CEFET/RJ
DIRETORIA DE PESQUISA E PÓS-GRADUAÇÃO

MIXED-MODE FRACTURE OF COMPOSITE-TO-METAL BONDED JOINTS: A STRAIN-BASED PARTITIONING METHOD

Marcio Moreira Arouche

Orientador: Dr. Silvio Romero de Barros
Coorientadora: Dra. Sofia Teixeira de Freitas

Rio de Janeiro
Julho de 2021

CEFET/RJ
DIRETORIA DE PESQUISA E PÓS-GRADUAÇÃO

MIXED-MODE FRACTURE OF COMPOSITE-TO-METAL BONDED JOINTS: A STRAIN-BASED PARTITIONING METHOD

Marcio Moreira Arouche

Tese apresentada ao Programa de Pós-Graduação em Engenharia Mecânica e Tecnologia de Materiais, do Centro Federal de Educação Tecnológica Celso Suckow da Fonseca, CEFET/RJ, como parte dos requisitos necessários à obtenção do título de Doutor em Engenharia Mecânica e Tecnologia de Materiais.

Orientador: Dr. Silvio Romero de Barros
Coorientadora: Dra. Sofia Teixeira de Freitas

Rio de Janeiro
Julho de 2021

MIXED-MODE FRACTURE OF COMPOSITE-TO-METAL BONDED JOINTS: A STRAIN-BASED PARTITIONING METHOD

Tese apresentada ao Programa de Pós-Graduação em Engenharia Mecânica e Tecnologia de Materiais, do Centro Federal de Educação Tecnológica Celso Suckow da Fonseca, CEFET/RJ, como parte dos requisitos necessários à obtenção do título de Doutor em Engenharia Mecânica e Tecnologia de Materiais.

Marcio Moreira Arouche

Banca Examinadora:

_____

Presidente, Professor Dr. Silvio Romero de Barros (CEFET/RJ) (orientador)

_____

Professora Dra. Sofia Teixeira de Freitas (TU Delft) (coorientadora)

_____

Professora Dra. Doina Mariana Banea (CEFET/RJ)

_____

Professor Dr. Volnei Tita (USP)

_____

Professor Dr. Marcelo Leite Ribeiro (USP)

_____

Professor Dr. João Pedro Ramôa Ribeiro Correia (IST – ULisboa)

Rio de Janeiro

Julho de 2021

Ficha catalográfica elaborada pela Biblioteca Central do CEFET/RJ

A771 Arouche, Marcio Moreira
Mixed-mode fracture of composite-to-metal bonded joints: a strain-based partitioning method / Marcio Moreira Arouche – 2021.
179f : il. color. , enc.

Tese (Doutorado). Centro Federal de Educação Tecnológica Celso Suckow da Fonseca, 2021.
Inclui bibliografia
Orientador: Silvio Romero de Barros
Coorientadora: Sofia Teixeira de Freitas

1. Mecânica da fratura. 2. Juntas adesivas. 3. Tecnologia de materiais. 4. Engenharia mecânica. 5. Confiabilidade (Engenharia). 6. Materiais – Fadiga. I. Barros, Silvio Romero de (Orient.). II. Freitas, Sofia Teixeira de (Coorient.). III. Título.

CDD 620.1126

Elaborada pela bibliotecária Tania Mello – CRB/7 nº 5507/04

ABSTRACT

The improvement of structural performance requires innovative applications of composite materials to replace traditional materials in the design of structures. In offshore industry, the deterioration of structures subjected to harsh environmental conditions motivates the development of new technologies for maintenance of structural integrity. Composite repair technology has emerged as a promising alternative for the rehabilitation of metal structures, introducing the application of composite-to-metal adhesively bonded joints. In this sense, literature reveals limitations of the current methodologies for optimizing the design and ensuring structural integrity of bi-material bonded structures. The determination of fracture mode ratio in cracks between different materials is challenging. Therefore, this Thesis addresses the fracture characterization of composite-to-metal bonded joints under mixed-mode loadings.

A new methodology was developed for the fracture characterization of bi-material crack propagation: the strain-based method (SBM). The SBM consists of an analytical approach based on beam analysis for the calculation of the total fracture energy and mode partitioning of bi-material crack propagation. It predicts a coupling relationship between the pure modes and allows obtaining the fracture mode ratio of bi-material cracks through a simple design criterion based on the longitudinal strain equivalence of the outer surfaces of the specimen. The new methodology was successfully applied on the experimental analysis of a composite-to-metal bonded joint using the mixed-mode bending (MMB) test. Limitations of the SBM include considerations of shear effects, crack tip rotation. Since the method relies on linear elastic fracture mechanics, the effect of a large fracture process zone (FPZ) developed ahead of the crack tip may also produce significant errors in the analytical solution.

A parametric study was performed to evaluate the SBM for the mixed-mode fracture characterization of bonded joints with asymmetric geometry and materials. The fracture energy obtained using SBM was benchmarked against the widely applied Williams' partitioning method (WM) and a finite element model (FEM) using the virtual crack closure technique (VCCT). Results showed that WM produces inaccurate fracture modes in asymmetric conditions while the SBM was able to obtain, with accuracy, the fracture mode ratio of bi-material cracks. The SBM proved to be an easy and reliable method that

allows characterizing mixed-mode fracture behavior of a crack propagation between different materials through a simple formulation. In contrast, the use of numerical solutions requires complex models and high computational cost.

The effect of design and manufacturing parameters on the performance of the composite-to-metal bonded joint was investigated using the SBM. Specimens were manufactured using a carbon fiber reinforced polymer (CFRP) co-bonded to a steel member with epoxy adhesive. A hand lay-up manufacturing process was applied with consolidation at room pressure or using vacuum bagging. Additionally, the influence of an inserted layer of glass fiber mat (GFM) was evaluated as a toughening mechanism to improve the fracture performance of the structure.

Results of MMB tests revealed that the insertion of a layer of GFM between adherends prevented the crack migration to the composite adherend and introduced a preferential crack propagation path. This shows that the adjacent composite layer to the adhesive interface has an important role in the fracture performance of the bonded joint. In addition, the fracture characterization revealed that the combination of vacuum pressure in the consolidation of the composite with the insertion of a layer of GFM increased the fracture toughness of the structure. The toughening mechanism is related with a more irregular crack path and higher surface roughness due to the increase in the energy required for the crack propagation. Moreover, the toughening effect showed to be more evident in higher mode II fracture conditions.

The effect of long-term environmental exposure on the performance of composite-to-metal bonded joints was investigated using the SBM. Specimens were aged in salt fog. Results showed that the environmental ageing did not have a drastic effect on the adhesive layer although it was extremely aggressive to the steel adherend. The fracture characterization revealed an increase of the toughness at crack initiation in aged specimens related to the shear behavior and plasticization of the adhesive, while the fracture toughness remained similar at crack propagation. In Addition, adhesive failure was observed in regions affected by moisture at the edges of the fracture surface while the failure mode at the unaffected regions shifted from cohesive to a combination of thin-layer cohesive and adhesive failure. These results contributed to describe the typical changes of the mechanical behavior of bonded joints at initial stages of ageing followed by a steady condition when pure adhesive failure is reached.

Keywords: fracture mechanics, composite materials, bonded joints, mixed-mode bending (MMB) test, strain-based method (SBM), finite element method, failure analysis, toughening mechanism, ageing.

RESUMO

A melhoria do desempenho estrutural requer aplicações inovadoras de materiais compósitos em substituição à materiais tradicionais no projeto de estruturas. Na indústria offshore, a deterioração de estruturas submetidas a condições ambientais severas motiva o desenvolvimento de novas tecnologias para manutenção da integridade estrutural. A tecnologia de reparo com compósitos surgiu como uma alternativa promissora para a reabilitação de estruturas metálicas, introduzindo a aplicação de juntas coladas de compósito em metal. Nesse sentido, a literatura revela limitações das metodologias atuais para otimização do projeto e garantia da integridade estrutural de juntas coladas bi-materiais. A determinação da razão do modo de fratura em trincas entre diferentes materiais é um desafio. Portanto, esta Tese aborda a caracterização da fratura de juntas coladas compósito-metal sob cargas de modo misto.

Uma nova metodologia foi desenvolvida para a caracterização da fratura em propagação de trincas bi-materiais: o método baseado na deformação, ou *strain-based method* (SBM). O SBM consiste em uma abordagem analítica, baseada em análise de vigas, para o cálculo da energia total de fratura e particionamento do modo de propagação em trincas bi-material. Ele prevê uma relação de acoplamento entre os modos puros e permite obter a razão do modo de fratura de trincas bi-materiais por meio de um critério simples baseado na equivalência da deformação longitudinal das superfícies externas do corpo de prova. A nova metodologia foi aplicada com sucesso na análise experimental de uma junta compósito-metal usando o ensaio *mixed-mode bending* (MMB). As limitações do SBM incluem considerações do efeito de cisalhamento e rotação da ponta de trinca. Uma vez que o método depende da mecânica de fratura elástica linear, o efeito da chamada *fracture process zone* (FPZ) desenvolvida à frente da ponta da trinca também pode produzir erros significativos na solução analítica.

Um estudo paramétrico foi realizado para avaliar o uso do SBM na caracterização da fratura em modo misto de juntas coladas com geometria e materiais assimétricos. A energia de fratura obtida usando o SBM foi comparada com o amplamente usado método de particionamento de Williams (WM) e com um modelo de elementos finitos (FEM) usando a *virtual crack closure technique* (VCCT). Os resultados mostraram que o WM produz modos de fratura imprecisos em condições assimétricas, enquanto o SBM foi

capaz de obter, com precisão, a razão do modo de fratura de trincas bi-materiais. O SBM provou ser um método fácil e confiável que permite caracterizar o comportamento da fratura em modo misto na propagação de uma trinca entre diferentes materiais por meio de uma formulação simples. Em contraste, o uso de soluções numéricas requer modelos complexos e alto custo computacional.

O efeito de parâmetros de projeto e fabricação no desempenho da junta colada compósito-metal foi investigado usando o SBM. Corpos de prova foram fabricados usando um polímero reforçado com fibra de carbono (CFRP) colado a uma parte de aço com adesivo epóxi. O processo de fabricação por laminação manual foi aplicado com consolidação à pressão ambiente ou usando bolsa de vácuo. Além disso, a influência da inserção de uma camada de manta de fibra de vidro (GFM) foi avaliada como um mecanismo de aumento de resistência para melhorar o desempenho em fratura da estrutura.

Resultados dos ensaios MMB revelaram que a inserção de uma camada de GFM entre os aderentes evitou a migração da trinca para o aderente compósito e introduziu um caminho preferencial de propagação da trinca. Isso mostra que a camada de compósito adjacente à interface adesiva tem um papel importante no desempenho em fratura da junta colada. Além disso, a caracterização da fratura revelou que a combinação da pressão de vácuo na consolidação do compósito com a inserção de uma camada de GFM aumentou a resistência à fratura da estrutura. O mecanismo de aumento de resistência está relacionado a um percurso mais irregular da trinca e uma maior rugosidade superficial, devido ao aumento da energia requerida para a propagação da trinca. Adicionalmente, o efeito do aumento de resistência à fratura mostrou-se mais evidente em condições de maior modo II.

O efeito da exposição ambiental de longo prazo no desempenho da junta colada compósito-metal foi investigado usando o SBM. Corpos de prova foram envelhecidos em névoa salina. Resultados mostraram que o envelhecimento ambiental não teve um efeito drástico na camada adesiva, embora tenha sido extremamente agressivo ao aderente de aço. A caracterização da fratura revelou um aumento da resistência na iniciação da trinca em corpos de prova envelhecidos relacionado ao comportamento ao cisalhamento e plastificação do adesivo, enquanto a resistência à fratura permaneceu similar na propagação da trinca. Além disso, a falha adesiva foi observada em regiões afetadas pela umidade nas bordas da superfície de fratura, enquanto o modo de falha em regiões não

afetadas mudou de coesiva para uma combinação de falha adesiva com coesiva de camada fina. Esses resultados contribuíram para descrever as mudanças típicas do comportamento mecânico de juntas coladas em estágios iniciais de envelhecimento, seguidos de uma condição estável quando a pura falha adesiva é atingida.

Palavras-chave: mecânica da fratura, materiais compósitos, juntas coladas, ensaio *mixed-mode bending* (MMB), *strain-based method* (SBM), método dos elementos finitos, análise de falha, mechanismo de aumento de resistência, envelhecimento.

List of Figures

Figure 1.1: Scheme of a unidirectional composite layer. 23
Figure 1.2: Composite repair of a ship hull. 24
Figure 1.3: Composite repair of a ballast tank 25
Figure 1.4: Scheme of a composite patch repair. 25
Figure 1.5: Fracture modes. 26
Figure 2.1: Beam analysis under pure bending moments. 32
Figure 2.2: (a) undeformed and (b) deformed finite element mesh. 36
Figure 2.3: VCCT for four-noded elements. 37
Figure 2.4: ADCB specimen free body diagram. 39
Figure 2.5: SLB specimen free body diagram. 41
Figure 2.6: MMB test scheme [75]. 43
Figure 2.7: MMB specimen free body diagram. 43
Figure 3.1: Crack propagation parameters. 64
Figure 3.2: Schematic of the MMB test. 65
Figure 3.3: Specimen geometry and boundary conditions. 69
Figure 3.4: Photo of the MMB test set up. 70
Figure 3.5: Detail of the FE mesh near the crack tip. 71
Figure 3.6: Mesh sensitivity analysis. 72
Figure 3.7: Load and crack length curves of Tests (a) 01 and (b) 02. 73
Figure 3.9: Load and crack length curves of Tests (a) 05 and (b) 06. 74
Figure 3.10: Load and crack length curves of Tests (a) 07 and (b) 08. 74
Figure 3.11: Load and crack length curves of Tests (a) 09 and (b) 10. 74
Figure 3.12: Fracture surfaces of (a) composite lower adherend
and (b) metal upper adherend. 75
Figure 3.13: Test 02 strain along steel (upper graph) and composite (lower graph)
surfaces at load of 456 N and crack length of 45 mm. 76
Figure 3.14: Test 02 strain along steel (upper graph) and composite (lower graph)
surfaces at load of 432 N and crack length of 55 mm. 77
Figure 3.15: Maximum steel arm strain during crack propagation. 78
Figure 3.16: Total fracture energy of Tests (a) 01 and (b) 02. 79

Figure 3.17: Total fracture energy of Tests (a) 03 and (b) 04. 79
Figure 3.18: Total fracture energy of Tests (a) 05 and (b) 06. 79
Figure 3.19: Total fracture energy of Tests (a) 07 and (b) 08. 80
Figure 3.20: Total fracture energy of Tests (a) 09 and (b) 10. 80
Figure 3.21: Fracture mode partitioning of the different test configurations. 80
Figure 4.1: Beam analysis under pure bending moments. 88
Figure 4.2: MMB test scheme. 93
Figure 4.3: MMB specimen. 94
Figure 4.4: Fracture mode of an asymmetric crack within arms of the same material, in terms of the element size. 95
Figure 4.5: Mesh of model with arms of the same material. 95
Figure 4.6: Fracture mode of a bi-material crack, in terms of the element size. 96
Figure 4.7: Mesh of model with bi-material crack. 96
Figure 4.8: Total fracture energy with the variation of the specimen thickness: cases (a) 1 – low, (b) 2 – intermediate and (c) 3 – high mode II. 98
Figure 4.9: Fracture mode ratio with the variation of specimen thickness: cases (a) 1 – low, (b) 2 – intermediate and (c) 3 – high mode II. 99
Figure 4.10: Influence of the coupling function on the fracture energy: cases (a) 1 – low, (b) 2 – intermediate and (c) 3 – high mode II. 100
Figure 4.11: Total fracture energy with the variation of the specimen material: cases (a) 4 – low, (b) 5 – intermediate and (c) 6 – high mode II. 102
Figure 4.12: Fracture mode ratio with the variation of specimen material: cases (a) 4 – low, (b) 5 – intermediate and (c) 6 – high mode II. 103
Figure 4.13: Influence of the coupling function on the fracture energy: cases (a) 4 – low, (b) 5 – intermediate and (c) 6 – high mode II. 104
Figure 4.14: MMB test results of thick specimens. 107
Figure 4.15: MMB test results of thin specimens. 108
Figure 4.16: Total fracture energy and mode ratio of thick specimens. 109
Figure 4.17: Total fracture energy and mode ratio of thin specimens. 109
Figure 5.1: MMB test scheme. 120

Figure 5.2: Load and crack length curves of specimens manufactured

at room pressure without GFM under 75% mode II fracture. 122
Figure 5.3: Load and crack length curves of specimens manufactured
at room pressure with GFM under 75% mode II fracture. 123
Figure 5.4: Load and crack length curves of specimens manufactured
using vacuum bagging without GFM under 75% mode II fracture..... 124
Figure 5.5: Load and crack length curves of specimens manufactured
using vacuum bagging with GFM under 75% mode II fracture..... 124
Figure 5.6: Load and crack length curves of specimens manufactured
using vacuum bagging without GFM under 40% mode II fracture..... 125
Figure 5.7: Load and crack length curves of specimens manufactured
using vacuum bagging with GFM under 40% mode II fracture..... 125
Figure 5.8: Crack propagation paths of (a) specimens without GFM
and (b) specimens with GFM. 126
Figure 5.9: Fracture toughness of specimens manufactured at room pressure
under 75% mode II fracture..... 127
Figure 5.10: Fracture toughness of specimens manufactured using
vacuum bagging under 75% mode II fracture. 128
Figure 5.11: Fracture toughness of specimens manufactured using
vacuum bagging under 40% mode II fracture. 129
Figure 5.12: Average fracture energy..... 130
Figure 5.13: Representative fracture surfaces of specimens manufactured
at room pressure under 75% mode II fracture. 131
Figure 5.14: Representative fracture height profiles of specimens manufactured
at room pressure under 75% mode II fracture (a) without and (b) with GFM. 131
Figure 5.15: Representative fracture surfaces of specimens manufactured using
vacuum bagging under 75% mode II fracture. 132
Figure 5.16: Representative fracture height profiles of specimens manufactured using
vacuum bagging under 75% mode II fracture (a) without and (b) with GFM. 133
Figure 5.17: Representative fracture surfaces of specimens manufactured using
vacuum bagging under 40% mode II fracture. 134

Figure 5.18: Representative fracture height profiles of specimens manufactured using

vacuum bagging under 40% mode II fracture (a) without and (b) with GFM. 134
Figure 5.19: Relationship between surface roughness and fracture energy. 137
Figure 5.20: SEM images of the steel side of specimens without GFM (a) RP-4 (G_{II}/G = 75%), (b) VB-2 (G_{II}/G = 75%) and (c) VB-5 (G_{II}/G = 40%). 138
Figure 5.21: SEM images of the steel side of specimens with GFM (a) RP/GFM-2 (G_{II}/G = 75%), (b) VB/GFM-3 (G_{II}/G = 75%) and (c) VB/GFM-5 (G_{II}/G = 40%). 139
Figure 6.1: Specimen geometry (dimensions in millimeters). 151
Figure 6.2: A specimen prepared for ageing. 151
Figure 6.3: MMB test scheme. 152
Figure 6.4: Model geometry and contour conditions. 153
Figure 6.5: Mesh sensitivity analysis. 154
Figure 6.6: Detail of the FE mesh around crack tip. 154
Figure 6.7: Steel outer surface (a) non-aged and (b) aged conditions. 157
Figure 6.8: Side view of a section of (a) non-aged and (b) aged specimens. 157
Figure 6.9: Load-displacement curves of tests with lever length of (a) 110 mm and (b) 150 mm. 158
Figure 6.10: Fracture energy of a representative specimen tested at a lever length of (a) 110 mm and (b) 150 mm. 160
Figure 6.11: Fracture mode ratio. 160
Figure 6.12: Average fracture energy at (a) crack initiation and (b) propagation. 161
Figure 6.13: Fracture surfaces of (a) non-aged and (b) aged specimens. 162
Figure 6.14: SEM images of non-aged specimen tested with c = 110 mm (20% mode II) at (a) x100 and (b) x500 and tested with c = 150 mm (15% mode II) at (c) x100 and (d) x500. 163
Figure 6.15: SEM images of aged specimen in 100x and 500x, respectively, at (a, b) center, (c, d) intermediate and (e, f) edge regions of the fracture surface. 164
Figure 6.16: EDS of aged specimen at (a) center, (b) intermediate and (c) edge regions. 165
Figure 6.17: EDS of aged specimen at center, intermediate and edge regions of the fracture surface. 166

List of Tables

Table 3.1: Mechanical properties of the materials. 68
Table 3.2: Test matrix..... 72
Table 4.1: Study cases of geometrical asymmetry. 97
Table 4.2: Results and errors of the analytical model in the condition of symmetric crack. 101
Table 4.3: Study cases of bi-material crack..... 101
Table 4.4: Results and errors of the analytical model in the condition of strain equivalence..... 104
Table 4.5: Mechanical properties of the materials. 106
Table 4.6: Test matrix..... 106
Table 5.1: Mechanical properties of the materials. 119
Table 5.2: Specimen measurements. 119
Table 5.3: Test matrix..... 121
Table 5.4: Roughness of the fracture surfaces..... 135
Table 6.1: Mechanical properties of the materials. 150
Table 6.2: Test matrix..... 157

List of Acronyms

4SLB: single leg 4-point bending

ADCB: asymmetric double cantilever beam

ATDCB: asymmetric tapered double cantilever beam

CBBM: compliance based beam method

CBON: cantilever beam opening notch

CBT: corrected beam theory

CFRP: carbon fiber-reinforced polymer

CLS: cracked lap shear

CLT: classical lamination theory

CPE4: 4-node bilinear plane strain quadrilateral solid elements

CTS: compact tension shear

CZM: cohesive zone model

DAL: dual actuator load

DCB: double cantilever beam

DCB-UBM: double cantilever beam with uneven bending moments

EDS: Energy-Dispersive Spectroscopy

ELS: end-loaded split

ENF: end-notched flexure

ENFR: end-notched flexure test with an inserted roller

FE: finite element

FEM: finite element method

FPSO: floating, production, storage and offloading

FPZ: fracture process zone

FRMM: fixed-ratio mixed-mode

FRP: fiber reinforced polymer

GFM: glass fiber mat

GFRP: glass fiber reinforced polymer

IDCB: imposed displacement cantilever beam

LEFM: linear elastic fracture mechanics

LVDT: linear variable differential transformers

MBT: modified beam theory

MEBT: modified elastic beam theory

MMB: mixed-mode bending

MMELS: mixed-mode end load split

MMF: mixed-mode flexure

OLB: over-leg bending

SACA: semi-analytical cohesive analysis

SBM: strain-based method

SEM: scanning electron microscope

SERR: strain energy release rate

SLB: single leg bending

TDCB: tapered double cantilever beam

VCCT: virtual crack closure technique

WM: Williams’ method

List of Symbols

Δa: element length

a: crack length

a_0: initial crack length

B: specimen width

c: lever length

c_g: lever center of gravity

E: elastic modulus

E_1: flexural longitudinal modulus of the upper arm

E_2: flexural longitudinal modulus of the lower arm

E_{11}: flexural longitudinal modulus

E_{eq}: equivalent flexural longitudinal modulus of the beam

f: function of the total fracture energy

f_I: function of the mode I fracture energy

f_{II}: function of the mode II fracture energy

f_c: coupling function between mode I and mode II fracture energy

G: total fracture energy

G_I: mode I fracture energy

G_{II}: mode II fracture energy

G_{II}: mode III fracture energy

G_c: critical strain energy release rate

h: specimen thickness

h_1: upper arm thickness

h_2: lower arm thickness

I: second moment of area

I_1: second moment of area of the upper arm

I_2: second moment of area of the lower arm

I_{eq}: equivalent second moment of area of the specimen

L: half-span

M: moment

M_1: moment on the upper arm

M_2: moment on the lower arm

P: test loading

P_I: opening loading

P_{II}: shear loadings

P_g: lever weight

Sq: root mean square height

T_g: glass transition temperature

U_e: external energy

U_s: strain energy

u_{ℓ_1}: displacement at nodal point ℓ_1 in x-direction

u_{ℓ_2}: displacement at nodal point ℓ_2 in x-direction

v_{ℓ_1}: displacement at nodal point ℓ_1 in y-direction

v_{ℓ_2}: displacement at nodal point ℓ_2 in y-direction

X_i: force at nodal point i in x-direction

Y_i: force at nodal point i in y-direction

β: longitudinal strain ratio between upper and lower arms

Δa: finite element size

ϕ: rotation angle of the specimen

ϕ_1: rotation angle of the upper arm

ϕ_2: rotation angle of the lower arm

ν: Poisson's ratio

ν_1: Poisson's ratio of the upper arm

ν_2: Poisson's ratio of the lower arm

ν_{12}: in-plane Poisson's ratio

ψ: bending stiffness ratio between upper and lower arms

Contents

1. Introduction 22

1.1 Background and motivation 23
1.2 Research goals and scope 26
1.3 Thesis outline 27
References 28

2. Literature Review of Mixed-Mode Fracture 30

2.1 Introduction 31
2.2 Fracture characterization models 32
2.2.1 Beam analysis 32
2.2.2 The virtual crack closure technique (VCCT) 35
2.3 Mixed-mode fracture tests 38
2.3.1 Asymmetric double cantilever beam (ADCB) Test 38
2.3.2 Single leg bending (SLB) test 40
2.3.3 Mixed-mode bending (MMB) test 42
2.3.4 Other testing methods 45
2.4 Conclusion 48
References 49

3. The Strain-Based Methodology 61

3.1 Introduction 62
3.2 Analytical model for bi-material bonded joints 64
3.3 Experimental procedures 67
3.3.1 Materials and specimens 67
3.3.2 Test set-up 69
3.4 Numerical model 70
3.5 Results and discussion 72
3.5.1 Experimental results 72
3.5.2 Validation of the numerical model 75
3.5.3 Fracture energy 77
3.6 Conclusion 81

References....81

4. Parametric Study....85

4.1 Introduction....86
4.2 Analytical models....88
4.2.1 Williams' partitioning method....90
4.2.2 Strain-based partitioning method....91
4.3 Numerical models....92
4.3.1 Asymmetric crack within the same material....94
4.3.2 Bi-material crack....95
4.4 Results and discussion....97
4.4.1 Asymmetric crack within the same material....97
4.4.2 Bi-material crack....101
4.5 Case study....105
4.5.1 Materials and methods....105
4.5.2 Results and discussion....107
4.6 Conclusion....110
References....110

5. Design and Manufacturing Parameters....115

5.1 Introduction....116
5.2. Materials and methods....118
5.2.1 Specimen design and manufacture....118
5.2.2 Experimental method....120
5.3 Test results....121
5.4. Discussion....126
5.4.1 Fracture toughness....126
5.4.2 Surface profile....130
5.4.3 Fractography....137
5.5 Conclusion....139
References....140

6. Environmental Ageing....145

6.1 Introduction....146

6.2 Materials and methods 150
6.2.1 Specimen manufacturing 150
6.2.2 Conditioning 151
6.2.3 Experimental method 152
6.3 Fracture data analysis 153
6.3.1 Numerical model 153
6.3.2 Analytical model 155
6.4 Results and discussion 156
6.4.1 Effect of ageing on the materials 156
6.4.2 Test results 157
6.4.3 Fracture toughness 158
6.4.4 Fractography 161
6.5 Conclusion 166
References 167
7. Conclusions and Final Remarks 173
7.1 Main conclusions and contributions 174
7.1.1 Mixed-mode fracture characterization of bi-material cracks 174
7.1.2 Effect of design and manufacturing parameters on composite-to-metal bonded joints 175
7.1.3 Effect of environmental conditions on composite-to-metal bonded joints 176
7.2 Future works 177

Chapter 1

Introduction

There is an increasing requirement for optimization of energy consumption and safety in industrial activities. The composite materials technology introduces new combination of properties that allows the developed of lighweight structures and the achievement of a superior structural performance. As innovative industrial applications of composites increase, the development of adhesive bonding technology is required due to their inherent integration and mutual benefit. With the expansion of these technologies, new opportunities become available for reseach in multi-material bonded structures. This research aims to address the chalenges of improving the design and ensuring structural integrity of bi-material bonded joints. The focus is placed on the crack propagation of bi-material bonded joints under mixed-mode fracture.

1.1 Background and motivation

The requirement of lightweight structures has encouraged the development of new materials. In this sense, composite materials technology has become the most suitable alternative to industrial applications [1]. First applications of composite structures are found in aerospace industry [2-5] and have been expanded to many other fields, such as automotive [6], maritime [7] and civil construction [8]. Advanced composite materials provide high strength with a relatively low weight and thus enable superior structural performance to be achieved. Inovative composite applications are developed as manufacturers replace traditional materials in the design of structures.

In a broad sense, a composite material is a new material made of a combination of two existing materials. In this context, advanced composites are usually made of a polymer matrix, which provides the shape, combined with a fiber reinforcement, which provides mechanical strength, as shown in Figure 1.1. These materials are called fiber reinforced polymers (FRPs). Since the mechanical properties are high only in the fiber direction, the FRPs are usually manufactured as multilayered structures. The main advantages of the laminate composites are the high mechanical properties, relatively low weight, design flexibility and high environmental resistance.

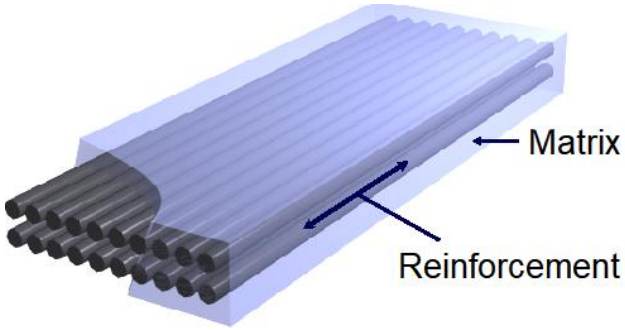


Figure 1.1: Scheme of a unidirectional composite layer.

The deterioration of structures subjected to harsh environmental conditions motivates the development of new technologies for maintenance of structural integrity. In recent years, the composite repair technology has emerged as a promising alternative for the rehabilitation of metal structures in aircrafts [9], vessels [10-12] and pipes [13-15]. In the offshore industry, oil and gas production platforms remain more than 20 years subjected to harsh environment and a large maintenance routine is necessary in order to

ensure structural integrity and continuous production. Composite repairs have the advantage of avoiding hot work, which is safer and does not require to stop the production. A composite patch is bonded or laminated directly on a metal structure in order to re-establish the structural integrity. Figure 1.2 [16] shows an example of composite repair applied to a ship hull and Figure 1.3 [17] shows the repair of a corroded floor of a ballast tank of a floating, production, storage and offloading (FPSO) unit. The composite patch is usually manufactured by hand lay-up using multidirectional carbon fibers and epoxy resin [18]. This results in a bi-material bonded structure between composite and metal parts, as shown in Figure 1.4 [18, modified]. The adhesive bonding technology has several advantages for joining composite materials, such as high strength-to-weight ratio, enhanced stress transfer mechanisms and design flexibility [1]. The advent of composite-to-metal bonded joints requires the development of new reliable methodologies for optimizing design and assuring structural integrity.



Figure 1.2: Composite repair of a ship hull.

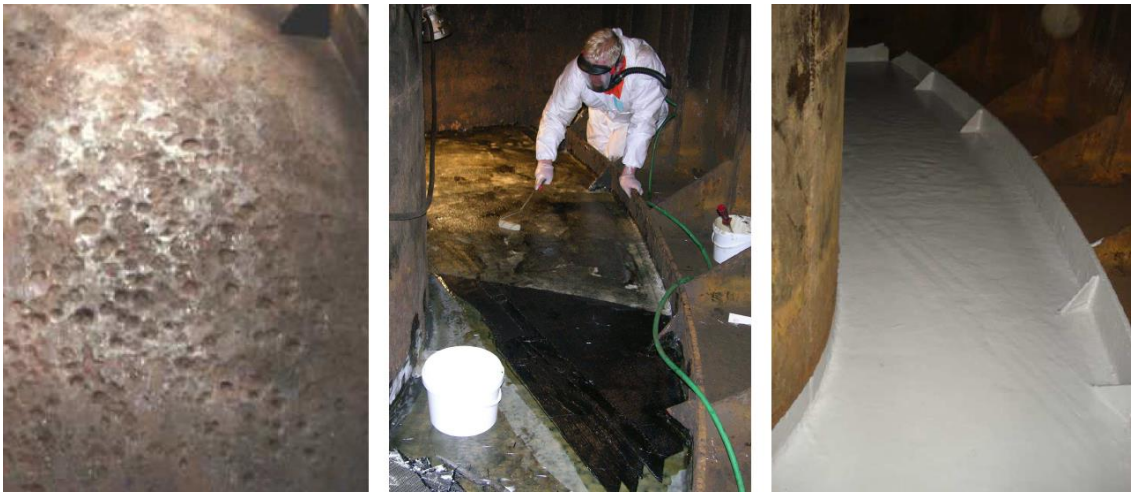


Figure 1.3: Composite repair of a ballast tank.

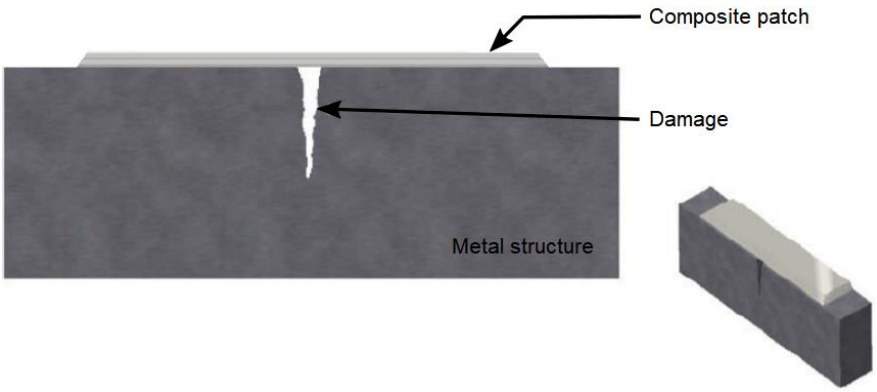


Figure 1.4: Scheme of a composite patch repair.

The fracture mechanics approach is widely applied to improve the design and evaluate the performance of structures. Imperfections present within materials are points of stress concentration and therefore fracture initiation. Fracture mechanics models the defect as a crack and evaluates if its size overcome the critical fracture size leading to structural failure. The strain energy release rate (SERR) is the most important property to consider in the calculation of fracture toughness of damaged structures. The crack propagation occurs when the available energy at the crack tip exceeds the critical energy for crack propagation. A crack in a structure may propagate in three different modes: opening (mode I), in-plane shear (mode II), and out-of-plane shear (mode III). An scheme is presented in Figure 1.5. In the cases of delamination and debonding, the crack propagates along a defined path at an interface, in a condition of mixed-mode (I+II) loadings.

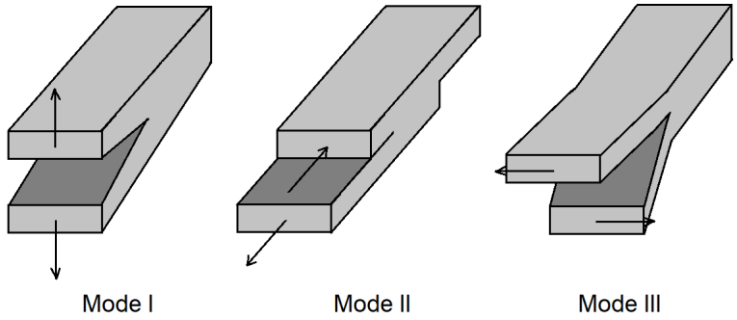


Figure 1.5: Fracture modes.

Literature reveals a need for the development of new methodologies for the characterization of mixed-mode fracture in bi-material bonded joints [19]. In this case, not only the total fracture toughness must be determined but also the proportion of mode I and mode II fracture.

1.2 Research goals and scope

There are well-stablished and standardized experimental methods for the fracture characterization of symmetric adherends. However, in the case of cracks between different materials, the determination of fracture mode ratio is challenging. The lack of a straightforward method capable of describing the fracture behavior of bi-material bonded joints poses an obstacle to the widespread use of multi-material bonded structures. The available methods for the fracture analysis of crack propagations between different materials are complex and rely on the use of computational tools, that are viable only in research level. Literature does not offer any reliable solution that can be easily reproduced in industrial level.

The present research aims to introduce a new methodology to evaluate the performance of bi-material bonded joints under mixed-mode fracture conditions. In this Thesis, research was conducted in specimen at coupon scale. Materials and procedures were chosen to simulate the application of composite bonded repairs in metal structures of offshore industry. In addition, parameters of design and manufacturing process were investigated using the proposed method. The effect of environmental degradation was also addressed in order to access the long-term performance of the bonded structure.

1.3 Thesis outline

This Thesis is organized in seven chapters. First, the **Introduction** (Chapter 1) presented the background and motivation for the topics developed in this Thesis. The research goals and methodology were defined. From here, specific parts of the research are discussed. Every chapter works independently, with introduction, goals, methods, results, discussion and conclusion.

Chapter 2, **Review of Mixed-Mode Fracture**, summarizes the state-of-art on the methodologies for the characterization of the fracture behavior of bonded materials under mixed-mode conditions. The most relevant methods for the evaluation of the performance and quantification of fracture parameters are outlined, including analytical and numerical approaches. A review of the experimental methods is also performed. The knowledge gaps in the literature review reveals challenges and limitations regarding the mixed-mode fracture characterization of bi-material cracks.

In Chapter 3, **The Strain-Based Methodology**, a new methodology is proposed for the mixed-mode fracture characterization of bi-material bonded joints. A testing procedure is suggested for the experimental assessment of the fracture behavior of composite-to-metal bonded joints. In Addition, an analytical solution, based on beam analysis, is proposed and validated for the calculation of the fracture parameters of the bi-material specimens under mixed-mode loadings.

In Chapter 4, a **Parametric Study** is performed in order to verify the accuracy and limitations of the strain-based method (SBM) for the calculation of the fracture parameters. The effects of geometry and material asymmetry are examined using numerical models. This analysis corroborated the results obtained in Chapter 3 for the application of the SBM to the mixed-mode fracture characterization of bi-material bonded joints.

Chapter 5 presents an analysis of **Design and Manufacturing Parameters** on the mixed-mode fracture behavior of composite-to-metal bonded joints. Different procedures for the manufacturing of composite patch repairs in steel structures are evaluated using the SBM. The influence of crack propagation path, fracture surface profile and failure modes on the performance of the structure is described.

In Chapter 6, the effect of **Environmental Ageing** on the mixed-mode fracture behavior of composite-to-metal bonded joints is evaluated. The long-term performance

of the bi-material bonded structure under a moist and salty atmosphere is examined using the SBM. The failure modes and chemical composition of the fracture surfaces are examined.

Finally, Chapter 7 presents the **Conclusions and Final Remarks** of the research developed in this Thesis. The outcome of the research is summarized and future challenges are pointed out.

References

[1] Budhe, S.; Banea, M.D.; de Barros, S. An Updated Review of Adhesively Bonded Joints in Composite Materials. Int. J. Adhes. Adhes. 2017, 72, 30-42.

[2] Mangalgiri, P.D. Composite materials for aerospace applications. Bull. Mater. Sci. 1999, 22, 657-664.

[3] Budhe, S.; Banea, M.D.; de Barros, S. Bonded repair of composite structures in aerospace application: a review on environmental issues. Appl. Adhes. Sci. 2018, 6, 3.

[4] Teixeira de Freitas, S.; Sinke, J. Failure analysis of adhesively-bonded skin-to-stiffener joints: Metal–metal vs. composite–metal. Eng. Failure Anal. 2015, 56, 2-13.

[5] Teixeira de Freitas, S.; Sinke, J. Failure analysis of adhesively-bonded metal-skin-to-composite-stiffener: Effect of temperature and cyclic loading. Compos. Struct. 2017, 166, 27-37.

[6] Taub, A.I.; Krajewski, P.E.; Luo, A.A. The evolution of technology for materials processing over the last 50 years: the automotive example. JOM 2007, 59, 48-57.

[7] Saleh, M.N.; Saeedifar, M.; Zarouchas, D.; Teixeira de Freitas, S. Stress analysis of double-lap bi-material joints bonded with thick adhesive. Int. J. Adhes. Adhes. 2020, 97, 102480.

[8] Van Den Einde, L.; Zhao, L.; Seible, F. Use of FRP composites in civil structural applications. Constr. Build. Mater. 2003, 17(6-7), 389-403.

[9] Katnam, K.B.; da Silva, L.F.M.; Young, T.M. Bonded repair of composite aircraft structures: A review of scientific challenges and opportunities. Prog. Aerosp. Sci. 2013, 61, 26-42.

[10] McGeorge, D.; Echtermeyer, A.T.; Leong, K.H.; Melve, B.; Robinson, M.; Fischer, K.P. Repair of floating offshore units using bonded fibre composite materials. Compos. Part A 2009, 40(9), 1364-1380.

[11] Meniconi, L.C.; Lana, L.D.; Morikawa, S.R. Experimental fatigue and aging evaluation of the composite patch repair of a metallic ship hull. Appl. Adhes. Sci. 2014, 2, 27.
[12] Saleh, M.N.; Saeedifar, M.; Zarouchas, D.; Teixeira de Freitas, S. Stress analysis of double-lap bi-material joints bonded with thick adhesive. Int. J. Adhes. Adhes. 2020, 97, 102480.
[13] da Costa-Mattos, H.S; Reis, J.M.L; Sampaio, R.F.; Perrut, V.A. An alternative methodology to repair localized corrosion damage in metallic pipelines with epoxy resins. Mater. Des. 2009, 30(9), 3581-3591.
[14] de Barros, S.; Banea, M.D.; Budhe, S.; de Siqueira, C.E.R.; Lobão, B.S.P.; Souza, L.F.G. Experimental analysis of metal-composite repair of floating offshore units (FPSO). J. Adhes. 2016, 93(1-2), 147-158.
[15] da Costa Mattos, H.S.; Reis, J.M.L.; Paim, L.M.; da Silva, M.L.; Lopes Junior, R.; Perrut, V.A. Failure analysis of corroded pipelines reinforced with composite repair systems. Eng. Fail. Anal. 2016, 59, 223-236.
[16] Meniconi, L.C.M.; Lana, L.D.M.; Morikana, S.R.K. Experimental Fatigue Evaluation of the Composite Repair of a Metallic Ship Hull. 2nd Brazilian Conference on Composite Materials, São José dos Campos, São Paulo, Brazil, 15-18 September 2014.
[17] Meniconi, L.C.M.; Porciúncula, I.N.; McGeorge, D.; Pedersen, A. Structural repair at a production platform by means of a composite material patch. Offshore Technology Conference, Houston, Texas, USA, May 3-6, 2010.
[18] DNV-RP-C301. Design, Fabrication, Operation and Qualification of Bonded Repair of Steel Structures. Det Norske Veritas AS, 2015.
[19] Chaves, F.J.P.; da Silva, L.F.M.; de Moura, M.F.S.F.; Dillard, D.A.; Esteves, V.H.C. Fracture Mechanics Tests in Adhesively Bonded Joints - A Literature Review. J. Adhes. 2014, 90(12), 955-992.

Chapter 2

Literature Review of Mixed-Mode Fracture

The fracture mechanics approach is an important technique to improve the design and evaluate the performance of composite and adhesively bonded materials. In these structures, the crack usually propagates in a combination of opening (mode I) and shear (mode II) loadings along a defined path. The fracture characterization is primarily based on the determination of the strain energy release rate (SERR). Not only the total fracture energy must be determined but also the ratio between the two fracture modes. A solid understanding of the available methodologies for mixed-mode fracture characterization is essential to improve the development and application of composites and adhesion technologies. In this work, a review on theoretical and experimental procedures for the mixed-mode fracture characterization of composites and bonded joints is presented. Analytical and numerical solutions based on elastic fracture mechanics (LEFM) are described for the determination of the total fracture energy and mode ratio. Advantages and limitations of a variety of experimental procedures are discussed. The most suitable method depends on several parameters, such as the available equipment, type of materials and the range of fracture modes to be tested.

Keywords: fracture mechanics, mixed-mode fracture, beam analysis, finite element method, testing methods, literature review.

2.1 Introduction

In the last few decades, enormous amount of investigation has been carried out on the development of laminated fiber-reinforced polymers (FRPs) [1-3]. The advantages of composite materials include high strength-to-weight ratio, design flexibility and durability. These technologies have been developed first in the aerospace industry [4-6] and became essential in many other fields, such as automotive [7], marine [8], construction [9] and electronics [10]. The expansion of composite applications increases the application of multi-material structures. Adhesive bonding is the most efficient technique in terms of design and performance for joining composites to other materials, such as metals. The design of multi-material bonded structures requires the development of new methods for optimizing structural performance.

The fracture mechanics approach is an important technique to improve the design and evaluate the performance of structures [11]. In the cases of delamination and debonding, the crack is constrained to propagate along a defined path. The fracture characterization is primarily based on the determination of the strain energy release rate (SERR) during the propagation of a crack. However, the fracture usually propagates in a combination of opening (mode I) and shear (mode II) loadings. In a mixed-mode fracture (I+II), the total fracture energy must be determined as well as the ratio between the two fracture modes. Different models have been developed based on beam theory [12] and J-integral [13] for the calculation of the fracture energy. The finite element method (FEM) has also been an important tool for the analysis of cracked materials through concepts of fracture mechanics [14]. The development and application of fracture characterization methods are object of several experimental [15, 16] and numerical [17] studies.

Many authors addressed the challenges on the fracture characterization of composites and bonded joints. Chaves et al. [18] indicated that there is a need for development of simple and reliable methodologies for the characterization of mixed-mode (I+II) fracture. Several methods were developed for the analysis of cracked materials. However, these works are scattered. A solid understanding of the available methods for fracture characterization is essential to improve the development and application of composites and adhesion technologies.

This Chapter presents a critical literature review on theoretical and experimental methods for the mixed-mode fracture characterization of composites and bonded joints. The reliability of the available approaches for fracture mode partitioning is evaluated.

2.2 Fracture characterization models

In this section, a description is provided regarding the most relevant theories for the fracture characterization of composites and bonded joints.

2.2.1 Beam analysis

Analytical methods based on beam theory are the simplest way to characterize interlaminar and interfacial fracture. They are widely applied to the analysis of beam-like specimens under bending moments. The analysis considers a region (δa) mechanically affected by the presence of a crack (a), as shown in Figure 2.1.

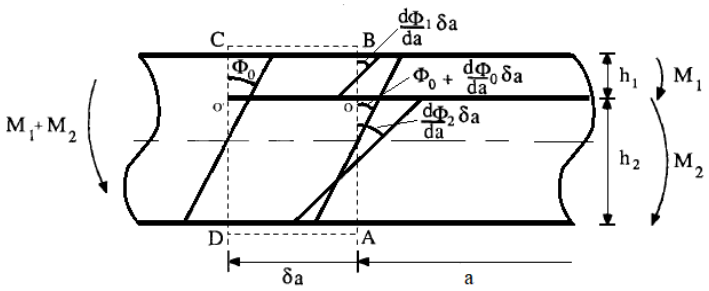


Figure 2.1: Beam analysis under pure bending moments.

The SERR is obtained through the law of conservation of energy:

$$G = \frac{1}{B}\left(\frac{dU_e}{da} - \frac{dU_s}{da}\right) \tag{2.1}$$

Where B is the width of the specimen, U_e is the external work performed and U_s is the strain energy and a is the crack length. When the crack moves from O on section AB to O' on section CD, the external work is:

$$\frac{\delta U_e}{\delta a} = M_1\left(\frac{\delta\phi_1}{\delta a} - \frac{\delta\phi_0}{\delta a}\right) + M_2\left(\frac{\delta\phi_2}{\delta a} - \frac{\delta\phi_0}{\delta a}\right) \tag{2.2}$$

Where M_1 and M_2 are the bending moments on the section of the crack tip in the upper and lower arms, respectively. For bending moments, the change in angle is given by:

$$\frac{\delta\phi}{\delta a} = \frac{M}{EI} \tag{2.3}$$

Where M is the moment, E is the axial Young's modulus parallel to the crack and I is the second moment of area. Similarly, the strain energy is:

$$\frac{\delta U_s}{\delta a} = \frac{M_1^2}{2E_1I_1} + \frac{M_2^2}{2E_2I_2} - \frac{(M_1 + M_2)^2}{2E_{eq}I_{eq}} \tag{2.4}$$

Where E_1, I_1, E_2, I_2, E and I are the flexural longitudinal moduli and second moments of the area in the section of the crack tip of the upper arm, lower arm and total specimen, respectively. Substituting (2) and (4) in (1), it can be reduced to the equation of the total fracture energy:

$$G = \frac{1}{2B}\left(\frac{M_1^2}{E_1I_1} + \frac{M_2^2}{E_2I_2} - \frac{(M_1 + M_2)^2}{E_{eq}I_{eq}}\right) \tag{2.5}$$

Equation (2.5) allows calculating the total fracture energy of a beam. However, it is essential to define the contribution of mode I and mode II fracture in the characterization of the mechanical behavior. Williams [1] presented a method for partitioning the fracture energy at the crack tip delamination of composites under bending loading. It is based on the following two assumptions:

(i) pure mode I exists when opposite moments act on the joint arms, i.e., $M_1 = M_I$ and $M_2 = -M_I$;

(ii) pure mode II is obtained when the curvatures of the two arms are the same, i.e., $M_1 = M_{II}$ and $M_2 = \psi M_{II}$, where ψ is defined as the bending stiffness ratio of upper and lower arms, as:

$$\psi = \frac{E_2 I_2}{E_1 I_1} \tag{2.6}$$

Based on these two assumptions, one can obtain:

$$M_1 = M_{II} - M_I \tag{2.7}$$

$$M_2 = \psi M_{II} + M_I \tag{2.8}$$

Substituting Equations (2.7) and (2.8) in Equation (2.5), the fracture energy can be partitioned in mode I, when $M_{II} = 0$, and mode II, when $M_I = 0$. G_I, G_{II} and G are then given by:

$$G_I = \frac{(\psi M_1 - M_2)^2}{2B(\psi + 1)^2}\left(\frac{1}{E_1 I_1} + \frac{1}{E_2 I_2}\right) \tag{2.9}$$

$$G_{II} = \frac{(M_1 + M_2)^2}{2B(\psi + 1)}\left(\frac{1}{E_1 I_1} - \frac{(\psi + 1)}{E_{eq} I_{eq}}\right) \tag{2.10}$$

$$G = G_I + G_{II} \tag{2.11}$$

The beam analysis is a full field measuring technique and is commonly referred in the literature as the ‘global’ method, as it considers the whole geometry of the beam.

Analytical models based only in simple beam analysis does not properly describe the crack propagation mechanism [19]. The two arms are not fixed against rotation at the delamination tip as assumed in simple beam analysis. Instead, they rotate slightly due to the elastic support that they provide one another. Such effects arise as a result of shear deformation and deflection at the crack tip, large deflections of the arm and stiffening of the arms due to the presence of the end-blocks. Williams [20] proposed a correction factor, based on Kanninen [21] elastic foundation model, for accounting these various effects in the mode I fracture. Wang and William [22] tested the same correction factor for mode II fracture component. The incorporation of crack tip correction factors in the beam model, Equations (2.9) and (2.10), resulted in the so-called corrected beam theory

(CBT). In this model, an effective crack length value is used to account for the contribution to the energy release rate from shear deformations.

The works of Williams [23], Hashemi et al. [24] and Ducept et al. [25] indicated that the beam analysis with crack tip corrections produces reliable values for the total fracture energy and partitioning ratio of symmetric cracks. However, Ducept el al. [26] showed that the global method does not provide reliable results of the fracture mode partitioning of cracks between asymmetric arms.

Conroy et al. [27] combined simple beam analysis with cohesive zone models (CZMs) and proposed a semi-analytical cohesive analysis (SACA) to obtain the fracture mode ratio of asymmetric geometries. It predicts a variation of the fracture mode ratio from the local to the global partitioning as the fracture process zone (FPZ) increases. The SACA has proven superior to the traditional beam analysis for the mixed mode fracture characterization of adhesively bonded joints [28]. However, it requires an iterative process for the estimation of the cohesive zone length to determine the fracture mode ratio from a numerically obtained dependency curve.

An alternative approach to obtain the fracture toughness of cracked materials is the J-integral. It can be defined as the decrease of potential energy per increment of cracked surface in an elastic linear or non-linear material [13]. The fracture energy can be calculated by evaluating the independent contour integral along a path following the external boundaries of the specimen. The J-integral approach uses non-linear fracture mechanics, which allows evaluating fracture under linear elastic as well as elastoplastic conditions. In conditions of linear-elastic behavior, the J-integral is equivalent to the definition of SERR from the LEFM.

2.2.2 The virtual crack closure technique (VCCT)

The fracture behavior of an interfacial crack can be predicted using a singular field-based approach. The virtual crack closure technique (VCCT), proposed by Rybicki and Kanninen [14], is a ‘local’ method based on LEFM that assumes that when a crack extends by a small amount, the energy released in the process is equal to the work required to close the crack to its original length. It allows obtaining the mode I, mode II and mode III fracture energy from the nodal forces and displacements obtained from the solution of a finite element model.

The VCCT became widely applied in the determination of the fracture energy and mode partitioning of plane (two-dimensional – 2D) and solid (three-dimensional – 3D) interfacial cracks [29]. In a 2D finite element plane stress or plane strain model, the crack (a) is represented as a one-dimensional discontinuity by a line of nodes, as shown in Figure 2.2a. Nodes at the top surface and the bottom surface of the discontinuity have identical coordinates but are not connected with each other. This allows the elements connected to the top surface to deform independently from those connected to the bottom surface. Consequently, the crack is allowed to open, as shown in Figure 2.2b.

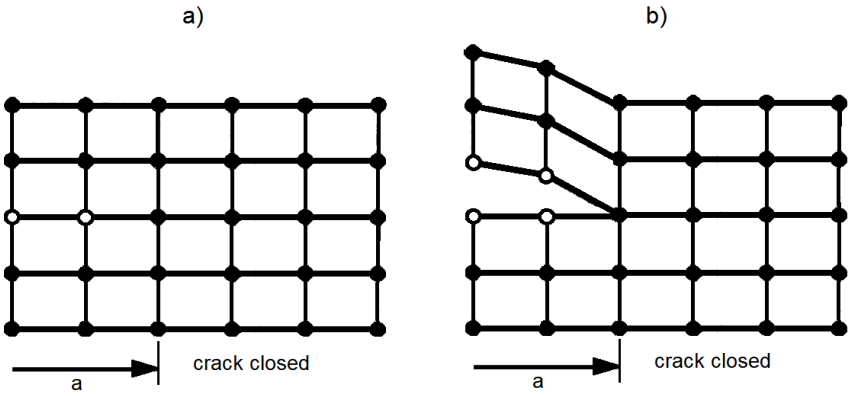


Figure 2.2: (a) undeformed and (b) deformed finite element mesh.

The mode I and mode II components of the strain energy release rate can be obtained using two-dimensional for four-noded finite element models, as shown in Figure 2.3.

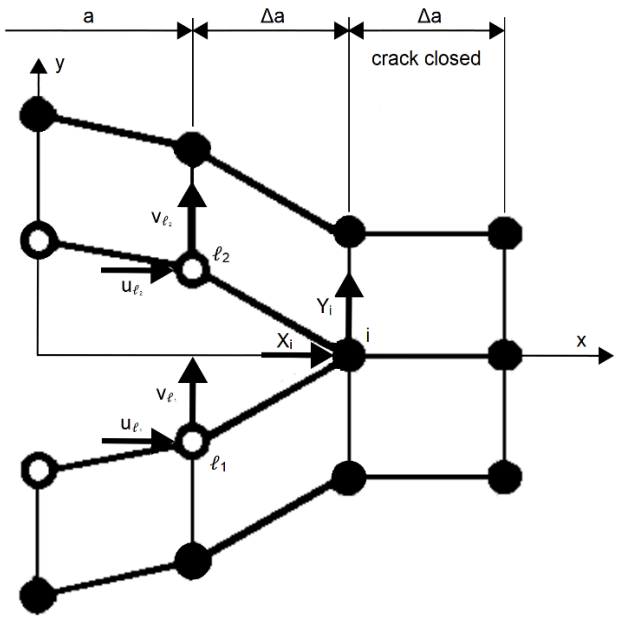


Figure 2.3: VCCT for four-noded elements.

Considering an element thickness equals 1, the equations are:

$$G_I = \frac{1}{2B\Delta a} Y_i \left(v_{\ell_2} - v_{\ell_1}\right) \tag{2.12}$$

$$G_{II} = \frac{1}{2B\Delta a} X_i \left(u_{\ell_2} - u_{\ell_1}\right) \tag{2.13}$$

Where Δa is the element length at the crack front, B is the element width in z direction, and X_i and Y_i are the forces at the crack tip (nodal point i). The relative displacements behind the crack tip are calculated from the nodal displacements u_{ℓ_1} and v_{ℓ_1} at the lower crack face (nodal point ℓ_1), and the nodal displacements u_{ℓ_2} and v_{ℓ_2} at the upper crack face (nodal point ℓ_2). The total energy release rate is calculated from the individual mode components.

$$G = G_I + G_{II} + G_{III} \tag{2.14}$$

Where $G_{III} = 0$ for the two-dimensional case discussed.

The VCCT has shown to be a reliable method for calculation of the fracture components at a crack between homogenous materials [29]. However, the mode partitioning becomes sensitive to the crack extension length when the crack is modelled at a bi-material interface [30]. One way to circumvent the problem is the insertion of an interlayer in both sides of the crack [31, 32]. The crack propagation occurs within a homogeneous path where the mode partition is not sensitive to the crack length.

The use of FEM allows obtaining the fracture of complex geometries but requires high computational effort. In general, the VCCT has been widely applied to the validation of analytical models for obtaining the fracture toughness of beam-like cracked structures [17]. However, the use of a local method the size of the singular field to be larger than the damage zone [35]. It is usually the case of crack propagation in ductile materials.

2.3 Mixed-mode fracture tests

In fracture tests, defects are modelled as pre-cracks that are artificially placed to simulate damage initiation. During the test, a cracked specimen is subjected to loadings that cause a stress concentration around the crack tip and consequently the crack propagation. In the case of mixed-mode fracture tests, the stresses result in mode I and mode II fracture simultaneously in a defined ratio. A variety of experimental methods has been developed for evaluation of the mixed-mode fracture. In this section, the most relevant test procedures are individually described and discussed.

2.3.1 Asymmetric double cantilever beam (ADCB) Test

The double cantilever beam (DCB) test was early developed for pure mode I fracture characterization of symmetric specimens [36]. The test specimen consists of a beam type geometry comprised of top and bottom arms with a crack (a) at one end along the interface. During the DCB test, an opening load (P) is applied to the specimen arms producing the crack propagation. When the crack is placed between arms with different geometry and/or materials, an amount of shear stress is experienced near the crack. In these cases, the asymmetric double cantilever beam (ADCB) test is indicated for the mixed-mode fracture characterization [37]. Figure 2.4 shows the ADCB test scheme. The

same procedure has also been called unsymmetric double cantilever beam (UDCB) test [38].

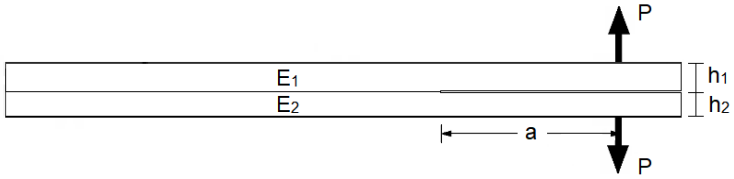


Figure 2.4: ADCB specimen free body diagram.

Ducept et al. [26] applied global and local methods for the fracture characterization of unidirectional asymmetric laminates. They verified that the simple beam analysis does not properly estimate the mode I and mode II fracture energy. Mollón et al. [39] successfully evaluated the fracture toughness of carbon-epoxy asymmetric laminates using the modified beam theory (MBT) [40]. The MBT is an experimental calibration parameter is introduced in the formulation in order to correct the beam theory to account for rotations at the delamination front during the DCB test. Alternatively, Shokrieh and Zeinedini [41] assumed each arm of the ADCB specimen as an elastic cantilever beam and proposed a modified elastic beam theory (MEBT) to calculate the SERR of multidirectional composite laminates.

Several methods have been proposed for the fracture characterization of mixed-mode fracture using the ADCB test [42-45]. Jernkvist [42, 43] developed criteria to evaluate the crack propagation in wood. The analysis considers the typical fiber structure from wood materials and relies on the concepts of LEFM for the formulation. Benatti et al. [44] proposed an analytical solution derived from a mechanical model of the ADCB test in which the specimen is an assembly of two arms partly connected by an elastic-brittle interface. However, the model does not account for the effects of geometric and material non-linearities. Risov and Mladensky [45] theoretically studied the non-linear fracture behavior of ADCB specimens made of unidirectional FRPs by means of path independent J-integral. They found that the material non-linearity contributes to the increase of the J-integral value. This effect is attributed to the strain energy dissipation due to plastic deformation of the beam.

Overall, the ADCB test is a simple solution to determine the mixed-mode fracture toughness of a reasonable range of fracture mode ratios by varying the relative

thicknesses of the two arms. The main drawback is that the mode II contribution is restricted by the tested material and geometrical limitations. Another inconvenient is the fact that one specimen geometry allows obtaining only one fracture mode ratio. Recently, Wang et al. [46] showed that pure mode I can be achieved in bi-material joints by matching the longitudinal strain distributions of the two adherends at the bond line. The longitudinal strain-based criterion showed to be more accurate in comparison with a flexural stiffness-based criterion for obtaining the pure mode I crack propagation.

Park and Dillard [47] proposed the asymmetric tapered double cantilever beam (ATDCB) test as a variation of the ADCB test combined with the tapered double cantilever beam (TDCB) [48]. The ATDCB specimen consists of a hybrid configuration, where one arm of the specimen has a constant section, and the other arm has wedge configuration. The relative stiffness of the adherends varies in a systematic manner, resulting in a range of the fracture mode ratio as the crack propagates. Similar to the ADCB test, the ATDCB test presents a limited partitioning range. Moreover, it has higher manufacturing complexity when compared with common ADCB, particularly for composite laminates.

2.3.2 Single leg bending (SLB) test

The end-notched flexure (ENF) test was early developed for pure mode II fracture characterization [49]. In the ENF test, a load (P) is applied to the specimen mid-span between the two supports points. The procedure has proven to produce pure shear loading in cracks between symmetric and asymmetric arms [50]. Russell and Street [51] introduced the mixed-mode flexure (MMF) test as an adaptation of the ENF test for mixed-mode fracture characterization. In the MMF test, the entire reaction force at this end is transmitted to the upper material through a loading block, inducing a portion of opening loading in the region of the crack tip. Later on, Yoon and Hong [52] proposed a similar procedure. In this case, a portion of the lower arm is removed from the cracked end so that the test can be applied using only simply supported ends. Davidson and Sundararaman [53] referred to a similar procedure as single-leg bending (SLB) test. The SLB test scheme is shown in Figure 2.5.

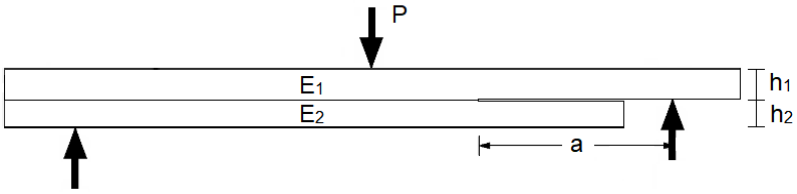


Figure 2.5: SLB specimen free body diagram.

The SLB test has been extensively applied to the analysis of composite laminates [54-56]. Abertsen et al. [54] and Rikards et al. [55] evaluated the influence of interface properties on the fracture toughness of unidirectional fiber composites using simple beam theory. Gong and Davidson et al. [56] confirmed the negligible effect out-of-plane shear (mode III) fracture from a tridimensional analysis of unidirectional and multidirectional symmetric specimens. Davidson et al. [57] verified the influence of geometric parameters on the energy release rate and mode ratio in symmetric SLB tests using the FEM. A design approach was proposed for obtaining accurate values of the fracture toughness from conventional data reduction methods. Gong and Benzeggagh [58] showed that both symmetrical and asymmetrical specimens allow testing a similar range of fracture mode ratios. The ratio depends only on the crack position and the thickness of the specimen and is independent of both the applied load and the crack length. Lee et al. [59] applied the SLB test to the analysis of composite-to-steel bonded joints. These works showed that the method is a simple solution to evaluate the mixed-mode fracture behavior of cracked specimens at a nearly constant mode ratio, but it is limited to smaller mode I contributions.

Szekrényes and Uj [60] incorporated transverse shear, elastic foundation effects to the beam analysis of unidirectional glass/polyester laminates. Oliveira et al. [61] proposed the compliance-based beam method (CBBM) for the mixed-mode fracture characterization of wood using SLB tests. The CBBM depends on the specimen compliance which is used to estimate an equivalent crack. Therefore, it does not require crack length monitoring during the test. Pereira et al. [62] successfully applied the same procedure to the fracture characterization of a bone specimens and Silva et al. [63] measured the crack tip opening displacements by digital image correlation. The same approach was applied to characterize the mixed-mode fracture of carbon-epoxy/cork hybrid laminates [64] and unidirectional carbon-fiber composites [65]. These works

proved the excellent performance of a crack equivalent beam model applied to the SLB test.

A variation of the SBL was suggested by Tracy et al. [66], the single leg 4-point bending (4SLB) test. The method utilizes a small test coupon and allows obtaining a constant mode ratio during crack propagation. Davidson et al. [67] verified the influence of geometric parameters on the energy release rate and mode ratio in symmetric 4SLB tests using the FEM. The 4SLB test has shown to provide an attractive alternative, as it can use the same type of test specimens and produces results with essentially the same accuracy of the SLB test.

Szekrényes and Uj [68] developed the over-leg bending (OLB) test as an adaptation of the SLB test modified by variating the position of the applied load between the two supports. The OLB test showed to promote a more stable crack propagation than the SLB due to the possibility of greater crack length. Additionally, Liu et al. [69] tested carbon fiber composites and verified that the crack propagates quicker in the SLB test than in the OLB test. However, the OLB test leads to a higher bending strength than the SLB for the same specimen.

2.3.3 Mixed-mode bending (MMB) test

Reeder and Crews [70] developed the mixed-mode bending (MMB) test method as a combination of the DCB and the ENF tests. In this test, the loading (P) is applied through a roller attached to a lever and loaded just above the mid-plane of the test specimen. The test loading is decomposed in opening (P_I) and shear (P_{II}) loadings in a constant ratio determined by the lever length (c). The original procedure was later redesigned in order to minimize geometrical nonlinearity effects [71] and to take into account the weight of the lever [72]. Chen et al. [73] proposed a modification to the test apparatus in order to avoid preloading on the specimens caused by the weight of the lever. The MMB test scheme is shown in Figure 2.6 and the loads applied to the specimen are shown in Figure 2.7. It has proved to be an easy and reliable method for measuring a wide range of mixed-mode ratios with only one specimen geometry [25, 74].

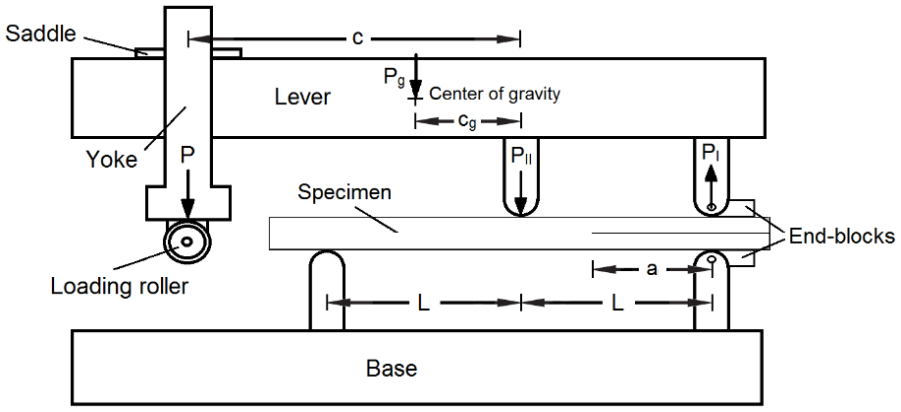


Figure 2.6: MMB test scheme [75].

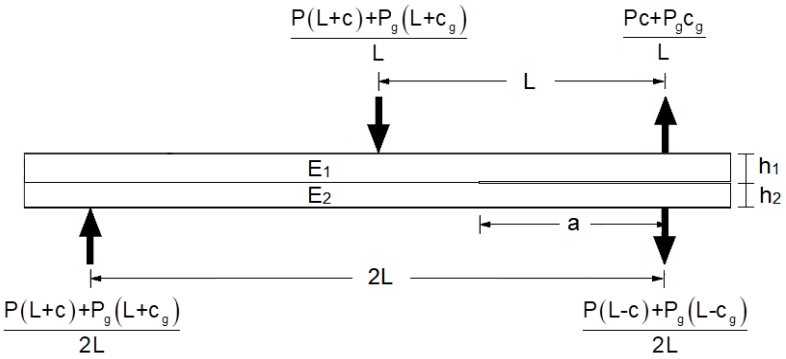


Figure 2.7: MMB specimen free body diagram.

The MMB test method has been extensively applied for evaluation of the delamination in unidirectional composites with a midplane crack [25, 73, 74, 76-80]. Martin and Hansen [77] proposed a constant opening-displacement ratio in order to achieve stable delamination growth and overcome potential inaccuracies. Ducept et al. [78] verified an atypical failure behavior concerning crack stability when testing a composite bonded joint in comparison with composite delamination. Reeder [79, 80] defined a criterion for choosing test parameters where nonlinear errors are insignificant. Bhashyam and Davidson [76] confirmed the accuracy of the CBT for fracture characterization of unidirectional symmetric delamination. Blanco and Turon [81] proposed a simple solution to determine the lever length with better accuracy. These works were led to the standard ASTM D6671M [82] that describes the MMB test procedure and incorporates the CBT for the fracture characterization of unidirectional symmetric composites.

Studies performed by de Morais and Pereira [83, 84] successfully applied the MMB test on the delamination analysis of multidirectional symmetric composites. Sarrado et al. [85] developed a method based on J-integral [13] for the experimental characterization of fractures with a large FPZ. However, it has the same specimen limitations as the standard method. Floros et al. [86] applied a CZM for a symmetric bonded joint between multidirectional laminates. In this case, modifications of the input parameters and the traction-separation law are needed to effectively simulate the mixed-mode fracture behavior of the joints.

The delamination in asymmetric composites has been consistently evaluated using the MMB test. Kim and Mayer [87] tested the fracture toughness between mismatch fiber directions. Pereira and de Morais [31] developed a compliance beam model to predict the fracture of multidirectional asymmetric laminates. Shahverdi et al. [88, 89] and Ševčík et al. [90] applied the global method for the analysis of asymmetric cracks between two different composite materials. They modeled cohesive interface elements based on an exponential traction-separation law to account for the effect of fiber bridging. The contribution of mode I fracture increases the effect of fiber bridging.

The MMB test method has also been expanded to several different materials. Oliveira et al. [91] performed a numerical study in order to confirm the adequacy of MMB test for fracture characterization of symmetric wood bonded joints. De Moura et al. [92, 93] applied an experimental compliance method for characterization of wood fracture. Yoshihara [94] demonstrated that the CBT predicts with accuracy the mixed-mode fracture of solid wood. Pereira et al. [95] tested the fracture of a relatively short beam specimens made of bone material. Many authors applied the MMB test for the analysis of symmetric metallic joints bonded [96-100]. Early study showed limitations to the specimen design due to extensive adherend yielding [96]. Stamoulis et al. [99] and Doubri et al. [100] successfully tested symmetric metallic joints using the standard procedure [82]. Ben Salem et al. [97, 98] proposed a method simple beam theory with elastic interfaces model to predict the damage development in bonded layers or interfaces. However, a reliable determination of the interface separation law requires experimental backface strain monitoring.

The most general applications of MMB tests concern the analysis of crack propagation in specimens where both geometry and material properties of the arms are

different. An early work performed by Soboyejo et al. [101] in a copper/molding compound specimen demonstrated the potential use of dissimilar specimens for interfacial fracture testing. Quispitupa et al. [102-104] evaluated the geometry of sandwich specimens for the evaluation of face/core debonding. They revealed a relationship between the fracture mode and the crack path.

2.3.4 Other testing methods

Apart from the already presented methods (ADCB, SLB and MMB), there are a variety of different experimental methods can be found in literature for the mixed-mode fracture characterization of composites and bonded joints. A classic experimental method to determine the fracture parameters of bonded materials is the cracked lap shear (CLS) test [105]. In CLS tests, the fracture mode ratio changes with the crack length and the thickness ratio between the two arms of the specimen, and the contribution of mode I fracture is limited. Moreover, an accurate measurement of the fracture energy during propagation may be difficult due to crack growth instability. Therefore, the fracture toughness is obtained only from the critical force.

Edde and Verreman [106] derived a closed-form analytical solution from the stress analysis of the CLS specimen. Rhee [107] and Albertsen [54] evaluated the delamination of unidirectional composites, Rhee and Chi [108] tested multidirectional laminates, and Azari et al. [109] tested metal bonded joints. Lai et al. [110] derived the fracture energy of CSL specimens using complex stress intensity factor [111]. Kanerva [112] verified a considerable effect of residual stresses on the fracture toughness of composite-to-metal CLS specimens. They stated that a 3D analysis is required to assess the total fracture energy and mode ratio from hybrid CLS specimens.

Arcan et al. [113] proposed a method for testing fiber reinforced materials under uniform plane-stress conditions. The test fixture allows testing a wide range of mixed-mode set ups as well as the pure modes by means of a simple tensile loading. Jurf and Pipes [114] proposed an adaptation of the method to accommodate a composite specimen containing an embedded interlaminar crack. The same experimental method was applied for the fracture analysis of isotropic materials [115] and wood [116] using the name of compact tension shear (CTS) specimen. Pang [117] determined the fracture toughness of symmetric bonded joints using a similar device. Rikards et al. [118] proposed an

adaptation of the CTS specimen for testing unidirectional composite specimen with a midplane crack. The modified version of Arcan specimen was applied in testing composite delamination [119] and bonded joints with composite or metallic adherends [120]. It has been shown that interfacial fracture toughness increases with the increase of mode II fracture. Additionally, a large scatter was observed in the results of composites materials and an unstable crack growth occurred in all cases.

The end-loaded split (ELS) [121] was developed to evaluate the pure mode II fracture behavior of cracked specimens. In the ELS test, a load is applied at the cracked end while the opposite end is clamped, producing the same curvature in both arms of the specimen. Hashemi et al. [121, 122] applied a variation of the ELS for evaluating the delamination of unidirectional symmetric FRPs under mixed-mode loadings. In the mixed-mode end load split (MMELS) test, an opening load is applied at the cracked end of one arm of the specimen while the opposite end is clamped. The work of Bao et al. [123] showed that the fracture mode ratio changes with the crack length during the MMELS test.

Kinloch et al. [124] proposed a modification to the MMELS test by employing a sliding clamped end. The procedure was recalled as fixed-ratio mixed-mode (FRMM) test as it allows obtaining a constant fracture mode ratio. For symmetrically cracked FRMM tests, the ratio of mode I to mode II loading is approximately constant throughout the test at 4:3. Additionally, they successfully applied the global method to the characterization of unidirectional fiber composites. However, the local singular-field approach [111] failed to predict the fracture mode ratio of FRMM tests. Later on, Choi et al [125] studied the delamination of multidirectional fiber composites using the beam theory with corrections for crack tip rotation and large displacements. Furthermore, Blanco et al [126] showed that the VCCT is able to predict the mode I and mode II fracture for any thickness ratio while the beam theory was capable of modelling only the case of a symmetric crack.

Benzeggagh et al. [127] suggested the cantilever beam opening notch (CBON) test to evaluate the fracture toughness of unidirectional composite materials. The test condition consists of a bending load applied at the upper surface of the uncracked free end while the lower arm is rigidly clamped at the opposite end. The main drawback of the CBON test is that it can only test over a very limited range of the fracture mode ratios.

In addition, the mode ratio varies with the crack length. Another alternative is the imposed displacement cantilever beam (IDCB) [58]. An initial displacement is imposed of the lower arm before loading the specimen. During the test, an opening load is applied at the upper arm while the uncrack end is fixed. The IDCB test is able to test over a wider range of fracture modes. However, the mode ratio also varies with the crack length.

Fernlung and Spelt [128] proposed a testing jig that allows testing over the entire range of mixed-mode fracture of adhesive joints and composite laminates by using a symmetrically cracked specimen. The jig also permits the realization of pure mode tests, namely the DCB for pure mode I and the ENF for pure mode II, thus being versatile in the context of fracture characterization. The fracture mode ratio is independent of the crack length. The Spelt testing jig was also applied by Azari et al. [109] for obtaining the fracture envelope of aluminum and steel bonded joints.

The dual actuator load (DAL) frame is a servo-hydraulic testing machine capable of imposing asymmetric loadings on symmetric bonded specimens [129]. The method has been applied to the fracture characterization of wood [129, 130], steel [131] and composite [132] bonded joints. The method is able to provide a large range of mixed-mode combinations. However, Chaves et al. [133] verified that the fracture mode ratio may change significantly during crack propagation when a constant displacement rate is imposed. To overcome this problem, Panettieri et al. [132] proposed a solution for obtaining a constant fracture ratio based on the force feedback control of the actuator position.

The double cantilever beam with uneven bending moments (DCB-UBM) was proposed by Sorensen et al. [134] for mixed-mode fracture characterization. It requires a special test fixture in order to create uneven bending moments on the two arms of a DCB specimen. Østergaard et al. [135] tested measured the interface fracture toughness of composite sandwich specimens. The DCB-UBM allows testing over the entire range of mixed-mode fracture and the mode ratio is independent of the crack length.

Boyano et al. [136, 137] proposed a modification to the ENF test [49], inserting a roller in the cracked part in order to promote mixed mode in unidirectional composites. The ENF test with an inserted roller (ENFR) allows obtaining a wide range of fracture modes with simple variations concerning the radius or the position of the inserted roller.

The mode ratio changes during crack propagation as a set of values is provided with increasing mode II fracture.

Costa et al. [138] proposed an apparatus for measuring the toughness of metal bonded joints relying exclusively on the load-displacement curve obtained from an universal testing machine and the displacement from two linear variable differential transformers (LVDT) connected to the specimen. It does not require visual crack length measurement, instead deducing the crack length from the displacement obtained from LVDTs.

2.4 Conclusion

This work summarized the current literature on the theories and experimental procedures for the mixed-mode fracture characterization of composites and bonded joints.

A description was provided regarding the most relevant theories for fracture characterization of delamination and debonding. The most applied methods rely on linear elastic fracture mechanics (LEFM). Analytical solutions based on beam theory are obtained for a simple beam-like geometries. Numerical solutions were developed allowing the characterization of more complex geometries and contour conditions. The virtual crack closure technique (VCCT) is the widely applied through the finite element method (FEM) to calculate the fracture energy. Numerical solutions are usually employed to the validation of more straight-forward analytical solutions. Literature reveals the lack of simple and reliable methods for the mixed-mode fracture characterization of bi-material bonded joints. Experimental and analytical solutions are a current object of studies for the mixed-mode fracture characterization of specimens with geometrical and material asymmetry.

The choice of experimental method to examinate the crack propagation depends on several parameters, such as the available equipment, type of materials and the range of fracture modes to be tested. Some testing methods, such as the ADCB and the SLB tests, are shown to be easy and reliable procedures for evaluating the fracture performance of composites and bonded materials. The require simple apparatus that are frequently available to researchers. The main limitation of these methods is the capacity of testing only a single fracture mode ratio from a specimen geometry. A second drawback is the limited range of fracture modes allowed even with geometrical changes. Therefore, these

test methods remain the best choice when a single fracture mode ratio is required and feasible.

It is an important advantage when the testing method allows examining a wide range of mixed-mode fracture ratios with only one simple specimen geometry. This saves considerable effort from the stage of specimens manufacturing. On the other hand, the requirement of a sophisticated apparatus may impose a significant disadvantage to the project. A simple testing jig is usually preferred. In this case, the MMB test method seems to be the most balanced option in terms of range, simplicity and reliability for examining the fracture of a variety of materials under mixed-mode loadings.

References

[1] Sela, N.; Ishai, O. Interlaminar fracture toughness and toughening of laminated composite materials: a review. Compos. 1989, 20(5), 423-435.

[2] Banea, M.D.; da Silva, L.F.M. Adhesively bonded joints in composite materials: An overview. Proc. Inst. Mech. Eng., Part L 2009, 223(1), 1-18.

[3] Budhe, S.; Banea, M.D.; de Barros, S.; da Silva, L.F.M. An updated review of adhesively bonded joints in composite materials. Int. J. Adhes. Adhes. 2017, 72, 30-42.

[4] Mangalgiri, P.D. Composite materials for aerospace applications. Bull. Mater. Sci. 1999, 22(3), 657-664.

[5] Budhe, S.; Banea, M.D.; de Barros, S. Bonded repair of composite structures in aerospace application: a review on environmental issues. Appl. Adhes. Sci. 2018, 6(1), 3.

[6] Katnam, K.B.; da Silva, L.F.M.; Young, T.M. Bonded repair of composite aircraft structures: A review of scientific challenges and opportunities. Prog. Aerosp. Sci. 2013, 61, 26-42.

[7] Taub, A.I.; Krajewski, P.E.; Luo, A.A.; Owens, J.N. The evolution of technology for materials processing over the last 50 years: The automotive example. JOM 2007, 59(2), 48-57.

[8] de Barros, S.; Banea, M.D.; Budhe, S.; De Siqueira, C.E.R.; Lobão, B.S.P.; Souza, L.F.G. Experimental analysis of metal-composite repair of floating offshore units (FPSO). J. Adhes. 2017, 93(1-2), 147-158.

[9] van den Einde, L.; Zhao, L.; Seible, F. Use of FRP composites in civil structural applications. Constr. Build. Mater. 2003, 17(6), 389-403.

[10] Nied, H.F. Mechanics of interface with applications in electronic packaging. IEEE Trans. Device Mater. Reliab. 2003, 3(4), 129-143.
[11] Ripling, E.J.; Mostovoy, S.; Corten, H.T. Fracture Mechanics: A Tool for Evaluating Structural Adhesives. J. Adhes. 1971, 3(2), 107-123.
[12] Williams, J.G. On the calculation of energy release rates for cracked laminates. Int. J. Fract. 1988, 36(2), 101-119.
[13] Rice, J.R. A Path Independent Integral and the Approximate Analysis of Strain Concentration by Notches and Cracks. J. Appl. Mech. 1968, 35(2), 379-386.
[14] Rybicki, E.F.; Kanninen, M.F. A finite element calculation of stress intensity factors by a modified crack closure integral. Eng. Fract. Mech. 1977, 9(4), 931-938.
[15] Pethrick, R.A. Design and ageing of adhesives for structural adhesive bonding – A review. Proc. Inst. Mech. Eng., Part L 2015, 229(5), 349-379.
[16] Viana, G.; Costa, M.; Banea, M.; da Silva, L. A review on the temperature and moisture degradation of adhesive joints. Proc. Inst. Mech. Eng., Part L 2017, 231(5), 488-501.
[17] He, X. A review of finite element analysis of adhesively bonded joints. Int. J. Adhes. Adhes. 2011, 31(4), 248-264.
[18] Chaves, F.J.P.; da Silva, L.F.M.; de Moura, M.F.S.F.; Dillard, D.A.; Esteves, V.H.C. Fracture Mechanics Tests in Adhesively Bonded Joints: A Literature Review. J. Adhes. 2014, 90(12), 955-992.
[19] Williams, J.G. Large Displacement and End Block Effects in the 'DCB' Interlaminar Test in Modes I and II. J. Compos. Mater. 1987, 21(4), 330-347.
[20] Williams, J.G. End corrections for orthotropic DCB specimens. Compos. Sci. Technol. 1989, 35(4), 367-376.
[21] Kanninen, M.F. A dynamic analysis of unstable crack propagation and arrest in the DCB test specimen. Int. J. Fract. 1974, 10(3), 415-430.
[22] Wang, Y.; Williams, J.G. Corrections for mode II fracture toughness specimens of composites materials. Compos. Sci. Technol. 1992, 43(3), 251-256.
[23] Williams, J.G. The fracture mechanics of delamination tests. J. Strain Anal. Eng. Des. 1989, 24(4), 207-214.

[24] Hashemi, S.; Kinloch, A.J.; Williams, J.M.; Ford, H. The analysis of interlaminar fracture in uniaxial fibre-polymer composites. Proc. R. Soc. London, Ser. A 1990, 427(1872), 173-199.
[25] Ducept, F.; Davies, P.; Gamby, D. An experimental study to validate tests used to determine mixed mode failure criteria of glass/epoxy composites. Composites, Part A 1997, 28(8), 719-729.
[26] Ducept, F.; Gamby, D.; Davies, P. A mixed-mode failure criterion derived from tests on symmetric and asymmetric specimens. Compos. Sci. Technol. 1999, 59(4), 609-619.
[27] Conroy, M.; Kinloch, A.J.; Williams, J.G.; Ivankovic, A. Mixed mode partitioning of beam-like geometries: A damage dependent solution. Eng. Fract. Mech. 2015, 149, 351-367.
[28] Álvarez, D.; Guild, F.J.; Kinloch, A.J.; Blackman, B.R.K. Partitioning of mixed-mode fracture in adhesively-bonded joints: experimental studies. Eng. Fract. Mech. 2018, 203, 224-239.
[29] Krueger, R. Virtual crack closure technique: History, approach, and applications. Appl. Mech. Rev. 2004, 57(2), 109-143.
[30] Agrawal, A.; Karlsson, A.M. Obtaining mode mixity for a bimaterial interface crack using the virtual crack closure technique. Int. J. Fract. 2006, 141(1), 75-98.
[31] Pereira, A.B.; de Morais, A.B. Mixed mode I+II interlaminar fracture of carbon/epoxy laminates. Composites, Part A 2008, 39(2), 322-333.
[32] Shahverdi, M.; Vassilopoulos, A.P.; Keller, T. Modeling effects of asymmetry and fiber bridging on Mode I fracture behavior of bonded pultruded composite joints. Eng. Fract. Mech. 2013, 99, 335-348.
[33] Valvo, P.S. A further step towards a physically consistent virtual crack closure technique. Int. J. Fract. 2015, 192(2), 235-244.
[34] Banks-Sills, L.; Farkash, E. A note on the Virtual Crack Closure Technique for a bimaterial interface crack. Int. J. Fract. 2016, 201(2), 171-180.
[35] Davidson, B.D.; Gharibian, S.J.; Yu, L. Evaluation of energy release rate-based approaches for predicting delamination growth in laminated composites. Int. J. Fract. 2000, 105(4), 343-365.

[36] ASTM D5528-13. Standard Test Method for Mode I Interlaminar Fracture Toughness of Unidirectional Fiber-Reinforced Polymer Matrix Composites. ASTM International, 2013.
[37] Xiao, F.; Hui, C.-Y.; Kramer, E.J. Analysis of a mixed mode fracture specimen: the asymmetric double cantilever beam. J. Mater. Sci. 1993, 28(20), 5620-5629.
[38] Sundararaman, V.; Davidson, B.D. An unsymmetric double cantilever beam test for interfacial fracture toughness determination. Int. J. Solids Struct. 1997, 34(7), 799-817.
[39] Mollón, V.; Bonhomme, J.; Viña, J.; Argüelles, A. Theoretical and experimental analysis of carbon epoxy asymmetric dcb specimens to characterize mixed mode fracture toughness. Polym. Test. 2010, 29(6), 766-770.
[40] Hashemi, S.; Kinloch, A.J.; Williams, J.G. Corrections needed in double-cantilever beam tests for assessing the interlaminar failure of fibre-composites. J. Mater. Sci. Lett. 1989, 8(2), 125-129.
[41] Shokrieh, M.M.; Zeinedini, A. A Novel Method for Calculation of Strain Energy Release Rate of Asymmetric Double Cantilever Laminated Composite Beams. Appl. Compos. Mater. 2014, 21(3), 399-415.
[42] Jernkvist, L.O. Fracture of wood under mixed mode loading: I. Derivation of fracture criteria. Eng. Fract. Mech. 2001, 68(5), 549-563.
[43] Jernkvist, L.O. Fracture of wood under mixed mode loading: II. Experimental investigation of Picea abies. Eng. Fract. Mech. 2001, 68(5), 565-576.
[44] Bennati, S.; Colleluori, M.; Corigliano, D.; Valvo, P.S. An enhanced beam-theory model of the asymmetric double cantilever beam (ADCB) test for composite laminates. Compos. Sci. Technol. 2009, 69(11), 1735-1745.
[45] Rizov, V.; Mladensky, A. Elastic–plastic analysis of Asymmetric Double Cantilever Beam specimen. Int. J. Mech. Sci. 2015, 92, 44-51.
[46] Wang, W.; Lopes Fernandes, R.; Teixeira De Freitas, S.; Zarouchas, D.; Benedictus, R. How pure mode I can be obtained in bi-material bonded DCB joints: A longitudinal strain-based criterion. Composites, Part B 2018, 153, 137-148.
[47] Park, S.; Dillard, D.A. Development of a simple mixed-mode fracture test and the resulting fracture energy envelope for an adhesive bond. Int. J. Fract. 2007, 148(3), 261-271.

[48] Blackman, B.R.K.; Hadavinia, H.; Kinloch, A.J.; Paraschi, M.; Williams, J.G. The calculation of adhesive fracture energies in mode I: revisiting the tapered double cantilever beam (TDCB) test. Eng. Fract. Mech. 2003, 70(2), 233-248.

[49] Carlsson, L.A.; Gillespie, J.W.; Pipes, R.B. On the Analysis and Design of the End Notched Flexure (ENF) Specimen for Mode II Testing. J. Compos. Mater. 1986, 20(6), 594-604.

[50] Mollón, V.; Bonhomme, J.; Argüelles, A.; Viña, J. Influence of the crack plane asymmetry over G_{II} results in carbon epoxy ENF specimens. Compos. Struct. 2012, 94(3), 1187-1191.

[51] Russell, A.J.; Street, K.N. Moisture and Temperature Effects on the Mixed-Mode Delamination Fracture of Unidirectional Graphite/Epoxy. Delamination and Debonding of Materials, 349-370, ASTM International, 1985.

[52] Yoon, S.H.; Hong, C.S. Modified end notched flexure specimen for mixed mode interlaminar fracture in laminated composites. Int. J. Fract. 1990, 43(1), R3-R9.

[53] Davidson, B.D.; Sundararaman, V. A single leg bending test for interfacial fracture toughness determination. Int. J. Fract. 1996, 78(2), 193-210.

[54] Albertsen, H.; Ivens, J.; Peters, P.; Wevers, M.; Verpoest, I. Interlaminar fracture toughness of CFRP influenced by fibre surface treatment: Part 1. Experimental results. Compos. Sci. Technol. 1995, 54(2), 133-145.

[55] Rikards, R.; Buchholz, F.G.; Bledzki, A.K.; Wacker, G.; Korjakin, A. Mode I, mode II, and mixed-mode I/II interlaminar fracture toughness of GFRP influenced by fiber surface treatment. Mech. Compos. Mater. 1996, 32(5), 439-462.

[56] Davidson, B.D.; Krüger, R.; König, M. Three-dimensional analysis of center-delaminated unidirectional and multidirectional single-leg bending specimens. Compos. Sci. Technol. 1995, 54(4), 385-394.

[57] Davidson, B.D.; Bansal, A.; Qida, B.; Xuekun, S. Geometrically Nonlinear Determination of Energy Release Rate and Mode Ratio in Single Leg Bending Tests. J. Reinf. Plast. Compos. 2008, 28(15), 1881-1901.

[58] Gong, X.J.; Benzeggagh, M. Mixed Mode Interlaminar Fracture Toughness of Unidirectional Glass/Epoxy Composite. Compos. Mat. Fatigue Fract. 100-123, ASTM International, 1995.

[59] Lee, M.J.; Kim, W.S.; Jang, C.J.; Kim, K.H.; Cho, T.M.; Lee, B.C.; Lee, J.J. Analysis and Simulation of the Failure Characteristic of a Single Leg Bending Joint with a Micro-Patterned Surface. J. Adhes. 2011, 87(7-8), 826-841.
[60] Szekrényes, A.; Uj, J. Beam and finite element analysis of quasi-unidirectional composite SLB and ELS specimens. Compos. Sci. Technol. 2004, 64(15), 2393-2406.
[61] Oliveira, J.M.Q.; de Moura, M.F.S.F.; Morais, J.J.L. Application of the end loaded split and single-leg bending tests to the mixed-mode fracture characterization of wood. 2009, 63(5), 597-602.
[62] Pereira, F.A.; de Moura, M.F.; Dourado, N.; Morais, J.J.; Dias, M.I. Bone fracture characterization under mixed-mode I+II loading using the single leg bending test. Biomech. Model. Mechanobiol. 2014, 13(6), 1331-1339.
[63] Silva, F.G.A.; de Moura, M.F.S.F.; Dourado, N.; Xavier, J.; Pereira, F.A.M.; Morais, J.J.L.; Dias, M.I.R. Mixed-mode I+II fracture characterization of human cortical bone using the Single Leg Bending test. J. Mech. Behav. Biomed. Mater. 2016, 54, 72-81.
[64] de Moura, M.F.S.F.; Cavaleiro, P.M.L.C.; Silva, F.G.A.; Dourado, N. Mixed-mode I+II fracture characterization of a hybrid carbon-epoxy/cork laminate using the Single-Leg Bending test. Compos. Sci. Technol. 2017, 141, 24-31.
[65] Reis, J.P.; de Moura, M.F.S.F.; Moreira, R.D.F.; Silva, F.G.A. Mixed mode I + II interlaminar fracture characterization of carbon-fibre reinforced polyamide composite using the Single-Leg Bending test. Mater. Today Commun. 2019, 19, 476-481.
[66] Tracy, G.D.; Feraboli, P.; Kedward, K.T. A new mixed mode test for carbon/epoxy composite systems. Composites, Part A 2003, 34(11), 1125-1131.
[67] Davidson, B.D.; Bansal, A.; Bing, Q.; Sun, X. Linear and nonlinear finite element analyses of unidirectional, symmetric single leg four-point bending tests. Eng. Fract. Mech. 2008, 75(8), 2130-2143.
[68] Szekrényes, A.; UJ, J. Over-leg Bending Test for Mixed-mode I/II Interlaminar Fracture in Composite Laminates. Int. J. Damage Mech. 2007, 16(1), 5-33.
[69] Liu, P.F.; Yang, J.; Wang, B.; Zhou, Z.F.; Zheng, J.Y. A Study on the Intralaminar Damage and Interlaminar Delamination of Carbon Fiber Composite Laminates Under Three-Point Bending Using Acoustic Emission. J. Failure Anal. Prev. 2015, 15(1), 101-121.

[70] Reeder, J.R.; Crews Jr., J.H. Mixed-mode bending method for delamination testing. AIAA J. 1990, 28(7), 1270-1276.
[71] Reeder, J.R.; Crews Jr, J.H. Redesign of the Mixed-Mode Bending Delamination Test to Reduce Nonlinear Effects. J. Compos. Technol. Res. 1992, 14(1), 12-19.
[72] Reeder, J.R. A Bilinear Failure Criterion for Mixed-Mode Delamination. Compos. Mater. Test. Des. 1993, 11, 303-322.
[73] Chen, J.H.; Sernow, R.; Schulz, E.; Hinrichsen, G. A modification of the mixed-mode bending test apparatus. Composites, Part A 1999, 30(7), 871-877.
[74] Benzeggagh, M.L.; Kenane, M. Measurement of mixed-mode delamination fracture toughness of unidirectional glass/epoxy composites with mixed-mode bending apparatus. Compos. Sci. Technol. 1996, 56(4), 439-449.
[75] Arouche, M.M.; Wang, W.; Teixeira de Freitas, S.; de Barros, S. Strain-based methodology for mixed-mode I+II fracture: A new partitioning method for bi-material adhesively bonded joints. J. Adhes. 2019, 95(5-7), 385-404.
[76] Bhashyam, S.; Davidson, B.D. Evaluation of Data Reduction Methods for the Mixed Mode Bending Test. AIAA J. 1997, 35(3), 546-552.
[77] Martin, R.H.; Hansen, P.L. Experimental Compliance Calibration for the Mixed-Mode Bending (MMB) Specimen. Compos. Mater. Fatigue Fract. 1997, 6, 305-323.
[78] Ducept, F.; Davies, P.; Gamby, D. Mixed mode failure criteria for a glass/epoxy composite and an adhesively bonded composite/composite joint. Int. J. Adhes. Adhes. 2000, 20(3), 233-244.
[79] Reeder, J.R. Refinements to the Mixed-Mode Bending Test for Delamination Toughness. J. Compos. Technol. Res. 2003, 25(4), 1-5.
[80] Reeder, J.R. (2003). A Criterion to Control Nonlinear Error in the Mixed-Mode Bending Test. Compos. Mater. Test. Des. 2003, 14, 349-371.
[81] Blanco, N.; Turon, A.; Costa, J. An exact solution for the determination of the mode mixture in the mixed-mode bending delamination test. Compos. Sci. Technol. 2006, 66(10), 1256-1258.
[82] ASTM D6671-19. Standard Test Method for Mixed Mode I-Mode II Interlaminar Fracture Toughness of Unidirectional Fiber Reinforced Polymer Matrix Composites ASTM International, 2019.

[83] de Morais, A.B.; Pereira, A.B. Mixed mode I+II interlaminar fracture of glass/epoxy multidirectional laminates – Part 1: Analysis. Compos. Sci. Technol. 2006, 66(13), 1889-1895.
[84] Pereira, A.B.; de Morais, A.B. Mixed mode I+II interlaminar fracture of glass/epoxy multidirectional laminates – Part 2: Experiments. Compos. Sci. Technol. 2006, 66(13), 1896-1902.
[85] Sarrado, C.; Turon, A.; Renart, J.; Costa, J. An experimental data reduction method for the Mixed Mode Bending test based on the J-integral approach. Compos. Sci. Technol. 2015, 117, 85-91.
[86] Floros, I.S.; Tserpes, K.I.; Löbel, T. Mode-I, mode-II and mixed-mode I+II fracture behavior of composite bonded joints: Experimental characterization and numerical simulation. Composites, Part B 2015, 78, 459-468.
[87] Kim, B.W.; Mayer, A.H. Influence of fiber direction and mixed-mode ratio on delamination fracture toughness of carbon/epoxy laminates. Compos. Sci. Technol. 2003, 63(5), 695-713.
[88] Shahverdi, M.; Vassilopoulos, A.P.; Keller, T. Mixed-Mode I/II fracture behavior of asymmetric adhesively-bonded pultruded composite joints. Eng. Fract. Mech. 2014, 115, 43-59.
[89] Shahverdi, M.; Vassilopoulos, A.P.; Keller, T. Mixed-mode quasi-static failure criteria for adhesively-bonded pultruded GFRP joints. Composites, Part A 2014, 59, 45-56.
[90] Ševčík, M.; Shahverdi, M.; Hutař, P.; Vassilopoulos, A.P. Analytical modeling of mixed-Mode bending behavior of asymmetric adhesively bonded pultruded GFRP joints. Eng. Fract. Mech. 2015, 147, 228-242.
[91] Oliveira, J.M.Q.; de Moura, M.F.S.F.; Silva, M.A.L.; Morais, J.J.L. Numerical analysis of the MMB test for mixed-mode I/II wood fracture. Compos. Sci. Technol. 2007, 67(9), 1764-1771.
[92] de Moura, M.F.S.F.; Oliveira, J.M.Q.; Morais, J.J.L.; Xavier, J. Mixed-mode I/II wood fracture characterization using the mixed-mode bending test. Eng. Fract. Mech. 2010, 77(1), 144-152.

[93] de Moura, M.F.S.F.; Oliveira, J.M.Q.; Morais, J.J.L.; Dourado, N. Mixed-mode (I+II) fracture characterization of wood bonded joints. Constr. Build. Mater. 2011, 25(4), 1956-1962.

[94] Yoshihara, H. Initiation and propagation fracture toughness of solid wood under the mixed Mode I/II condition examined by mixed-mode bending test. Eng. Fract. Mech. 2013, 104, 1-15.

[95] Pereira, F.A.M.; de Moura, M.F.S.F.; Dourado, N.; Morais, J.J.L.; Silva, F.G.A.; Dias, M.I.R. Bone fracture characterization under mixed-mode I+II loading using the MMB test. Eng. Fract. Mech. 2016, 166, 151-163.

[96] Liu, Z.; Gibson, R.F.; Newaz, G.M. The Use of a Modified Mixed Mode Bending Test for Characterization of Mixed-mode Fracture Behavior of Adhesively Bonded Metal Joints. J. Adhes. 2002, 78(3), 223-244.

[97] Ben Salem, N.; Jumel, J.; Budzik, M.K.; Shanahan, M.E.R.; Lavelle, F. Analytical and experimental investigations of crack propagation in adhesively bonded joints with the Mixed Mode Bending (MMB) test Part II: Investigation of cohesive stresses distribution with backface strain monitoring. Theor. Appl. Fract. Mech. 2014, 74, 222-232.

[98] Ben Salem, N.; Jumel, J.; Budzik, M.K.; Shanahan, M.E.R.; Lavelle, F. Analytical and experimental investigations of crack propagation in adhesively bonded joints with the Mixed Mode Bending (MMB) test Part I: Macroscopic analysis & Digital Image Correlation measurements. Theor. Appl. Fract. Mech. 2014, 74, 209-221.

[99] Stamoulis, G.; Carrere, N.; Cognard, J.Y.; Davies, P.; Badulescu, C. On the experimental mixed-mode failure of adhesively bonded metallic joints. Int. J. Adhes. Adhes. 2014, 51, 148-158.

[100] Droubi, M.G.; McAfee, J.; Horne, R.C.; Walker, S.; Klaassen, C.; Crawford, A.; Prathuru, A.K.; Faisal, N.H. Mixed-mode fracture characteristics of metal-to-metal adhesively bonded joints: experimental and simulation methods. Procedia Struct. Integr. 2017, 5, 40-47.

[101] Soboyejo, W.O.; Lu, G.-Y.; Chengalva, S.; Zhang, J.; Kenner, V. A modified mixed-mode bending specimen for the interfacial fracture testing of dissimilar materials. Fatigue Fract. Eng. Mater. Struct. 1999, 22(9), 799-810.

[102] Quispitupa, A.; Berggreen, C.; Carlsson, L.A. On the analysis of a mixed mode bending sandwich specimen for debond fracture characterization. Eng. Fract. Mech. 2009, 76(4), 594-613.
[103] Quispitupa, A.; Berggreen, C.; Carlsson, L.A. Design Analysis of the Mixed Mode Bending Sandwich Specimen. J. Sandwich Struct. Mater. 2010, 12(2), 253-272.
[104] Quispitupa, A.; Berggreen, C.; Carlsson, L.A. Face/core interface fracture characterization of mixed mode bending sandwich specimens. Fatigue Fract. Eng. Mater. Struct. 2011, 34(11), 839-853.
[105] Brussat, T.R.; Chiu, S.T.; Mostovoy, S. Fracture Mechanics for Structural Adhesive Bonds - Final Report. Wright-Patterson Air Force Base, Ohio, 1977.
[106] Edde, F.; Verreman, Y. On the fracture parameters in a clamped cracked lap shear adhesive joint. Int. J. Adhes. Adhes. 1992, 12(1), 43-48.
[107] Rhee, K.Y. Characterization of delamination behavior of unidirectional graphite/PEEK laminates using cracked lap shear (CLS) specimens. Compos. Struct. 1994, 29(4), 379-382.
[108] Rhee, K.Y.; Chi, C.H. Determination of Fracture Toughness, GC of Graphite/Epoxy Composites from a Cracked Lap Shear (CLS) Specimen. J. Compos. Mater. 2001, 35(1), 77-93.
[109] Azari, S.; Eskandarian, M.; Papini, M.; Schroeder, J.A.; Spelt, J.K. Fracture load predictions and measurements for highly toughened epoxy adhesive joints. Eng. Fract. Mech. 2009, 76(13), 2039-2055.
[110] Lai, Y.-H.; Dwayne Rakestraw, M.; Dillard, D.A. The cracked lap shear specimen revisited—a closed form solution. Int. J. Solids Struct. 1996, 33(12), 1725-1743.
[111] Suo, Z.; Hutchinson, J.W. Interface crack between two elastic layers. Int. J. Fract. 1990, 43(1), 1-18.
[112] Jokinen, J.; Kanerva, M. Analysis of cracked lap shear testing of tungsten-CFRP hybrid laminates. Eng. Fract. Mech. 2017, 175, 184-200.
[113] Arcan, M.; Hashin, Z.; Voloshin, A. A method to produce uniform plane-stress states with applications to fiber-reinforced materials. Exp. Mech. 1978, 18(4), 141-146.
[114] Jurf, R.A.; Pipes, R.B. Interlaminar Fracture of Composite Materials. J. Compos. Mater. 1982, 16(5), 386-394.

[115] Richard, H.A.; Benitz, K. A loading device for the creation of mixed mode in fracture mechanics. Int. J. Fract. 1983, 22(2), R55-R58.
[116] Valentin, G.; Caumes, P. Crack propagation in mixed mode in wood: a new specimen. Wood Sci. Technol. 1989, 23(1), 43-53.
[117] Pang, H.L.J. Mixed mode fracture analysis and toughness of adhesive joints. Eng. Fract. Mech. 1995, 51(4), 575-583.
[118] Rikards, R.; Buchholz, F.G.; Wang, H.; Bledzki, A.K.; Korjakin, A.; Richard, H.A. Investigation of mixed mode I/II interlaminar fracture toughness of laminated composites by using a CTS type specimen. Eng. Fract. Mech. 1998, 61(3), 325-342.
[119] Choupani, N. Experimental and numerical investigation of the mixed-mode delamination in Arcan laminated specimens. Mater. Sci. Eng., A 2008, 478(1), 229-242.
[120] Choupani, N. Interfacial mixed-mode fracture characterization of adhesively bonded joints. Int. J. Adhes. Adhes. 2008, 28(6), 267-282.
[121] Hashemi, S.; Kinloch, A.J.; Williams, J.G. The Effects of Geometry, Rate and Temperature on the Mode I, Mode II and Mixed-Mode I/II Interlaminar Fracture of Carbon-Fibre/Poly(ether-ether ketone) Composites. J. Compos. Mater. 1990, 24(9), 918-956.
[122] Hashemi, S.; Kinloch, A.J.; Williams, J.G. Mechanics and mechanisms of delamination in a poly(ether sulphone)—Fibre composite. Compos. Sci. Technol. 1990, 37(4), 429-462.
[123] Bao, G.; Ho, S.; Suo, Z.; Fan, B. The role of material orthotropy in fracture specimens for composites. Int. J. Solids Struct. 1992, 29(9), 1105-1116.
[124] Kinloch, A.J.; Wang, Y.; Williams, J.G.; Yayla, P. The mixed-mode delamination of fibre composite materials. Compos. Sci. Technol. 1993, 47(3), 225-237.
[125] Choi, N.S.; Kinloch, A.J.; Williams, J.G. Delamination Fracture of Multidirectional Carbon-Fiber/Epoxy Composites under Mode I, Mode II and Mixed-Mode I/II Loading. J. Compos. Mater. 1999, 33(1), 73-100.
[126] Blanco, N.; Gamstedt, E.K.; Costa, J.; Trias, D. Analysis of the mixed-mode end load split delamination test. Compos. Struct. 2006, 76(1), 14-20.
[127] Benzeggagh, M.L.; Davies, P.; Gong, X.J.; Roelandt, J.M.; Mourin, M.; Prel, Y.J. A mixed mode specimen for interlaminar fracture testing. Compos. Sci. Technol. 1989, 34(2), 129-143.

[128] Fernlund, G.; Spelt, J.K. Mixed-mode fracture characterization of adhesive joints. Compos. Sci. Technol. 1994, 50(4), 441-449.
[129] Singh, H.K.; Chakraborty, A.; Frazier, C.E.; Dillard, D.A. Mixed mode fracture testing of adhesively bonded wood specimens using a dual actuator load frame. Holzforschung 2010, 64(3), 353-361.
[130] Nicoli, E.; Dillard David, A.; Frazier Charles, E.; Zink-Sharp, A. Characterization of mixed-mode I/II fracture properties of adhesively bonded yellow-poplar by a dual actuator test frame instrument Holzforschung 2012, 66, 623-631.
[131] Chaves, F.J.P.; de Moura, M.F.S.F.; da Silva, L.F.M.; Dillard, D.A. Fracture characterization of bonded joints using the dual actuator load apparatus. J. Adhes. Sci. Technol. 2014, 28(5), 512-524.
[132] Panettieri, E.; Leclerc, G.; Jumel, J.; Guitard, J. Mixed-mode crack propagation tests of composite bonded joints using a dual-actuator load frame – Constant and variable G_{II}/G_I conditions. Eng. Fract. Mech. 2018, 202, 471-486.
[133] Chaves, F.J.P.; de Moura, M.F.S.F.; da Silva, L.F.M.; Dillard, D.A. Numerical analysis of the dual actuator load test applied to fracture characterization of bonded joints. Int. J. Solids Struct. 2011, 48(10), 1572-1578.
[134] Sørensen, B.F.; Jørgensen, K.; Jacobsen, T.K.; Østergaard, R.C. DCB-specimen loaded with uneven bending moments. Int. J. Fract. 2006, 141(1), 163-176.
[135] Østergaard, R.C.; Sørensen, B.F.; Brøndsted, P. Measurement of Interface Fracture Toughness of Sandwich Structures under Mixed Mode Loadings. J. Sandwich Struct. Mater. 2007, 9(5), 445-466.
[136] Boyano, A.; Mollón, V.; Bonhomme, J.; De Gracia, J.; Arrese, A.; Mujika, F. Analytical and numerical approach of an End Notched Flexure test configuration with an inserted roller for promoting mixed mode I/II. Eng. Fract. Mech. 2015, 143, 63-79.
[137] Boyano, A.; De Gracia, J.; Arrese, A.; Mujika, F. Experimental assessment of an End Notched Flexure test configuration with an inserted roller for analyzing mixed-mode I/II fracture toughness. Eng. Fract. Mech. 2016, 163, 462-475.
[138] Costa, M.; Carbas, R.; Marques, E.; Viana, G.; da Silva, L.F.M. An apparatus for mixed-mode fracture characterization of adhesive joints. Theor. Appl. Fract. Mech. 2017, 91, 94-102.

Chapter 3

The Strain-Based Methodology

The dissemination of composite materials introduces applications of hybrid structures with composite and metal parts. The development of reliable methodologies to evaluate the performance of these structures is required. In this Chapter, the mixed-mode fracture behavior of a bi-material adhesively bonded joint is investigated. A new strain-based criterion for the design of the mixed-mode bending (MMB) bi-material specimen is suggested. A new analytical partitioning method, based on beam analysis, is proposed and tested on a composite-to-metal bonded joint and compared with a finite element model using the virtual crack closure technique (VCCT). The results show that the proposed strain-based design methodology can be successfully used in MMB test for bi-material joints. The fracture mode partitioning is accurately predicted by the strain-based partitioning method (SBM). However, the total fracture energy predicted by the analytical method can be inaccurate due to a significant effect of transverse shear in thick specimens.

Keywords: fracture mechanics, fracture toughness, mixed-mode fracture, MMB test, strain-based partitioning method (SBM), bi-material bonded joints, finite element analysis.

This chapter is based on the journal article: "Strain-based methodology for mixed-mode I+II fracture: A new partitioning method for bi-material adhesively bonded joints", published in The Journal of Adhesion 95(5-7):385-404 (2019).

3.1 Introduction

In recent years, composite materials have become widely used in structural applications. This technology has been developed in aerospace industry [1] and disseminated to numerous fields, such as automotive [2], marine [3] and construction [4]. Fiber-reinforced polymers (FRPs) are most commonly applied due to their high strength-to-weight ratio. The dissemination of these materials introduces applications of hybrid structures with composite and metal parts [5]. Adhesive bonding is the most efficient technology in terms of weight and performance to join these two materials. The advent of composite-to-metal bonded joints requires the development of reliable methodologies to evaluate the performance of these structures [6-8].

Fracture mechanics is an important instrument to improve the design and performance of adhesively bonded structures. Imperfections present within materials are points of stress concentration and therefore fracture initiation. Fracture mechanics models the defect as a crack and evaluates if its size overcome the critical fracture size leading to structural failure. The strain energy release rate (SERR) is the most important property to consider in the calculation of fracture toughness of cracked structures. The crack propagation occurs when the available energy at the crack tip (G) exceeds the critical energy for crack propagation (G_c) [9]. In-service structures are commonly subjected to a combination of peeling and shear stresses. This means that a combination of modes I and II loadings occur at the crack tip.

A variety of mixed-mode fracture test methods has been developed for evaluation of the mixed-mode (I+II) fracture toughness. The crack lap shear (CLS) test [10] has been widely used for characterization of the fracture toughness of adhesively bonded joints. The asymmetric double cantilever beam (ADCB) test [11] was suggested from a generalization of the DCB test using a specimen with asymmetric arms. The single-leg bending (SLB) test [12] has proposed as a three-point bending test with one extremity supported only by the specimen upper arm. However, these test methods have a limited range of mode-mixities with small contribution of mode II. Different mixed mode ratios can only be obtained by changing the thickness ratios of the upper and lower arms, which requires the manufacture of specimens with different geometries.

Several mixed-mode fracture test methods have been proposed for the characterization of a wide range of mode-mixities [13-18]. Some of these works are

adaptations of pure mode test methods [13-15]. Other authors developed testing jigs that induce a combination of opening and shear loadings to the specimen [16-18]. Among them, the mixed-mode bending (MMB) test [17] stands out for its easy implementation, reliability and capability of testing a wide range of mode-mixities with only one specimen geometry.

The MMB test method was originally developed for evaluation of delamination in unidirectional composites [19-20]. A number of authors evaluated symmetric and asymmetric delamination of multidirectional composites [21-23]. A recent work addressed the fracture toughness in dissimilar composite bonded joints [24]. Few works addressed mixed-mode fracture of metal bonded joints [25-27]. They show that the MMB test presented a difficulty due to extensive adherend yielding. Tests with wood bonded joints [28-30] and bone fracture [31] can also be found in the literature. However, no work is available on mixed-mode fracture of composite-to-metal bonded joints.

The linear elastic fracture behavior of a bonded joint can be predicted using finite element analysis. A number of formulations are available in literature for mixed-mode failure of bonded joints [32-33]. Among them, the virtual crack closure technique (VCCT) is widely applied and commonly available in most of the commercial softwares of finite element analysis. The VCCT is based on the assumption that the energy released when the crack is extended a crack tip element size is identical to the energy required to close the crack in the same length. This is an accurate method for calculation of the fracture energy at the crack tip in homogenous materials [33]. However, when the crack is located in a bi-material interface, the mode partitioning become sensitive to the crack extension length [34]. One method proposed by literature to circumvent this problem is the introduction of an interlayer between the crack interface and placing the crack within it [23-24]. The crack propagation occurs within a homogeneous path where the mode partition is not sensitive to the crack length.

In this Chapter, the mixed-mode fracture behavior of a bi-material adhesively bonded joint is investigated. The aim is to propose and evaluate a new strain-based criterion for the design of MMB bi-material specimens and a new analytical partitioning method to characterize their fracture behavior under mixed-mode loadings. A composite-to-metal adhesively bonded joint is used as a case study to evaluate the proposed method.

3.2 Analytical model for bi-material bonded joints

The strain energy release rate of a cracked material can be defined as [35]:

$$G = \frac{1}{B}\left(\frac{dU_e}{da} - \frac{dU_s}{da}\right) \tag{3.1}$$

Where B is the specimen width, a is the crack length, U_e is the external work and U_s is the strain energy. The formulation for the total fracture (G) is then obtained for linear elastic material behavior [36]:

$$G = \frac{1}{2B}\left(\frac{M_1^2}{E_1 I_1} + \frac{M_2^2}{E_2 I_2} - \frac{(M_1 + M_2)^2}{E_{eq} I_{eq}}\right) \tag{3.2}$$

Where E_1, I_1, E_2, I_2, E_{eq} and I_{eq} are the flexural longitudinal moduli and second moments of area in the section of the crack tip of the upper arm, lower arm and beam, respectively. M_1 and M_2 are the bending moments on the section of the crack tip in the upper and lower arms, respectively. This equation is valid for a crack propagation along a defined path between two arms under bending moments, as shown in Figure 3.1.

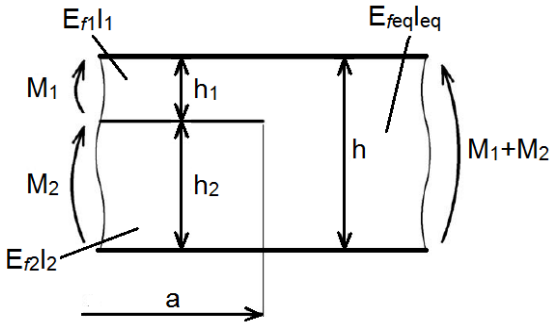


Figure 3.1: Crack propagation parameters.

Regarding the MMB test, mixed-mode fracture is induced by opening and shear loadings applied to the specimen. A schematic of the MMB test set-up is shown in Figure 3.2.

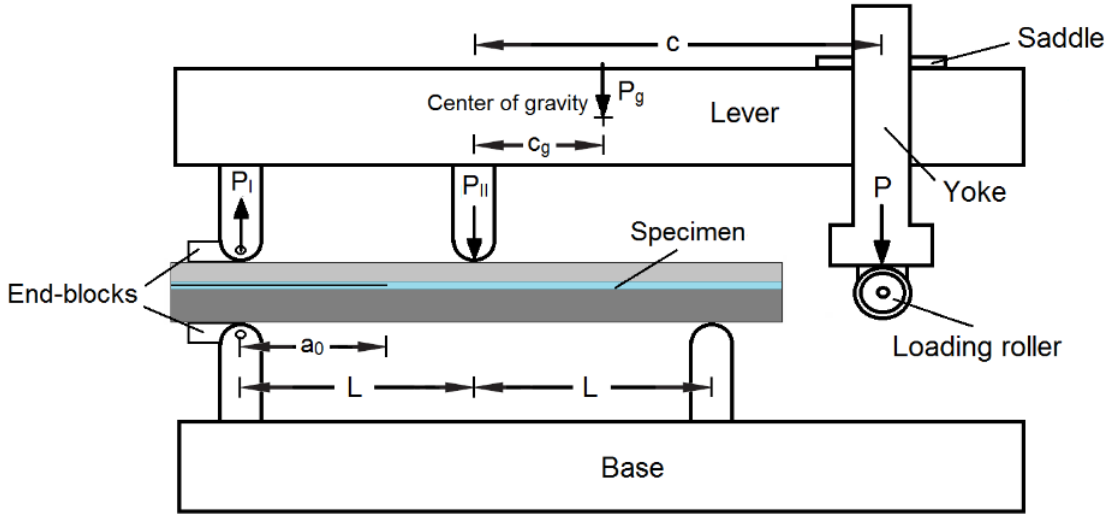


Figure 3.2: Schematic of the MMB test.

Where L is the half-span, P is the test load, c is the lever length, P_g is the lever weight, and c_g is the distance of the lever center of gravity. The resulting bending moments are:

$$M_1 = \frac{Pc + P_g c_g}{L} a \tag{3.3}$$

$$M_2 = \frac{P(L - c) + P_g(L - c_g)}{2L} a \tag{3.4}$$

The total fracture energy of a MMB test can be obtained by replacing Equations (3.3) and (3.4) in Equation (3.2). However, it is essential to distinguish the contribution of mode I and mode II fracture in order to characterize the mixed mode fracture behavior of the structure.

Literature suggests different methods for the partitioning of mixed-mode fracture [37]. The so-called ‘global method’, proposed by Williams [35] was one of the earliest analytical methods that successfully identified the pure modes fracture and mixed-mode partition of specimens under bending moments. Williams partitioning method (WM) is based on the following two assumptions for the fracture mode separations:

(i) pure mode I exists when opposite moments act on the joint arms, i.e. $M_1 = M_I$ and $M_2 = -M_I$;
(ii) pure mode II is obtained when the curvatures of the two arms are the same, i.e. $M_1 = M_{II}$ and $M_2 = \psi M_{II}$, where ψ is defined as the bending stiffness ratio of upper and lower arms, as:

$$\psi = \frac{E_2 I_2}{E_1 I_1} \tag{3.5}$$

Based on these two assumptions, one can obtain:

$$M_1 = M_{II} - M_I \tag{3.6}$$

$$M_2 = \psi M_{II} + M_I \tag{3.7}$$

Substituting (3.6) and (3.7) in (3.2), the fracture energy can be partitioned in mode I, when $M_{II} = 0$, and mode II, when $M_I = 0$. G_I and G_{II} are then given by:

$$G_I = \frac{(\psi M_1 - M_2)^2}{2B(\psi + 1)^2}\left(\frac{1}{E_1 I_1} + \frac{1}{E_2 I_2}\right) \tag{3.8}$$

$$G_{II} = \frac{(M_1 + M_2)^2}{2B(\psi + 1)}\left(\frac{1}{E_1 I_1} - \frac{(\psi + 1)}{E_{eq} I_{eq}}\right) \tag{3.9}$$

Similar formulations for delamination of composite materials can be found in the literature [20, 24]. However, WM is only able to give the correct partition of symmetric specimens and is limited on the prediction of fracture behavior in asymmetric geometries and materials [37].

A recent study [38] has proven that in the case of bi-material bonded joints, i.e., arms of different material, simply guaranteeing opposite moments, as assumed by the global method, i.e. $M_1 = M_I$ and $M_2 = -M_I$, is not sufficient to guarantee pure mode I and introduces a certain amount of mode II fracture. That same study proves that to assure pure mode I in bi-material bonded joints, the longitudinal strain distribution at the faying

surfaces of both arms must be identical. Therefore, the assumption of pure mode I is replaced by:

(i) i.e. $M_1 = M_I$ and $M_2 = -\beta M_I$, where β is the longitudinal strain ratio of upper and lower arms, defined by:

$$\beta = \frac{E_2 h_2^2}{E_1 h_1^2} \tag{3.10}$$

Based on the new assumption for pure mode I and preserving the assumption of pure mode II, one can obtain:

$$M_1 = M_{II} - M_I \tag{3.11}$$

$$M_2 = \psi M_{II} + \beta M_I \tag{3.12}$$

The strain equivalence between arms assures pure mode I fracture while pure mode II is obtained when the curvatures of the two arms are the same. When the strain-based design equivalence geometry is adopted for the design of the MMB specimens, i.e., the arms of bi-material bonded joint geometry are chosen such as $E_2 h_2^2 = E_1 h_1^2$ (β = 1), equations (3.11) and (3.12) reduce to (3.6) and (3.7) and the fracture mode partitioning is obtained from Equations (3.8) and (3.9).

3.3 Experimental procedures

In order to test the proposed methodology, a test campaign has been conducted in which MMB tests were performed in composite-to-metal bonded joints. The geometry of the joint was designed to satisfy the criterion of strain equivalence (β = 1).

3.3.1 Materials and specimens

Composite-to-metal test specimens were manufactured. A 6.35 mm thickness (h_1) carbon steel plate (σ_y = 250 MPa) was taken as metal adherend. Carbon fiber fabrics with a nominal area weight of 424 g/m^2 (LTC450-C10-C, DEVOLD AMT, Langevåg, Norway) were selected to make the composite adherend. Each fabric is composed of two

orthogonal plies of unidirectional fibers. An epoxy resin (PIPEFIX, Novatec, Rio de Janeiro, Brazil) was chosen as impregnation resin of the composite. The adhesive material is an epoxy (NVT201E, Novatec, Rio de Janeiro, Brazil). Mechanical properties of the materials are shown in Table 3.1. The mechanical properties of the materials were obtained from a previous work [39].

Table 3.1: Mechanical properties of the materials.

Material	**Elastic Modulus, E_{11} (GPa)**	**Poisson's Ratio, ν_{12}**
Steel	200	0.27
Composite 0/90	46	0.24
Adhesive	2.25	0.38

The manufacturing process tried to mimic as much as possible the application of composite patch repairs in oil and gas production platforms [40]. Surface preparation of the steel plate was achieved with grit blasting of G-40 steel grit and degreasing with acetone. An anti-friction material was applied over the steel surface to produce the pre-crack. The adhesive was then applied over the treated steel surface. One layer of glass fiber dry chopped strand mat with a density of 300 g/m^2 was applied to avoid direct contact between carbon fibers and metal. Then, the hand lay-up process started by alternating application of carbon fiber fabrics layers and the impregnation resin. Finally, a layer of peel ply was applied over the last composite ply in order to produce a smoother outer surface. The number of composite plies was determined in order to comply with the strain-based design criterion ($\beta = 1$). The final lay-up consisted of a $[0/90]_{20}$ carbon fiber reinforced polymer (CFRP). The curing process was performed at room temperature for 2 hours.

A CFRP-to-steel plate was manufactured (180 x 400 mm) with total thickness (h) of 20.3±0.7 mm and cut to specimens of 180±1 mm length and 25±1 mm width (B). Measurements were obtained with a digital caliper from three different regions: 30 mm from the sides and at the half-length of the specimens. Finally, aluminum end-blocks (25 x 15 x 7 mm) were bonded to the specimens using an epoxy adhesive, producing a initial crack length (a_0). Specimen geometry and boundary conditions are shown in Figure 3.3.

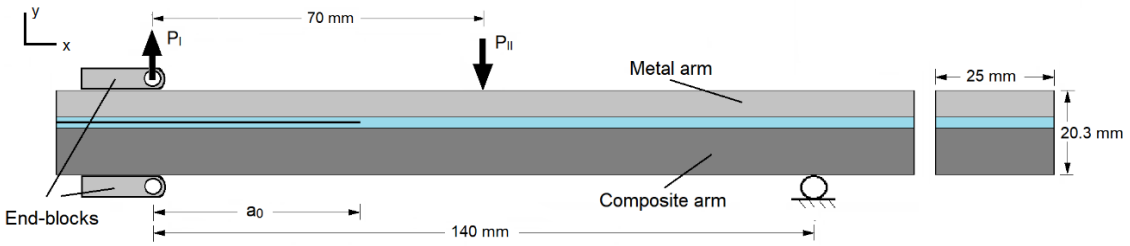


Figure 3.3: Specimen geometry and boundary conditions.

3.3.2 Test set-up

In the MMB test, a load (P) is applied by the yoke on the loading rollers attached to the lever and loaded just above the mid-plane of the test specimen. The lever applies the opening (P_I) and shear (P_{II}) loadings on the specimen in a ratio defined by the lever length (c). The contribution of shear loading increases when the lever length is reduced. A typical MMB test apparatus [41] was used in the test, as shown in Figure 3.4. The lever weight (P_g) is 17.3 N. The test set-up was chosen to have the steel arm on top in order to avoid crack migration to the composite layers.

The side of the specimens was coated with a water-based correction fluid and millimeter paper was placed for crack length measurements. A high-resolution camera system was positioned to take photos of the crack side. Crack propagation points were acquired from the photos. Strains gauges were used in order to measure the longitudinal strain. Six strain gauges (KFG-5-120-C1-11, Kyowa Electronic Instruments, Tokyo, Japan) were glued at the free surfaces of the specimen (four on the steel adherend and two on the composite adherend). Tests were performed in a servo-hydraulic testing machine (MTS 831, MTS Systems Corporation) coupled with a 10 kN load cell. The procedure was configured for a constant displacement of 0.5 mm/min.

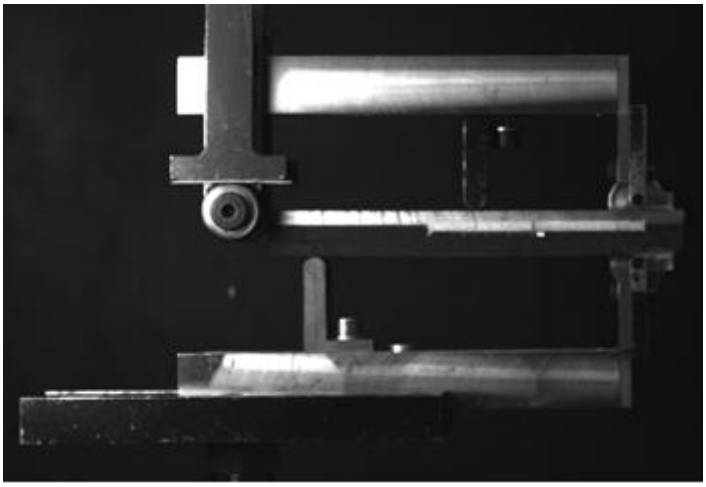


Figure 3.4: Photo of the MMB test set up.

3.4 Numerical model

A 2D finite element (FE) model was developed in Abaqus Standard (version 2019.HF2). The numerical model is intended to calculate the strain fields in the specimen and the fracture energy at load-crack length points obtained from the of the experimental results. The geometry, loadings and contour conditions were applied in order to simulate the of the MMB test configuration. The specimen supports were modelled as a constraint from all displacements and rotations around x and y axis, on the left side, and a constraint from displacements in y direction, on the right side, as shown in Figure 3.3. The opening load (P_I) was applied in the right top end and the shear loading (P_{II}) was applied in the center top surface. In this case, isotropic materials were selected with the properties derived from Table 3.1. A FE mesh with 4-node bilinear plane strain quadrilateral solid elements (CPE4) was applied in the whole model. Elements of the same size were applied in both sides of the crack and the aspect ratio of the elements in the vicinity of the crack tip was maintained at 1/1. Non-linear effects of large deformations and displacements are considered in the analysis.

The VCCT was applied for calculation of the fracture parameters. This method is implemented as a crack propagation tool in Abaqus. The crack propagates when the fracture energy around the crack tip exceeds a critical value. Since the simulation of the damage progression is not the aim of this study, high values of critical SERR were inserted to assure that the crack will not propagate. This allows obtaining the fracture

energy at defined crack propagation points. A crack propagation between different materials leads to dependent results on the element size around the crack tip. In order to circumvent the problem, literature suggests the model of an artificial interlayer around the crack [23, 24]. Therefore, a thin symmetric layer with adhesive properties (see Table 3.1) was modelled in both sides of the crack, resulting a total adhesive layer of 0.4 mm thickness, as shown in Figure 3.5. The effect of the adhesive layer on the stiffness of the arms is negligible.

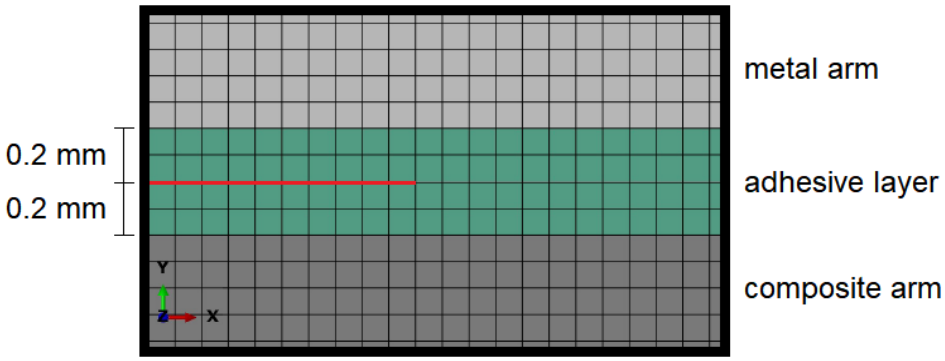


Figure 3.5: Detail of the FE mesh near the crack tip.

A crack length (a) of 30 mm was defined for the mesh sensitivity analysis. A nonlinear-elastic analysis was performed, and the results of the mesh sensitivity analysis are shown in Figure 3.6. The calculated fracture mode ratio (G_{II}/G) of the model without adhesive layer presented dependent on the element size around the crack tip (Δa) and did not represent the actual fracture development. However, the fracture mode ratio of the model with adhesive layer showed to be independent from the element size. A global mesh with elements of 0.1 mm was chosen for the determination of fracture energy at crack propagation points.

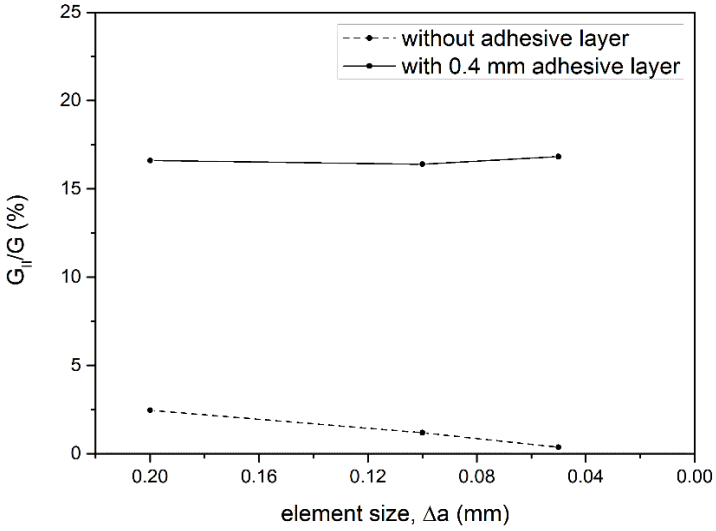


Figure 3.6: Mesh sensitivity analysis.

3.5 Results and discussion

3.5.1 Experimental results

A total of ten specimens were tested with five different test parameters. The test parameters are detailed in Table 3.2. Figures 3.7, 3.8, 3.9, 3.10 and 3.11 show the load and crack-displacement curves of each test configuration. There is an acceptable scatter in the load-displacement curves of similar test parameters. Some non-linearity may occur in the beginning of the test due to accommodation of the test apparatus. The first test series, Tests 01 and 02 (Figure 3.7), was performed with an initial crack of 45 mm. This initial crack length was reduced to 30 mm, in Tests 03 and 04 (Figure 3.8), in order to increase the propagation zone. Then, the lever length was changed between series in order to change the fracture mode ratio. It is observed that the test loadings are higher when using lower lever lengths. This was expected since the reduction of the lever length decreases the mode I fracture component, and the contribution of mode I loading has a major influence in the crack propagation. Figure 3.12 shows images of the typical final fracture surfaces taken from an optical microscope. All tests exhibited cohesive fracture within the adhesive layer.

Table 3.2: Test matrix.

Test	Lever length, c (mm)	Lever center of gravity, c_g (mm)	Initial crack, a_0 (mm)
01	104	38	45
02	104	38	45
03	104	38	30
04	104	38	30
05	78	32	30
06	78	32	30
07	64	29	30
08	64	29	30
09	50	27	30
10	50	27	30

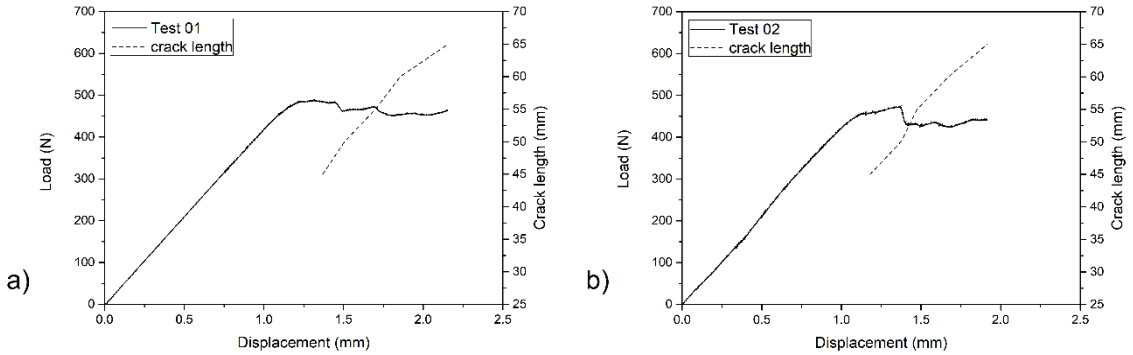


Figure 3.7: Load and crack length curves of Tests (a) 01 and (b) 02.

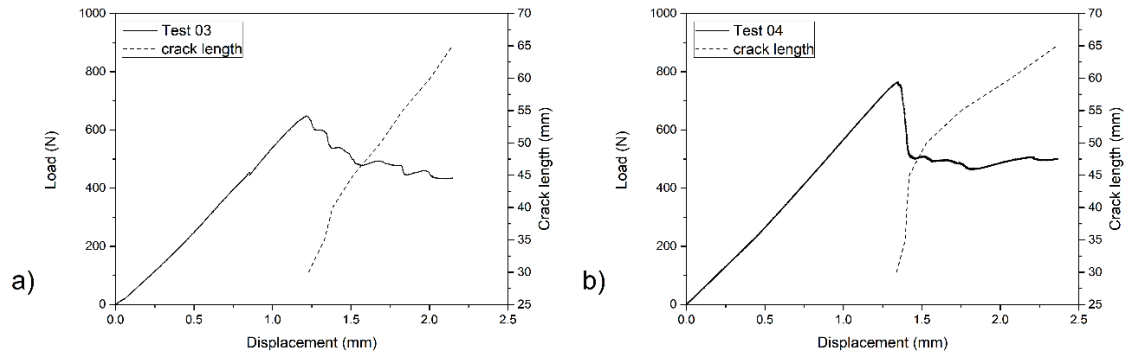


Figure 3.8: Load and crack length curves of Tests (a) 03 and (b) 04.

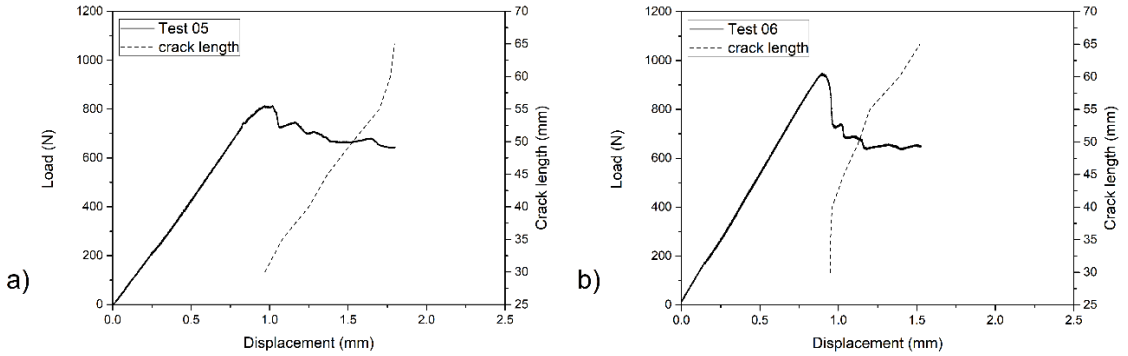


Figure 3.9: Load and crack length curves of Tests (a) 05 and (b) 06.

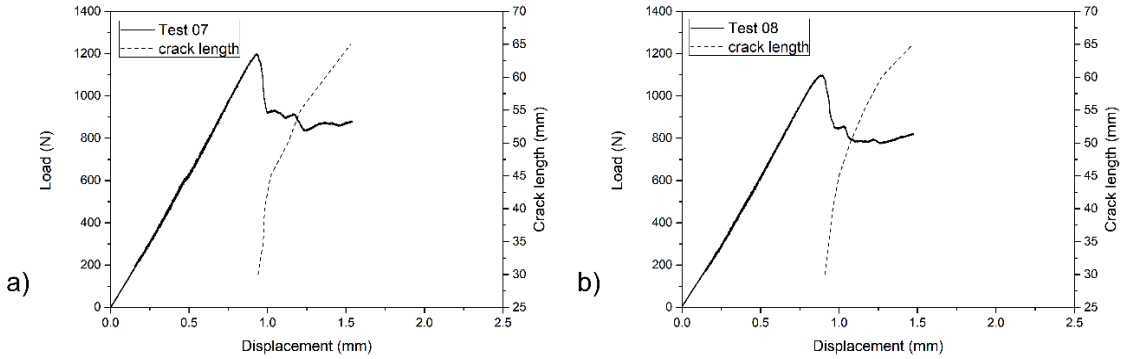


Figure 3.10: Load and crack length curves of Tests (a) 07 and (b) 08.

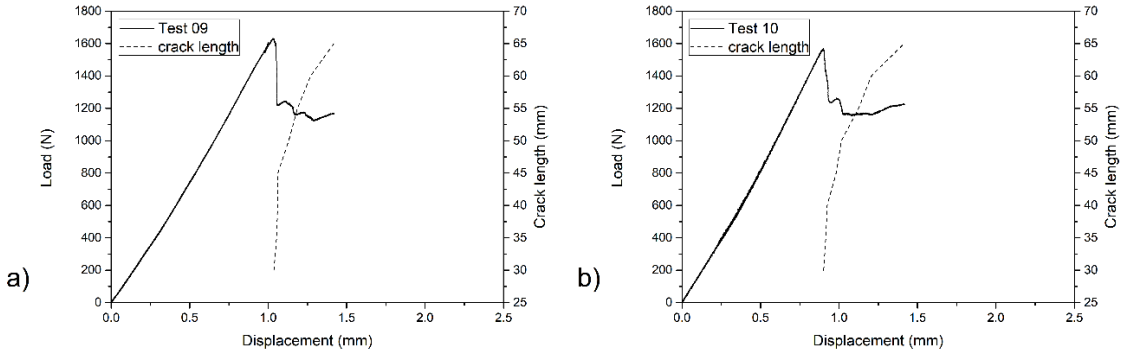


Figure 3.11: Load and crack length curves of Tests (a) 09 and (b) 10.

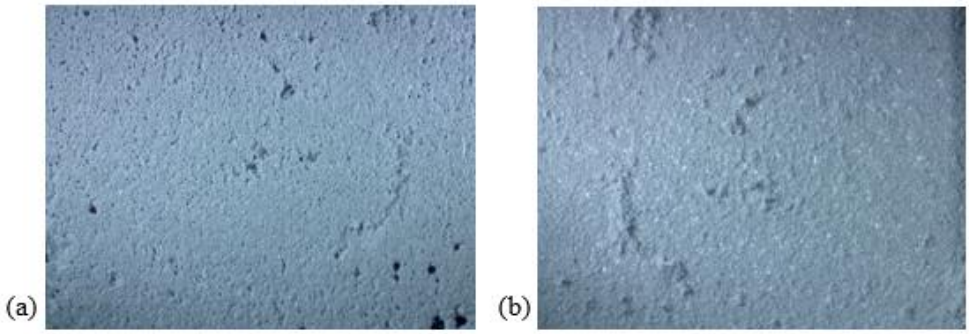


Figure 3.12: Fracture surfaces of (a) composite lower adherend and (b) metal upper adherend.

3.5.2 Validation of the numerical model

For validation of the numerical model, the strains obtained from the strain gauges during experiments were compared with the FE model at loading vs. crack size specific points. Two loading cases at the crack length of 45 mm and 55 mm were considered from Test 02. The numerical strain curves were obtained along the steel and composite outer surfaces at half-width – location of the strain gauges. Figures 3.13 and 3.14 show the comparison between numerical and experimental longitudinal strain. The length axis is defined from the application point of the opening load. There is a good agreement between numerical and experimental results.

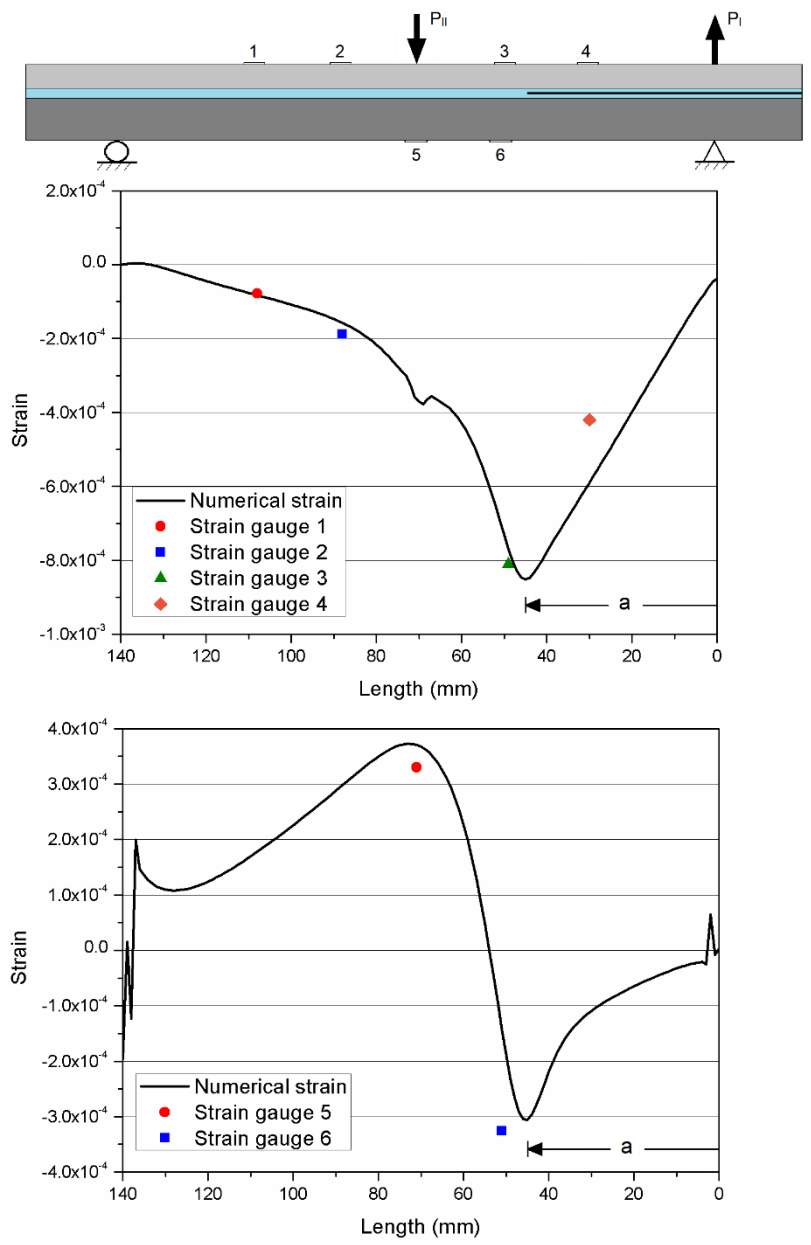


Figure 3.13: Test 02 strain along steel (upper graph) and composite (lower graph) surfaces at load of 456 N and crack length of 45 mm.

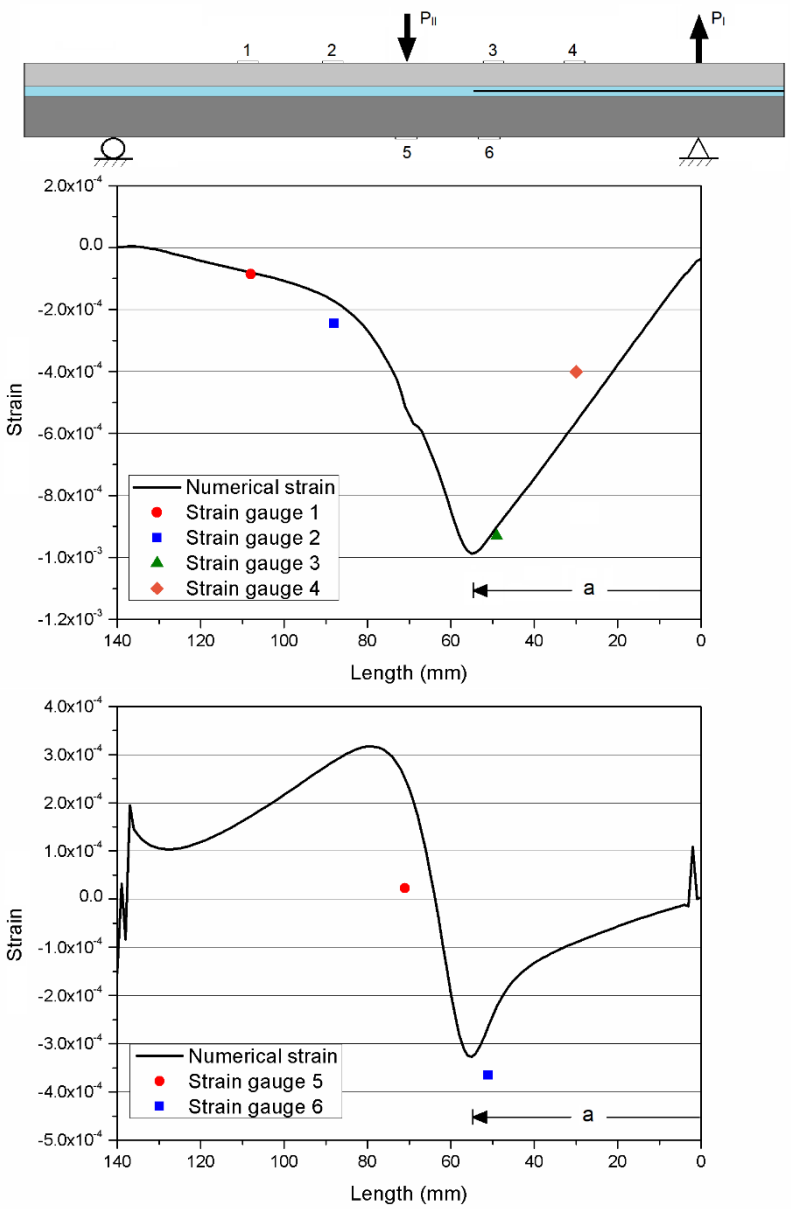


Figure 3.14: Test 02 strain along steel (upper graph) and composite (lower graph) surfaces at load of 432 N and crack length of 55 mm.

3.5.3 Fracture energy

Linear elastic condition is required for the calculation of fracture energy using the analytical approach. To assure that, numerical simulations were performed with experimental loading-crack propagation points. The maximum strain in the metal arm was obtained in every 5 mm of crack propagation. As shown in Figures 3.13 and 3.14, the region of maximum strain coincides with the crack tip length and the strain increases with the crack size. Additionally, the FE model of the MMB test presented significant

stresses only in the longitudinal direction. Figure 3.15 shows the maximum strain during crack propagation for each tested lever length (c). The metal yielding point imposes a limitation for the analysis of the test results using a linear elastic model.

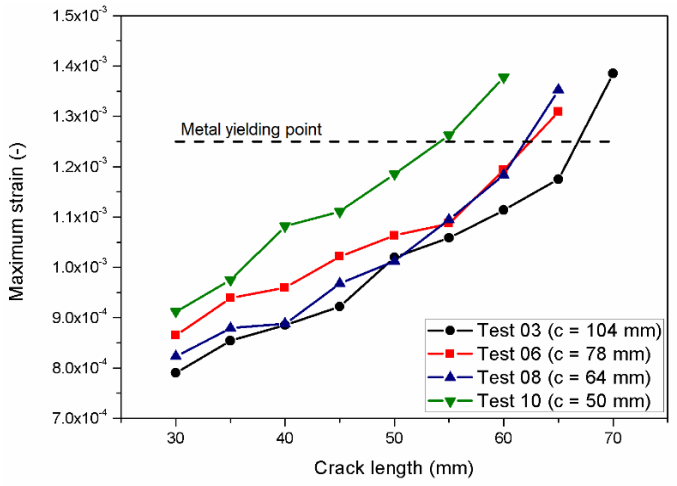


Figure 3.15: Maximum steel arm strain during crack propagation.

The numerical and analytical SERR was calculated from test propagation points in the region of linear elastic behavior. Figures 3.16, 3.17, 3.18, 3.19 and 3.20 show the total fracture energy (G) of each test. The analytical curves were obtained using the SBM (Equations 3.8 and 3.9), and the numerical curves were obtained using the finite element model (FEM/VCCT). It is observed that the analytical fracture energy increases as the crack propagates while the numerical fracture energy remains in a narrow range. There is a considerable difference between analytical and numerical results in the first propagation point (30 mm) and the difference reduces as the crack propagates. However, the fracture energy becomes similar when the crack length reaches 60 to 65 mm. This can be explained by the fact that the analytical methods consider only the deformation due to bending when determining the energy but neglect the shear effect. The latter is significant when testing thick beams and becomes smaller as the thickness to span ratio decreases. In the early stages of propagation, the thickness to crack length ratio is significantly higher than at further propagation stages when the crack length increases. Therefore, the effect of shear stresses decreases as the crack increases, hence the analytical results get closer to the numerical ones.

The analytical and numerical fracture mode partitioning (G_{II}/G) are shown in Figure 3.21. Even though the analytical method did not give very accurate predictions of the total fracture energy, it calculated with good accuracy the fracture mode ratio of the tests. The difference between the fracture mode ratio obtained with analytical and numerical models is limited to approximately 3%. Therefore, the SBM is able to determine the fracture mode of remarkably asymmetric specimens.

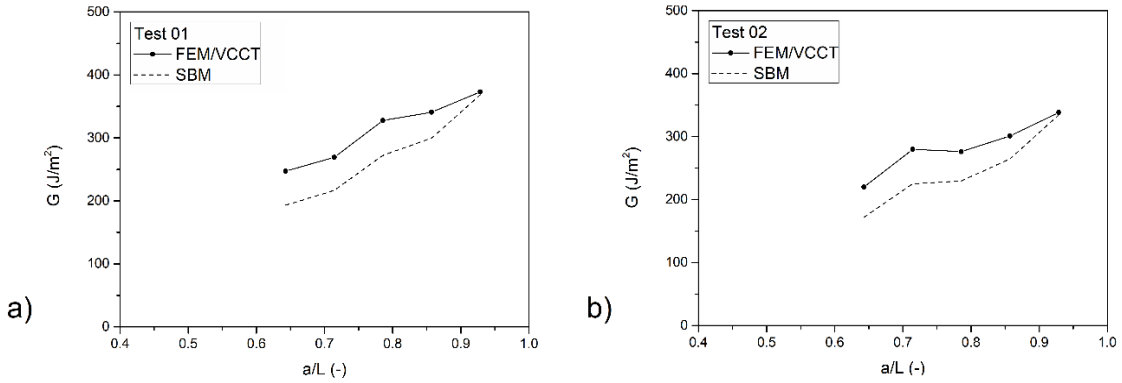


Figure 3.16: Total fracture energy of Tests (a) 01 and (b) 02.

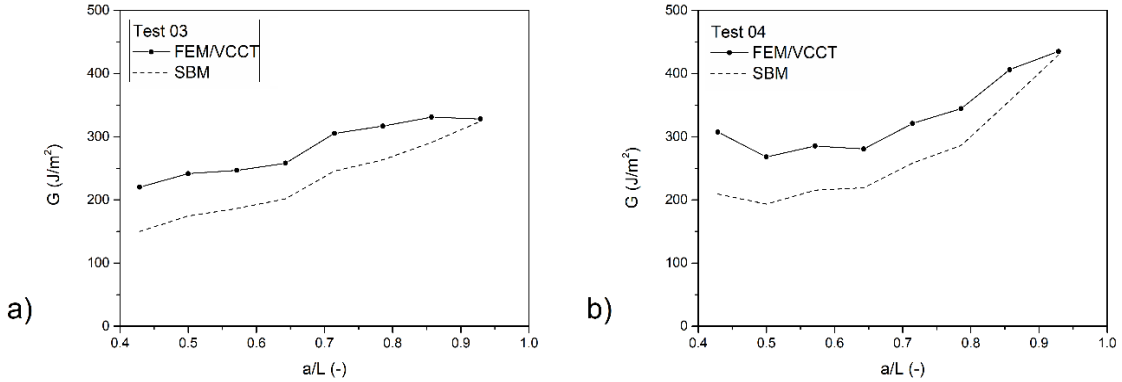


Figure 3.17: Total fracture energy of Tests (a) 03 and (b) 04.

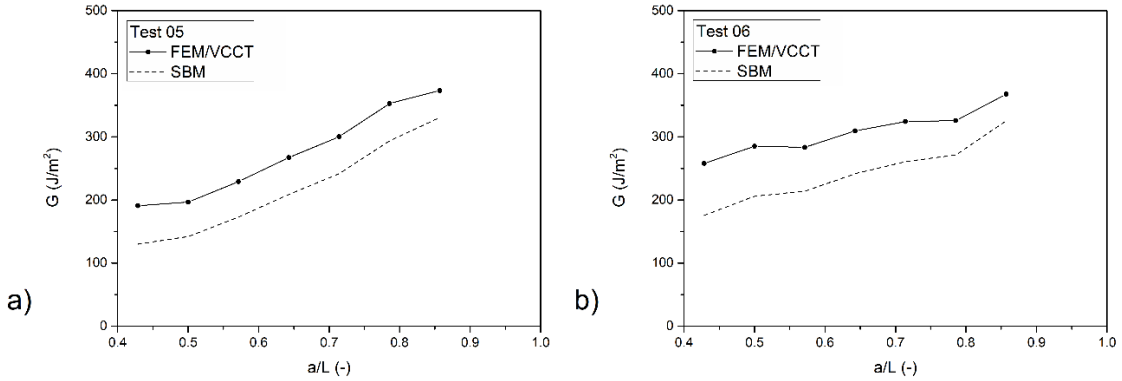


Figure 3.18: Total fracture energy of Tests (a) 05 and (b) 06.

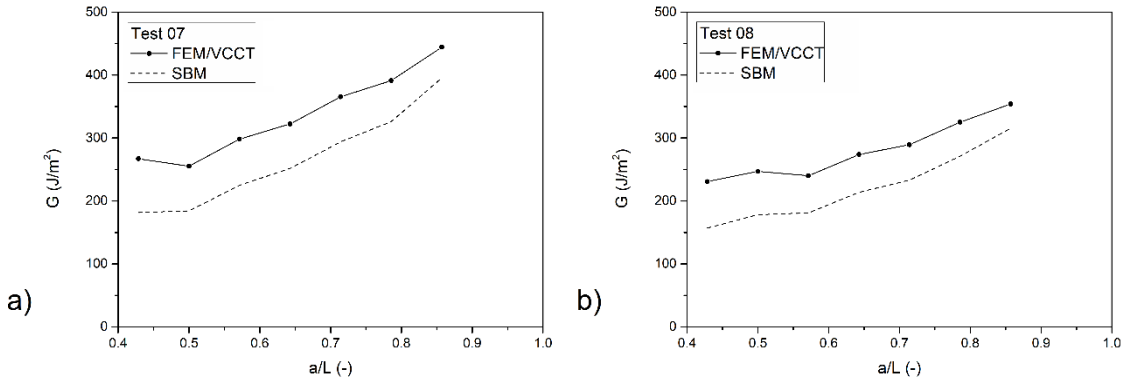


Figure 3.19: Total fracture energy of Tests (a) 07 and (b) 08.

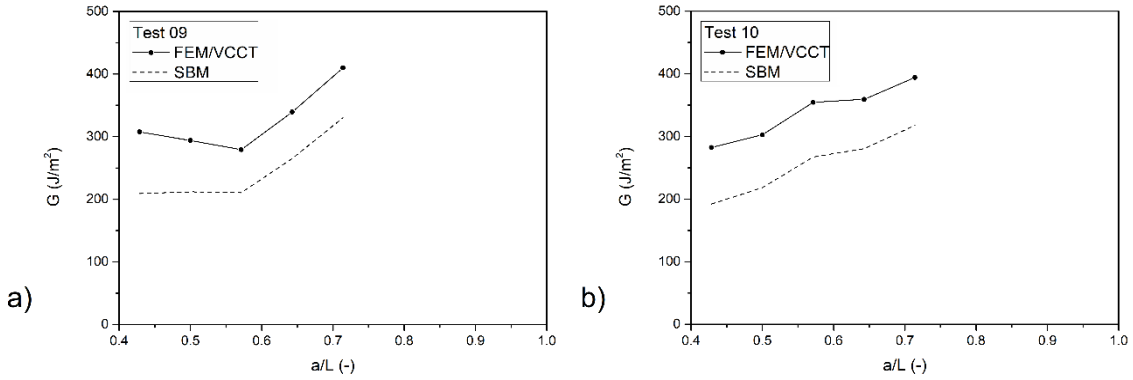


Figure 3.20: Total fracture energy of Tests (a) 09 and (b) 10.

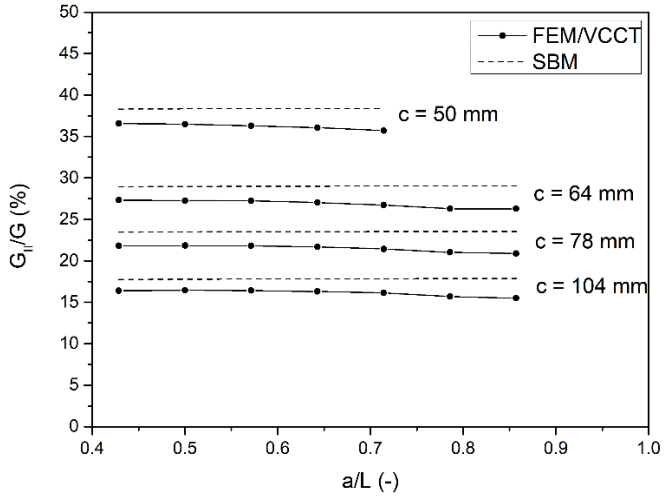


Figure 3.21: Fracture mode partitioning of the different test configurations.

3.6 Conclusion

The mixed-mode fracture behavior of a composite-to-metal adhesively bonded joint was investigated. A new strain-based criterion for the design of the mixed-mode bending (MMB) bi-material specimen was suggested. A new analytical partitioning method was proposed – the strain-based partitioning method (SBM) – and tested on a composite-to-metal bonded joint. A finite element model of the tests was developed and validated with strain gauges. The fracture energy was obtained from the numerical model using the VCCT. Analytical and numerical results were compared and conclusion can be drawn.

The MMB test method showed potential for the experimental evaluation of the mixed-mode fracture of bi-material bonded joints. The new strain-based specimen design was successfully applied to the MMB test although the metal yielding point imposes limitations on the maximum contribution of mode II fracture in the MMB test.

The SBM successfully predicted the fracture mode partitioning of bi-material bonded joints. However, it is necessary to cosider the transverse shear effect in order to obtain accurate values of the total fracture energy of thick specimens.

A finite element model of the MMB test using the VCCT with a bi-material joint produces mesh size dependent results. This problem can be circumvented by modelling a thin layer with the same material on both sides of the crack. Then, the total fracture energy and mode ratio of bi-material cracks can be predicted.

References

[1] Mangalgiri, P.D. Composite materials for aerospace applications. Bull. Mater. Sci. 1999, 22, 657-664.

[2] Taub, A.I.; Krajewski, P.E.; Luo, A.A. The evolution of technology for materials processing over the last 50 years: the automotive example. JOM 2007, 59, 48-57.

[3] de Barros, S.; Banea, M.D.; Budhe, S. Experimental analysis of metal-composite repair of floating offshore units (FPSO). J. Adhes. 2016, 93(1-2), 147-158.

[4] Van Den Einde, L.; Zhao, L.; Seible, F. Use of FRP composites in civil structural applications. Constr. Build. Mater. 2003, 17(6-7), 389-403.

[5] Budhe, S.; Banea, M.D.; de Barros, S. An updated review of adhesively bonded joints in composite materials. Int. J. Adhes. Adhes. 2017, 72, 30-42.

[6] Teixeira de Freitas, S.; Sinke, J. Failure analysis of adhesively-bonded skin-to-stiffener joints: Metal–metal vs. composite–metal. Eng. Failure Anal. 2015, 56, 2-13.
[7] Teixeira de Freitas, S.; Sinke, J. Failure analysis of adhesively-bonded metal-skin-to-composite-stiffener: Effect of temperature and cyclic loading. Compos. Struct. 2017, 166, 27-37.
[8] Teixeira de Freitas, S.; Sinke, J. Adhesion Properties of Bonded Composite-to-Aluminium Joints Using Peel Tests. J. Adhes. 2014, 90(5-6), 511-525.
[9] Chaves, F.J.P.; da Silva, L.F.M.; de Moura, M.F.S.F.; Dillard, D.A.; Esteves, V.H.C. Fracture Mechanics Tests in Adhesively Bonded Joints - A Literature Review. J. Adhes. 2014, 90(12), 955-992.
[10] Lai, Y.-H.; Rakestraw, M.D.; Dillard, D.A. The cracked lap shear specimen revisited—a closed form solution. Int. J. Solids Struct. 1996, 33(12), 1725-1743.
[11] Xiao, F.; Hui, C.-Y.; Kramer, E. J. Analysis of a mixed mode fracture specimen: the asymmetric double cantilever beam. J. Mater. Sci. 1993, 28, 5620-5629.
[12] Davidson, B.D.; Sundararaman, V. A single leg bending test for interfacial fracture toughness determination. Int. J. Fract. 1996, 78, 193-210.
[13] Park, S; Dillard, D.A. Development of a simple mixed-mode fracture test and the resulting fracture energy envelope for an adhesive bond. Int. J. Fract. 2007, 148, 261-271.
[14] Sørensen, B.F.; Jørgensen, K.; Jacobsen, T.K.; Østergaard, R.C. DCB-specimen loaded with uneven bending moments. Int. J. Fract. 2006, 141, 163-176.
[15] Boyano, A.; Mollón, V.; Bonhomme, J.; de Gracia, J.; Arrese, A.; Mujika F. Analytical and numerical approach of an End Notched Flexure test configuration with an inserted roller for promoting mixed mode I/II. Eng. Fract. Mech. 2015, 143, 63-79.
[16] Fernlund, G.; Spelt, J.K. Mixed-mode fracture characterization of adhesive joints. Compos. Sci. Technol. 1994, 50(4), 441-449.
[17] Reeder, J.R.; Crews Jr, J.H. Mixed-Mode bending method for delamination testing. AIAA J. 1990, 28(7), 1270-1276.
[18] Costa, M.; Carbas, R.; Marques, E.; Viana, G.; da Silva, L.F.M. An apparatus for mixed-mode fracture characterization of adhesive joints. Theor. Appl. Fract. Mech. 2017, 91, 94-102.
[19] Reeder, J.R.; Crews Jr., J.H. Redesign of the Mixed-mode Bending Delamination Test to Reduce Non-linear Effects. J. Compos. Technol. Res. 1992, 14(1), 12-19.

[20] Ducept, F.; Gamby, D.; Davies, P. A mixed-mode failure criterion derived from tests on symmetric and asymmetric specimens. Compos. Sci. Technol. 1999, 59(4), 609-619.
[21] Pereira, A.B; de Morais, A.B. Mixed mode I + II interlaminar fracture of glass-epoxy multidirectional laminates – Part 2 Experiments. Compos. Sci. Technol. 2006, 66(13), 1896-1902.
[22] Kim, B.W.; Mayer, A.H. Influence of fiber direction and mixed-mode ratio on delamination fracture toughness of carbon/epoxy laminates. Compos. Sci. Technol. 2003, 63(5), 695-713.
[23] Pereira, A.B.; de Morais, A.B. Mixed mode I + II interlaminar fracture of carbon/epoxy laminates. Compos. Part A 2008, 39(2), 322-333.
[24] Shahverdi, M.; Vassilopoulos, A.P.; Keller, T. Mixed-Mode I/II fracture behavior of asymmetric adhesively-bonded pultruded composite joints. Eng. Fract. Mech. 2014, 115, 43-59.
[25] Liu, Z.; Gibson, R.F.; Newaz, G.M. The Use of a Modified Mixed Mode Bending Test for Characterization of Mixed-Mode Fracture Behavior of Adhesively Bonded Metal Joints. J. Adhes. 2010, 78(3), 223-244.
[26] Stamoulis, G.; Carrere, N.; Cognard, J.Y.; Davies, P.; Badulescu, C. On the experimental mixed-mode failure of adhesively bonded metallic joints. Int. J. Adhes. Adhes. 2014, 51, 148-158.
[27] Droubi, M.G.; Mcafee, J.; Horne, R.C.; Walker, S.; Klaassen, C.; Crawford, A.; Prathuru, A.K.; Faisal, N.H. Mixed-mode fracture characteristics of metal-to-metal adhesively bonded joints - experimental and simulation methods. Procedia Structural Integrity 2016, 5, 40-47.
[28] Oliveira, J.M.Q.; de Moura, M.F.S.F.; Silva, M.A.L.; Morais, J.J.L. Numerical analysis of the MMB test for mixed-mode I/II wood fracture. Compos. Sci. Technol. 2007, 67(9), 1764-1771.
[29] de Moura, M.F.S.F.; Oliveira, J.M.Q.; Morais J.J.L; Dourado, N. Mixed-mode (I + II) fracture characterization of wood bonded joints. Constr. Build. Mater. 2011, 25(4), 1956-1962.
[30] Yoshihara, H. Initiation and propagation fracture toughness of solid wood under the mixed Mode I-II condition examined by mixed-mode bending test. Eng. Fract. Mech. 2013, 104, 1-15.

[31] Pereira, F.A.M.; de Moura, M.F.S.F.; Dourado, N.; Morais, J.J.L.; Silva, F.G.A.; Dias, M.I.R. Bone fracture characterization under mixed-mode I + II loading using the MMB test. Eng. Fract. Mech. 2016, 166, 151-163.
[32] Távara, L.; Reinoso, J.; Castillo, D.; Mantič, V. Mixed-mode failure of interfaces studied by the 2D linear elastic–brittle interface model: Macro- and micro-mechanical finite-element applications in composites. J. Adhes. 2018, 94(8), 627-656.
[33] Krueger, R. Virtual crack closure technique: History, approach, and applications. Appl. Mech. Rev. 2004, 57(2), 109–143.
[34] Agrawal, A.; Karlsson, A.M. Obtaining mode mixity for a bimaterial interface crack using the virtual crack closure technique. Int. J. Fract. 2006, 141, 75-98.
[35] Williams, J.G. On the calculation of energy release rates for cracked laminates. Int. J. Fract. 1988, 36, 101-119.
[36] Hibbeler, R. C. Mechanics of Materials, seventh edition; Pearson Prentice Hall: São Paulo, 2010.
[37] Harvey, C.M.; Wang, S. Experimental assessment of mixed-mode partition theories. Compos. Struct. 2012, 94(6), 2057-2067.
[38] Wang, W.; Fernandes, R.L.; Teixeira de Freitas, S.; Zarouchas, D. How pure mode I can be obtained in bi-material bonded DCB joints: A longitudinal strain-based criterion. Compos. Part B 2018, 153, 137-148.
[39] Teixeira de Freitas, S.; Banea, M.D.; Budhe, S.; de Barros, S. Interface adhesion assessment of composite-to-metal bonded joints under salt spray conditions using peel tests. Compos. Struct. 2017, 164, 68-75.
[40] Meniconi, L.C.M.; Porciúncula, I.N.; McGeorge, D.; Pedersen, A. Structural repair at a production platform by means of a composite material patch. Offshore Technology Conference, Houston, Texas, USA, May 3-6, 2010.
[41] ASTM D6671M-19. Standard Test Method for Mixed Mode I-Mode II Interlaminar Fracture Toughness of Unidirectional Fiber Reinforced Polymer Matrix Composites. ASTM International, 2019.

Chapter 4

Parametric Study

The goal of this Chapter is to evaluate the strain-based partitioning method (SBM), an analytical method based on beam analysis, for the mixed-mode fracture characterization of asymmetric cracks. The fracture energy is calculated at the crack tip of mixed-mode bending (MMB) test with asymmetric geometry and material parameters. The fracture energy obtained using SBM is benchmarked against the widely applied Williams' partitioning method (WM) and numerical results from finite element models using the virtual crack closure technique (VCCT). Results show that WM produces inaccurate fracture modes in asymmetric conditions. However, if using SBM, the fracture mode ratio of bi-material cracks was obtained with accuracy. SBM describes a coupling function between mode I and mode II fracture that allows the mode partitioning as long the specimen complies with a simple design criterion based on the longitudinal strain equivalence between arms. Experimental results of composite-to-metal bonded joints support the results of the parametric study. SBM showed to be a simple and reliable solution for the mixed-mode fracture characterization of bi-material cracks.

Keywords: fracture toughness; crack propagation; mixed mode fracture; strain-based method (SBM); interfacial fracture, delamination; bi-material bonded joints; finite element analysis.

This chapter is based on the journal article: "Evaluation of the Strain-Based Partitioning Method for Mixed-Mode I+II Fracture of Bi-Material Cracks", under review in The Journal of Adhesion.

4.1 Introduction

Adhesive bonding technology is the most efficient method in terms of strength-to-weight ratio and design flexibility for joining composites to other materials, such as metals [1]. This leads to the application of bonded structures between dissimilar materials with asymmetric interfaces, the bi-material bonded joints. First applications of bi-material structures are found in aerospace industry [2-4] and nowadays have become essential in many other fields, such as automotive industry [5], maritime [6-7] and civil construction [8]. In addition, laminated composite structures usually have multidirectional sections due to different fiber orientations, which also result in asymmetric interfaces. The emergence of new structures and applications requires the development of new methodologies for optimizing design and assuring structural integrity.

The fracture mechanics approach is widely applied to improve the design and evaluate the performance of structures. In the cases of delamination and debonding, the crack usually propagates along an interface. In real-life application, interfacial fracture often propagates in a combination of opening (mode I) and shear (mode II) loadings. Chaves et al. [9] indicated that there is a need for development of new methodologies for the characterization of mixed-mode (I+II) interfacial fracture. In mixed-mode fracture, not only the total fracture toughness must be determined but also the proportion of mode I and mode II fracture. Hence, it is essential to develop reliable methods for evaluation of asymmetric crack propagation under mixed-mode I+II loadings.

A variety of experimental procedures is available for mixed-mode fracture testing. The asymmetric double cantilever beam (ADCB) test [10] is a simple solution but allows only testing a limited range of low mode II. The asymmetric tapered double cantilever beam (ATDCB) test [11] also presents a limited partitioning range and has higher manufacturing complexity. The mixed-mode flexure (MMF) test [12-13], also called single leg bending (SLB) test [11], is another simple solution to characterize mixed-mode fracture. However, the test is limited to small range of mode I contribution. The over-leg bending (OLB) test [15] allows obtaining a greater crack length but has the same limitation of the SLB test. The mixed-mode bending (MMB) test [16-17] stands out for its easy implementation and capability of testing a wide range of partitioning ratios with only one specimen geometry. The MMB test method was originally developed for fracture propagation of unidirectional symmetric composites and was later extended to

multidirectional laminates [18-20]. Other applications include metal bonded joints [21-23], wood bonded joints [24-26] and bone fracture [27].

A reliable method to determine the fracture toughness of a cracked structure relies on the finite elements method (FEM) in combination with the virtual crack closure technique (VCCT). The VCCT is based on the assumption that the energy released when the crack is extended a crack tip element size is identical to the energy required to close the crack in the same length [28]. This method has been successfully applied for calculation of the fracture toughness at the crack located between different materials [28-29]. The VCCT is commonly applied for fracture characterization in research and development projects. However, numerical solutions have limited industrial application due to high implementation costs.

Analytical methods based on beam theory analysis have arisen as a simple approach for the fracture characterization. Williams [30] proposed a solution for the calculation of the total fracture energy and mode ratio of a given specimen geometry and testing condition. Williams [31] and Wang and William [32] proposed corrections factors to the mode I and mode II fracture modes for accounting the effects of shear deformation and deflection at the crack tip. Shahverdi et al. [33] applied the same assumptions of Williams` partitioning method (WM) [30] to the delamination of a multidirectional composite. These analytical solutions are reliable in the cases of symmetric specimens, where both sides of the crack have the same material and geometry. However, they showed to give inaccurate results for the fracture mode ratio when the crack propagates in an interface between different materials [34-35]. Innovative solutions are required for the analysis of multilateral structures.

The mixed-mode fracture characterization of asymmetric cracks has been object of recent studies [36-37]. Valvo [38] developed a solution based on simple kinematic assumption for obtaining the fracture mode ratio of delaminated beams under general loading conditions. His work evidenced the influence of curvatures, strains and thicknesses of the arms on the determination of pure modes. Alternatively, Wang et al. [39] proposed a longitudinal strain equivalent geometry between arms for the pure mode I fracture characterization of bi-material bonded joints. Then, Arouche et at. [40] extended this criterion for the mixed-mode fracture characterization of asymmetric cracks and introduced a new method: the strain-based partitioning method (SBM). It showed to be

an easy and consistent method to obtain the fracture mode ratio of bi-material cracks. However, more studies are required on the performance of the SBM considering parameters of materials and geometry.

The present study aims to evaluate the SBM for the mixed-mode fracture characterization of asymmetric cracks. The widely applied WM is also verified for comparison between the analytical methods. The performance of both methods is studied on a wide range of geometrical and material asymmetry between crack sides. The fracture toughness obtained from the analytical methods are benchmarked against numerical results of finite elements models of MMB tests using the VCCT. Finally, the application and limitations of the SBM are verified in a study case with composite-to-metal bonded joints.

4.2 Analytical models

The strain energy release rate (SERR) is the most important property to consider in the calculation of fracture toughness of cracked structures. For linear elastic behavior, the total SERR can be obtained by the balance of fracture energy through the following equation:

$$G = \frac{1}{B}\left(\frac{\delta U_e}{\delta a} - \frac{\delta U_s}{\delta a}\right) \tag{3.1}$$

Where B is the width of the specimen, U_e is the external work performed, U_s is the strain energy and a is the crack length. The analysis considers a region ABCD mechanically affected by the presence of a crack under pure bending moments, as shown in Figure 4.1.

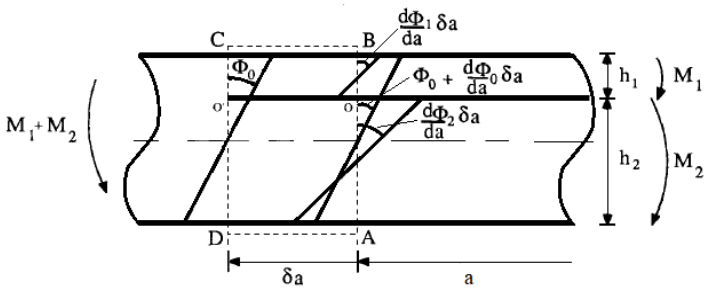


Figure 4.1: Beam analysis under pure bending moments.

The upper and lower arm thickness are h_1 and h_2, and the bending moments applied on the upper and lower arms are M_1 and M_2, respectively. The angles Φ_0, Φ_1 and Φ_2 represent the slopes of the beam, upper arm and lower arm, respectively. When the crack grows a length δa from O on section AB to O' on section CD, the external work is:

$$\frac{\delta U_e}{\delta a} = M_1\left(\frac{\delta\phi_1}{\delta a} - \frac{\delta\phi_0}{\delta a}\right) + M_2\left(\frac{\delta\phi_2}{\delta a} - \frac{\delta\phi_0}{\delta a}\right) \tag{4.2}$$

For pure bending, the change in angle is given by:

$$\frac{\delta\phi}{\delta a} = \frac{M}{EI} \tag{4.3}$$

Where M is the moment, E is the flexural modulus and I is the second moment of area. Similarly, the strain energy is:

$$\frac{\delta U_s}{\delta a} = \frac{M_1^2}{2E_1I_1} + \frac{M_2^2}{2E_2I_2} - \frac{(M_1+M_2)^2}{2E_{eq}I_{eq}} \tag{4.4}$$

Where E_1, I_1, E_2, I_2, E_{eq} and I_{eq} are the flexural longitudinal moduli and second moments of the area in the section of the crack tip of the upper arm, lower arm and total specimen, respectively. Substituting (4.2) and (4.4) in (4.1), it can be reduced to the equation of the total fracture energy:

$$G = \frac{1}{2B}\left(\frac{M_1^2}{E_1I_1} + \frac{M_2^2}{E_2I_2} - \frac{(M_1+M_2)^2}{E_{eq}I_{eq}}\right) \tag{4.5}$$

Equation (4.5) allows determining the total fracture energy of a crack between two arms. However, it is essential to the characterization of the mechanical behavior to define the contribution of mode I and mode II fracture.

4.2.1 Williams' partitioning method

Williams [30] proposed a partitioning method (WM) based on the assumptions that: (i) pure mode I exists when opposite moments act on the joint arms; and (ii) pure mode II is obtained when the curvature in the two arms are the same. This means:

$$M_1 = M_{II} - M_I \tag{4.6}$$

$$M_2 = \psi M_{II} + M_I \tag{4.7}$$

Where the bending stiffness ratio between upper and lower arms is:

$$\psi = \frac{E_2 I_2}{E_1 I_1} \tag{4.8}$$

Substituting (4.6) and (4.7) in (4.5), the equation of the total fracture energy can be reduced to:

$$G = \frac{1}{2B}\left[M_I^2\left(\frac{\psi+1}{E_2 I_2}\right) + M_{II}^2\left(\frac{\psi+\psi^2}{E_2 I_2} - \frac{(1+\psi)^2}{E_{eq} I_{eq}}\right)\right] \tag{4.9}$$

Notice that no cross-product term is observed. Therefore, the partitioning can be obtained by rewriting Equation (4.9) as function of M_I and M_{II}:

$$f(M_I, M_{II}) = f_I(M_I) + f_{II}(M_{II}) \tag{4.10}$$

Finally, the equations of mode I and mode II fracture can be written as:

$$G_I = \frac{M_I^2}{2B}\left(\frac{\psi+1}{E_2 I_2}\right) \tag{4.11}$$

$$G_{II} = \frac{M_{II}^2}{2B}\left(\frac{\psi+\psi^2}{E_2 I_2} - \frac{(1+\psi)^2}{E_{eq} I_{eq}}\right) \tag{4.12}$$

$$G = G_I + G_{II} \tag{4.13}$$

WM is widely applied in the fracture characterization of symmetric cracks. However, literature has shown that it does not predict with accuracy the fracture mode ratio of cracks between asymmetric arms [18, 33-34]. The assumptions do not describe with precision the interaction between mode I and mode II fracture. Therefore, it is not recommended for the characterization of asymmetric cracks.

4.2.2 Strain-based partitioning method

The strain-based partitioning method (SBM) [40] introduced a new criterion for the fracture mode partitioning. The main difference in comparison with the WM lies on the condition for pure mode I: it incorporates the condition of strain equivalence for mode pure mode I, identified by Ouyang [41] and confirmed by Wang et al. [39]. In the case of pure mode II, similarly to WM, the SBM assumes that it is produced when both arms have the same curvature, as observed by Mollón et al. [42]. Therefore, the partitioning assumptions become: (i) the longitudinal strain distribution at the faying surfaces of both arms must be identical in order to produce pure mode I; and (ii) pure mode II is obtained when the curvature in the two arms are the same. This gives:

$$M_1 = M_{II} - M_I \tag{4.14}$$

$$M_2 = \psi M_{II} + \beta M_I \tag{4.15}$$

Where the longitudinal strain ratio between upper and lower arms is:

$$\beta = \frac{E_2 h_2^2}{E_1 h_1^2} \tag{4.16}$$

Substituting Equations (4.14) and (4.15) in Equation (4.5), the equation of the total fracture energy is obtained:

$$G = \frac{1}{2B}\left[\begin{matrix} M_I^2\left(\frac{\psi+\beta^2}{E_2I_2} - \frac{(\beta-1)^2}{E_{eq}I_{eq}}\right) + M_{II}^2\left(\frac{\psi+\psi^2}{E_2I_2} - \frac{(1+\psi)^2}{E_{eq}I_{eq}}\right) + \\ M_I M_{II}\left(\frac{2\psi\beta - 2\psi}{E_2I_2} - \frac{2(1+\psi)(\beta-1)}{E_{eq}I_{eq}}\right) \end{matrix}\right] \quad (4.17)$$

Equation (4.17) shows that the mode I fracture energy affects the mode II fracture energy and vice-versa. Consequently, the equation can only be written in the form of:

$$f(M_I, M_{II}) = f_I(M_I) + f_{II}(M_{II}) + f_c(M_I, M_{II}) \quad (4.18)$$

Equation (4.18) displays a coupling function $f_c(M_I, M_{II})$ beyond the functions of pure mode I and pure mode II – $f_I(M_I)$ and $f_{II}(M_{II})$, respectively. This implies that the fracture mode partitioning is obtained when the coupling function $f_c(M_I, M_{II})$ is zero. This is achieved in the condition of $\beta = 1$. Therefore, the specimen design condition of longitudinal strain equivalence has to be satisfied. It means:

$$E_1 h_1^2 = E_2 h_2^2 \quad (4.19)$$

In this case, the mode I and mode II equations of fracture energy are the same as in WM – Equations (4.11) and (4.12). However, WM does not reinforce any specific specimen design since it was derived for symmetric specimens in which β is always equal to 1. It ignores the coupling function that contributes to the total fracture energy. This is believed to be the reason why WM is inaccurate if applied to asymmetric specimens where the longitudinal strain-based design criterion is not applied ($\beta \neq 1$). This assumption will be verified in this paper.

4.3 Numerical models

A virtual mixed-mode bending (MMB) test was chosen to evaluate the analytical fracture characterization method. In this test, a loading is applied through a roller attached to a lever and loaded just above the mid-plane of the test specimen, as shown in Figure 4.2. The test loading (P) is decomposed in opening (P_I) and shear (P_{II}) loadings in a

constant ratio determined by the lever length (c). A longer lever length c produces a fracture with higher portion of mode I.

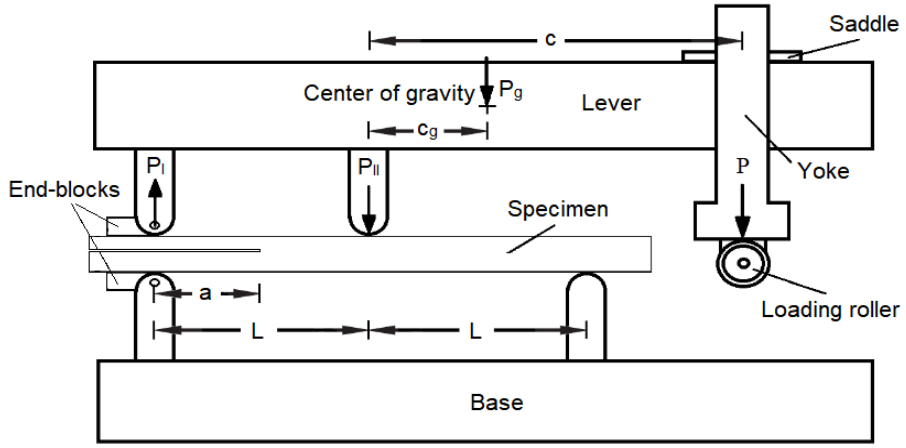


Figure 4.2: MMB test scheme.

A 2D finite element model was created in Abaqus Standard (version 2019.HF2). Figure 4.3 shows the geometric features of the model: 70 mm half-span (L) and 50 mm crack length (a). The upper and lower arm thicknesses (h_1 and h_2, respectively) and materials (E_1 and E_2, respectively) are the parameters varied in the analysis. Loads and boundary conditions were applied to the model in order to simulate the MMB testing conditions. Mode I and mode II loads (P_I and P_{II}, respectively) were derived from a test load (P) of 100 N, according with the applied lever length (c). The specimen supports were modelled as a constraint from all displacements and rotations around x and y axis, on the left side, and a constraint from displacements in y direction, on the right side, as shown in Figure 4.3. The left bottom end was only constrained from displacements in y direction. Plane strain 4-nodes bilinear quadrilateral elements (CPE4) were applied in the whole geometry. Non-linear effects of large deformations and displacements are included in the analysis.

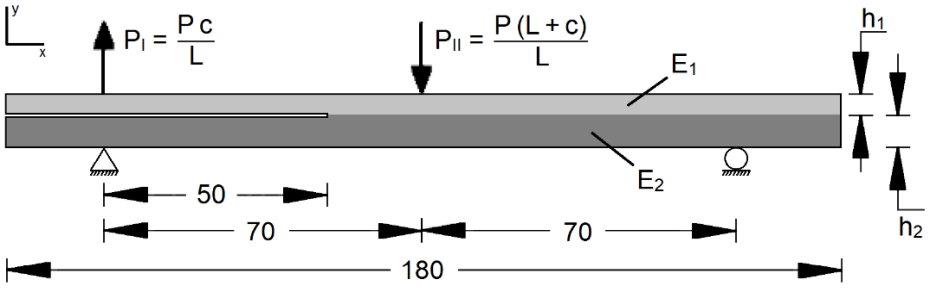


Figure 4.3: MMB specimen.

The virtual crack closure technique (VCCT) was applied for calculation of the mode I and mode II fracture energy. High values of critical fracture energy were inserted to ensure that the crack did not propagate. This allows obtaining the fracture energy at defined crack propagation points. The mesh sensitivity analysis was performed in two models with different conditions of asymmetry. The first model is an asymmetric crack between arms of the same material, and the second model is a bi-material crack. Both studies will be discussed hereafter.

4.3.1 Asymmetric crack within the same material

A mesh sensitivity analysis was performed on an asymmetric crack between arms of the same material. The model consists of an MMB test specimen with an upper arm thickness (h_1) of 1.50 mm and a lower arm thickness (h_2) of 3.00 mm. An elastic isotropic material was applied to both arms with elastic modulus (E_1 and E_2) of 70 GPa and Poisson's ratio (ν_1 and ν_2) of 0.33. The test loadings refer to lever length (c) of 61 mm. Figure 4.4 shows the fracture mode (G_{II}/G) obtained from the node at the crack tip, using different square element sizes. As can be seen, the model achieved good convergency. The mesh with elements of 0.20 mm presented a variation of 0.72% in the mode I fracture energy and 1.02% in the mode II fracture energy to the model with 0.10 mm elements. Therefore, the model with 20700 elements of 0.20 mm was selected for the numerical calculation of the fracture parameters, as shown in Figure 4.5.

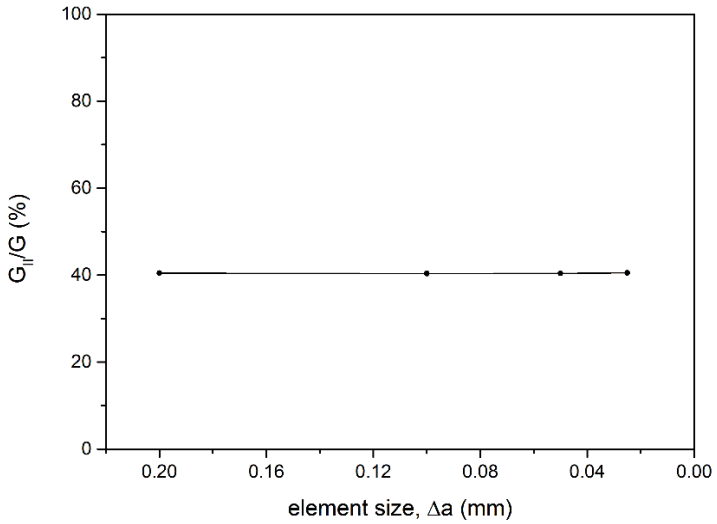


Figure 4.4: Fracture mode of an asymmetric crack within arms of the same material, in terms of the element size.

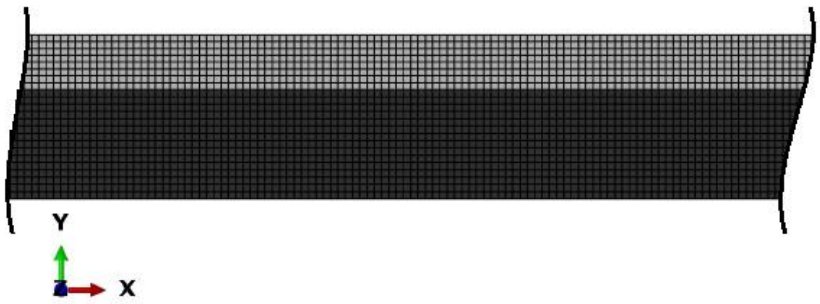


Figure 4.5: Mesh of model with arms of the same material.

4.3.2 Bi-material crack

A second mesh sensitivity analysis was performed on a crack between arms made of different materials. The model consists of an MMB test specimen with an upper arm thickness (h_1) of 2.12 mm and a lower arm thickness (h_2) of 3.00 mm. Elastic isotropic materials were applied to both arms, with elastic modulus of the upper (E_1) and lower (E_2) arms of 140 GPa and 70 GPa, respectively, and Poisson's ratio of 0.33 in both arms (ν_1 and ν_2). In order to avoid mesh size dependent results in cracks between different materials, literature recommends modeling a thin interlayer and make the crack propagates within it [28, 34]. Therefore, a 0.10 mm adhesive layer was inserted on both sides of the crack. The adhesive has elastic modulus of 2.25 GPa and Poisson's ratio of 0.38, and the inserted layer is thin enough to have a negligible effect (< 1%) on the

stiffness of the arms. Figure 4.6 shows the fracture mode (G_{II}/G) obtained from the node at the crack tip, using different square element sizes. A good convergence is observed in the model with adhesive layer. The mesh with elements of 0.05 mm presented a variation of 0.29% in the mode I fracture energy and 0.44% in the mode II fracture energy to the model with 0.25 mm elements. Therefore, the model with 381600 elements of 0.05 mm was selected for the numerical calculation of the fracture parameters, as shown in Figure 4.7.

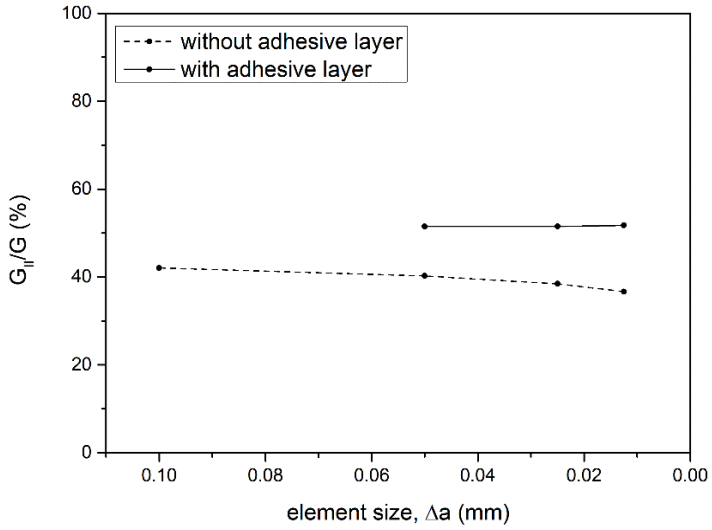


Figure 4.6: Fracture mode of a bi-material crack, in terms of the element size.

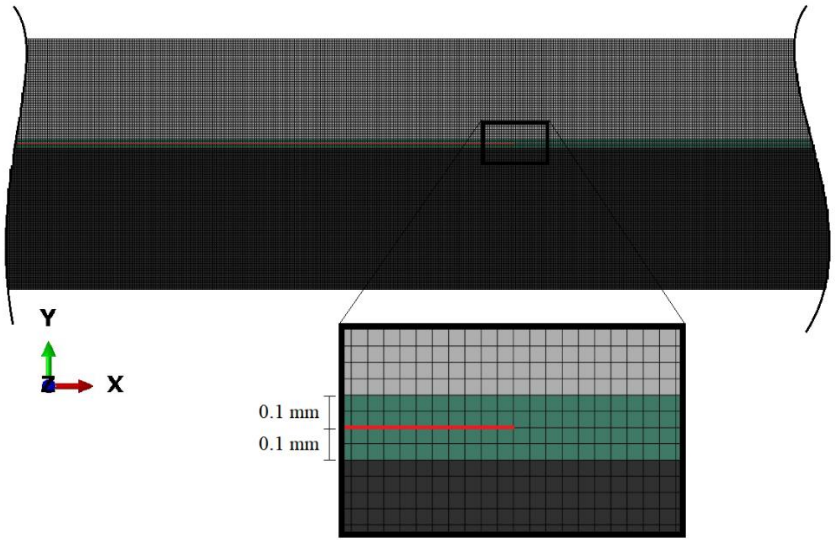


Figure 4.7: Mesh of model with bi-material crack.

4.4 Results and discussion

In this section, the results from the analytical methods are benchmarked against the numerical results. The total fracture energy and the fracture mode ratio are presented for the WM, the SBM (which coincides with the WM for $\beta = 1$, Equation 16), and the finite element model (FEM/VCCT). The arms thicknesses and materials vary, and therefore β. The accuracy of the analytical methods is verified for general specimen design. The aim is to verify the assumption proposed in the SBM that the accurate fracture mode ratio is only obtained if the longitudinal strain-based design criterion is applied ($\beta = 1$). This proposition is evaluated, firstly, for asymmetric cracks within the same material and, secondly, for bi-material cracks.

4.4.1 Asymmetric crack within the same material

The first parametric study was performed on an asymmetric crack within the same material. Both arms have elastic modulus (E_1 and E_2) of 70 GPa and Poisson's ratio (ν_1 and ν_2) of 0.33. In order to verify the influence of the fracture mode ratio in the accuracy of the analytical methods, three different conditions were considered: low (c = 117 mm), intermediate (c = 61 mm) and high (c = 42 mm) mode II ratio. Table 4.1 shows the three cases of geometrical asymmetry. The upper arm thickness (h_1) is varied in a wide range of geometries applied to the MMB test specimen while the lower arm thickness (h_2) remains 3.0 mm. The crack length is kept at 50 mm and the test load (P) is 100 N.

Table 4.1: Study cases of geometrical asymmetry.

Case	Lever length, c (mm)	h_1 (mm)	h_2 (mm)	E_1; E_2 (GPa)	ν_1; ν_2
1	117	**$1.5 < h_1 < 6.0$**	3.0	70	0.33
2	61	**$1.5 < h_1 < 6.0$**	3.0	70	0.33
3	42	**$1.5 < h_1 < 6.0$**	3.0	70	0.33

Analytical and numerical results of the total fracture energy (G) are presented in Figure 4.8. Notice that the SBM – Equation (17) – gives the same total fracture energy as WM – Equation (9) – for any geometry. This occurs because both methods are derived from the same equation of the total fracture energy – Equation (5). Figures 4.8a, 4.8b and

4.8c show the three cases of low (case 1), intermediate (case 2) and high (case 3) mode II fracture, respectively. Overall, the total fracture energy obtained from analytical solutions based on beam analysis are in very good agreement with the numerical results.

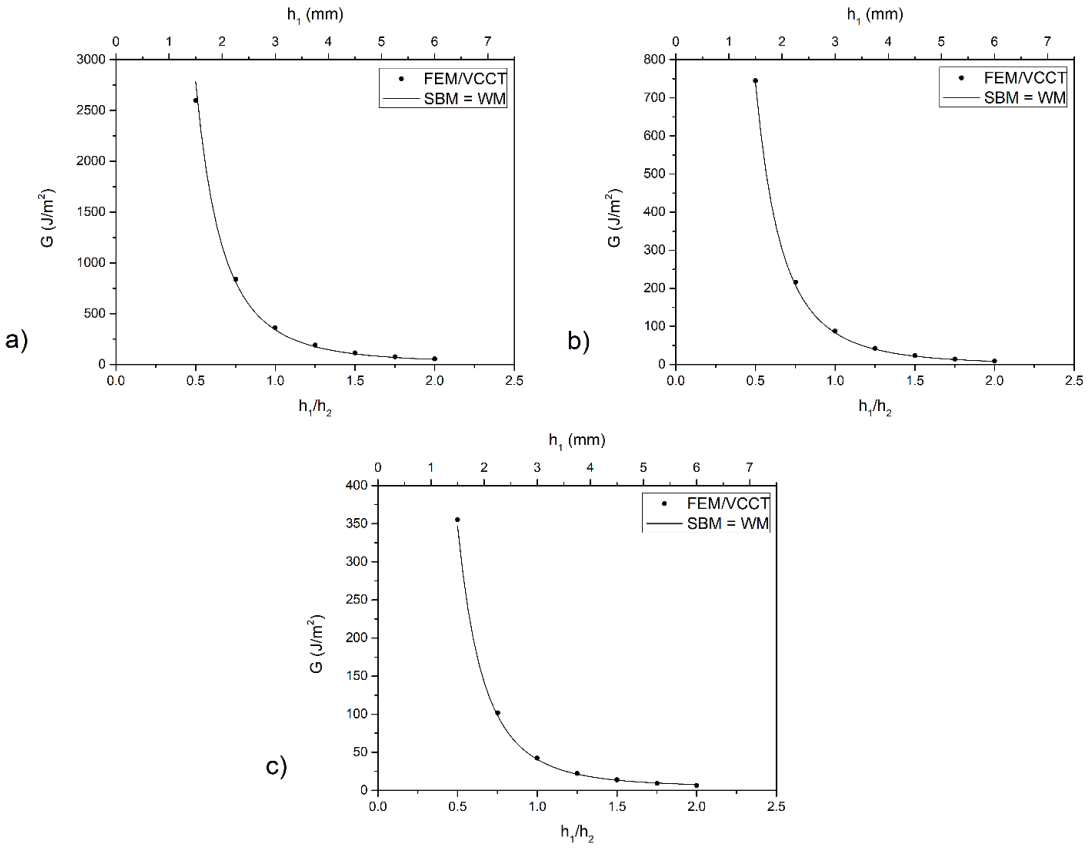


Figure 4.8: Total fracture energy with the variation of the specimen thickness: cases (a) 1 – low, (b) 2 – intermediate and (c) 3 – high mode II.

Figure 4.9 shows the analytical and numerical fracture mode ratio (G_{II}/G). Notice that the SBM is applied only when the specimen design condition is satisfied ($\beta = 1$) and, for this condition, gives the same result of WM. Figure 4.9a shows the results for low mode II (case 1). When $\beta = 1$, the crack is symmetric ($h_1/h_2 = 1$) and both analytical methods show good agreement with numerical results. As β differs from 1, WM gives significant discrepancies from the FEM/VCCT results. This shows that WM is only valid for the condition $\beta = 1$. Similar results are observed as the mode II fracture ratio increases, in Figures 4.9b and 4.9c (cases 2 and 3, respectively). Moreover, it is noticeable that WM gives inaccurate fracture partitioning ratios on asymmetric cracks within the same material [30-31]. This can be explained by the influence of the mode I and mode II

coupling on the fracture energy, shown in Figure 4.10, which plots the coupling function (see Equation 18) over the total fracture energy (f_c/G). It can be seen that the influence of the mode I and mode II coupling in the total fracture energy is zero in the case of a symmetric crack ($\beta = 1$). The coupling effect increases largely with the asymmetry of the specimen. This explains the fact that WM is not well suited for the mixed-mode fracture characterization of cracks between asymmetric geometries.

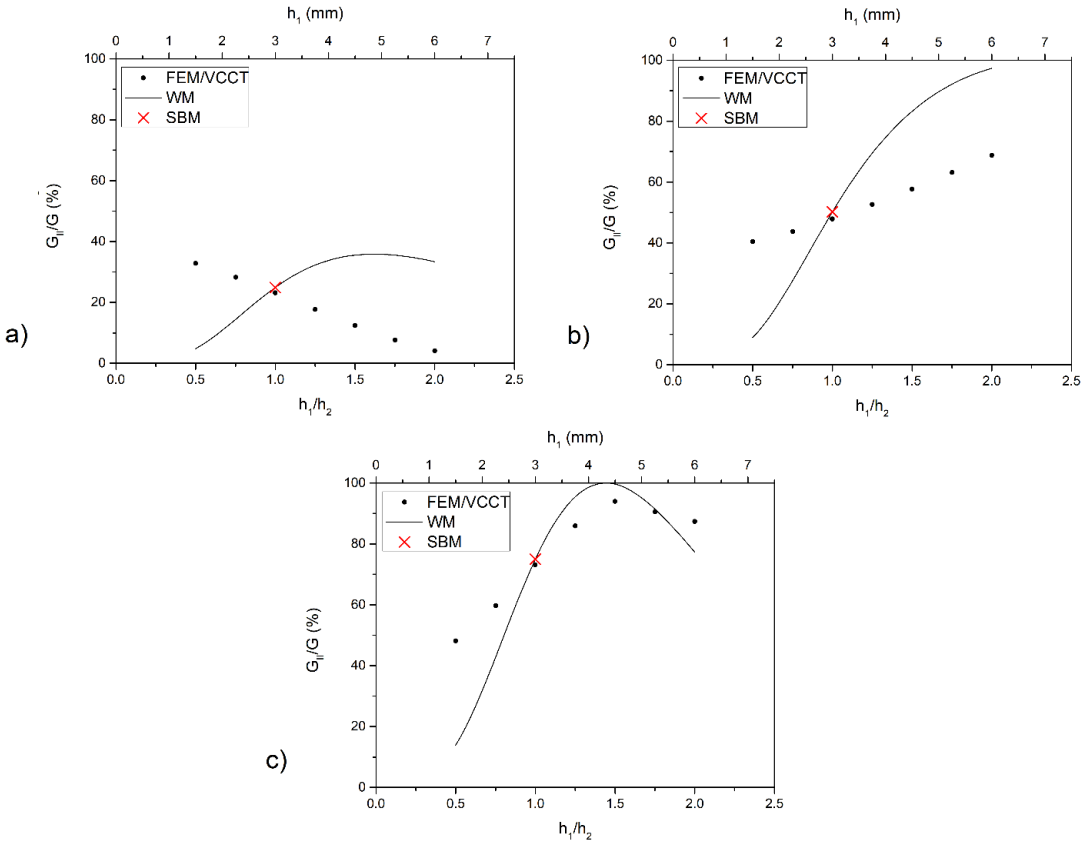


Figure 4.9: Fracture mode ratio with the variation of specimen thickness: cases (a) 1 – low, (b) 2 – intermediate and (c) 3 – high mode II.

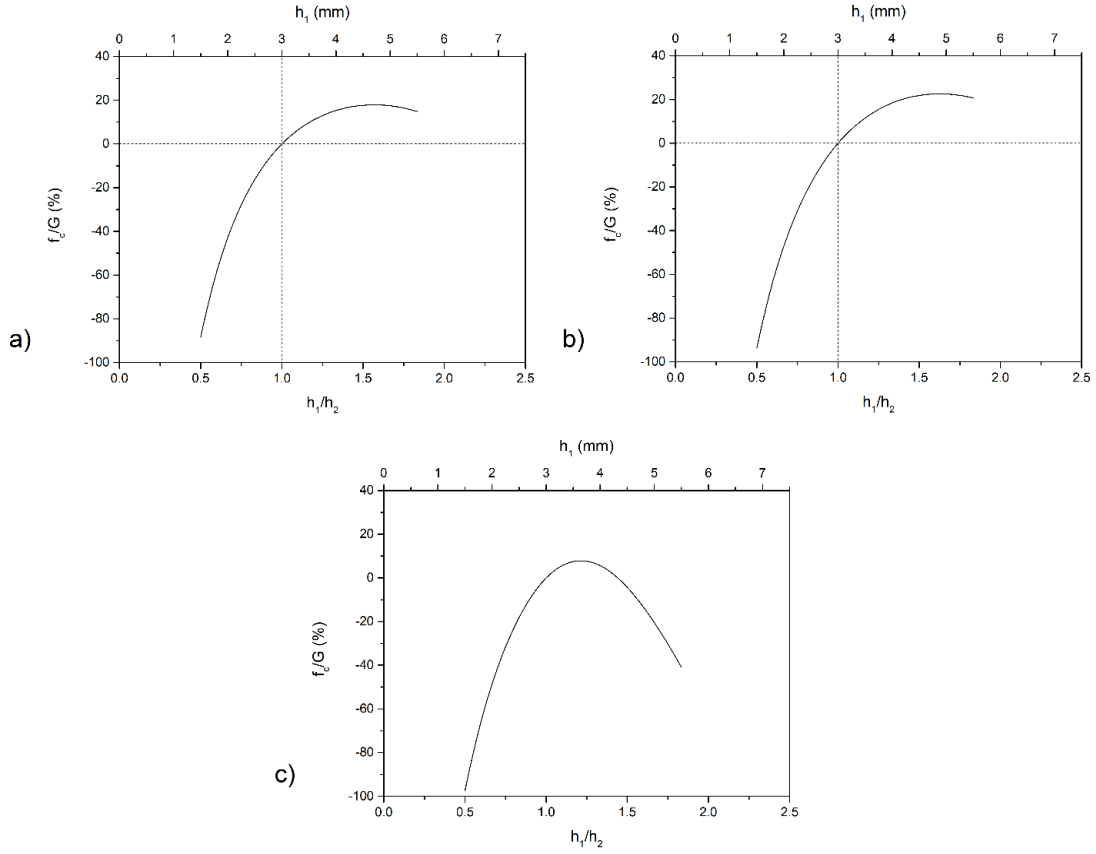


Figure 4.10: Influence of the coupling function on the fracture energy: cases (a) 1 – low, (b) 2 – intermediate and (c) 3 – high mode II.

Table 4.2 shows the results and errors of the analytical model in comparison with the numerical model for the condition of symmetric crack. Slight errors between -4.2% and -6.0% are observed in the calculation of the total fracture energy and between 2.6% and 7.6% in the fracture mode ratio. In the particular condition of a symmetric crack, literature suggests crack tip corrections in order to account for the effect of crack tip rotation under mode I [31] and mode II [32] fracture. The analytical method with the application of these correction factors presented insignificant errors for the calculation of the total fracture energy and errors lower than 4.0% for the fracture mode ratio – see Table 4.2. In both cases, the use of correction factors resulted in more accurate results. This shows that the effect of crack tip rotation during the experiments may have a non-negligible effect on the fracture behavior although the simple analytical model proved to be reliable.

Table 4.2: Results and errors of the analytical model in the condition of symmetric crack.

Case	Numerical model		Analytical model				Analytical model with crack tip corrections			
	G (J/m^2)	G_{II}/G (%)	G (J/m^2)	Error (%)	G_{II}/G (%)	Error (%)	G (J/m^2)	Error (%)	G_{II}/G (%)	Error (%)
1	362.3	23.2	340.7	-6.0	24.9	7.6	364.7	0.6	24.1	4.0
2	87.7	47.9	83.1	-5.2	50.2	4.8	87.9	0.3	49.1	2.5
3	42.4	73.1	40.6	-4.2	75.0	2.6	42.5	0.2	74.1	1.4

4.4.2 Bi-material crack

A second parametric study was carried out on a bi-material crack with asymmetric geometry. The upper arm has thickness (h_1) of 2.12 mm and the lower arm has thickness (h_2) of 3.0 mm. In order to verify the influence of the fracture mode ratio in the accuracy of the analytical methods, three different conditions were considered: low (c = 95 mm), intermediate (c = 49 mm) and high (c = 34 mm) mode II ratio. Table 4.3 shows the three cases of bi-material crack. The upper arm elastic modulus (E_1) is varied in a wide range of reasonable specimen materials applied to the MMB test. The lower arm has elastic modulus (E_2) of 70 GPa and both arms have Poisson's ratio (ν_1 and ν_2) of 0.33. The crack length is kept at 50 mm and the test load (P) is 100 N, likewise the previous cases.

Table 4.3: Study cases of bi-material crack.

Case	Lever length, c (mm)	h_1 (mm)	h_2 (mm)	E_1 (GPa)	E_2 (GPa)	ν_1; ν_2
4	95	2.12	3.0	**$35 \leq E_1 \leq 210$**	70	0.33
5	49	2.12	3.0	**$35 \leq E_1 \leq 210$**	70	0.33
6	34	2.12	3.0	**$35 \leq E_1 \leq 210$**	70	0.33

Analytical and numerical results of the total fracture energy (G) are presented in Figure 4.11. Both analytical methods give the same results for any material. Figures 4.11a, 4.11b and 4.11c show the three cases of low, intermediate and high mode II fracture, respectively. Both analytical methods are in very good agreement with the

FEM/VCCT results, hence, the analytical methods based on beam analysis provide reliable results of the total fracture energy on bi-material cracks.

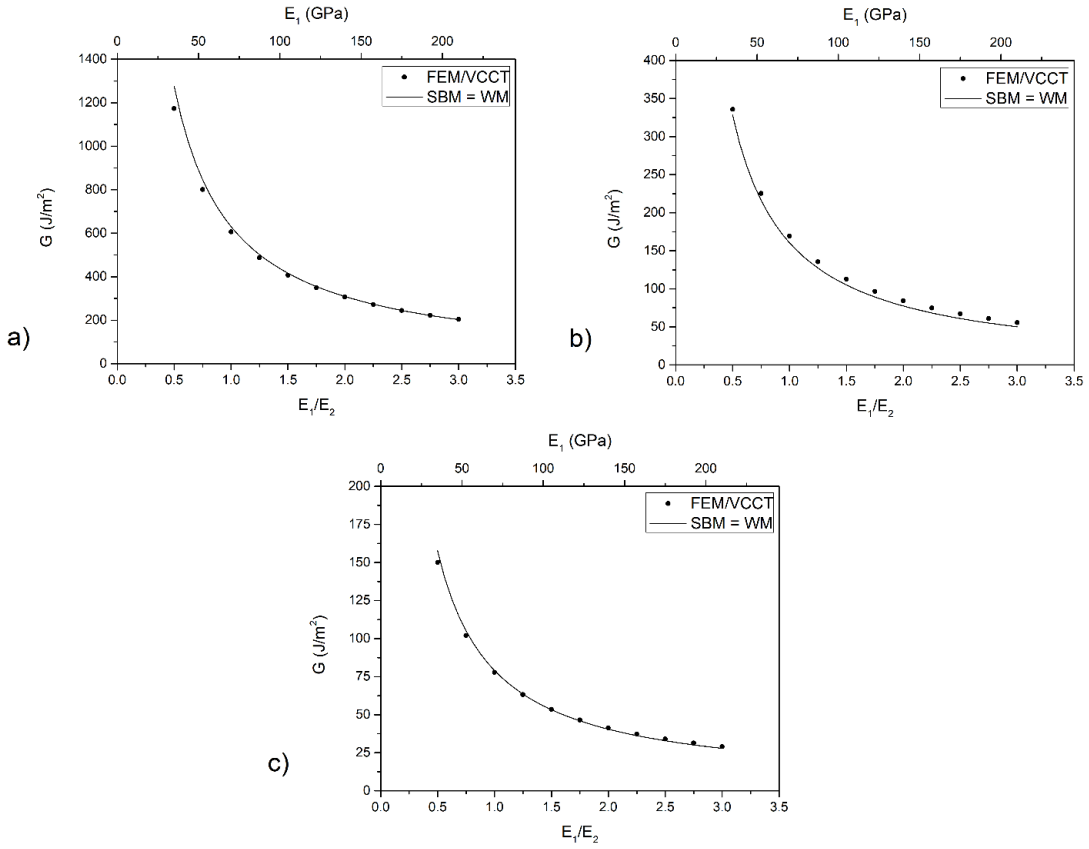


Figure 4.11: Total fracture energy with the variation of the specimen material: cases (a) 4 – low, (b) 5 – intermediate and (c) 6 – high mode II.

Figure 4.12 shows the analytical and numerical fracture mode ratio (G_{II}/G). For the applied parameters, the strain-equivalent geometry ($\beta = 1$) is achieved when E_1/E_2 equals 2.0. In the case of low mode II (case 4), shown in Figure 4.12a, the SBM shows good agreement with the FEM/VCCT despite the remarkable asymmetry of the materials and geometry. However, as β differs from 1, WM gives significant discrepancies from the FEM/VCCT results. This shows that the analytical method based on beam analysis is only valid for when the strain-equivalence condition is respected. Similar results are observed as the mode II fracture ratio increases, presented in Figures 4.12b and 4.12c (cases 5 and 6, respectively). Moreover, it is shown once more that WM is only valid when the condition of strain equivalence is satisfied ($\beta = 1$). For any other geometry, it gives incorrect fracture mode ratios because it ignores the coupling effect between

fracture modes. Figure 4.13 shows that the coupling function f_c is zero in the case of a strain-equivalent geometry ($\beta = 1$). In any other geometry, the influence of the mode I and mode II coupling may have a large effect on the fracture mode of bi-material cracks. This explains the requirement of the strain-based design criterion for obtaining the correct partitioning ratio.

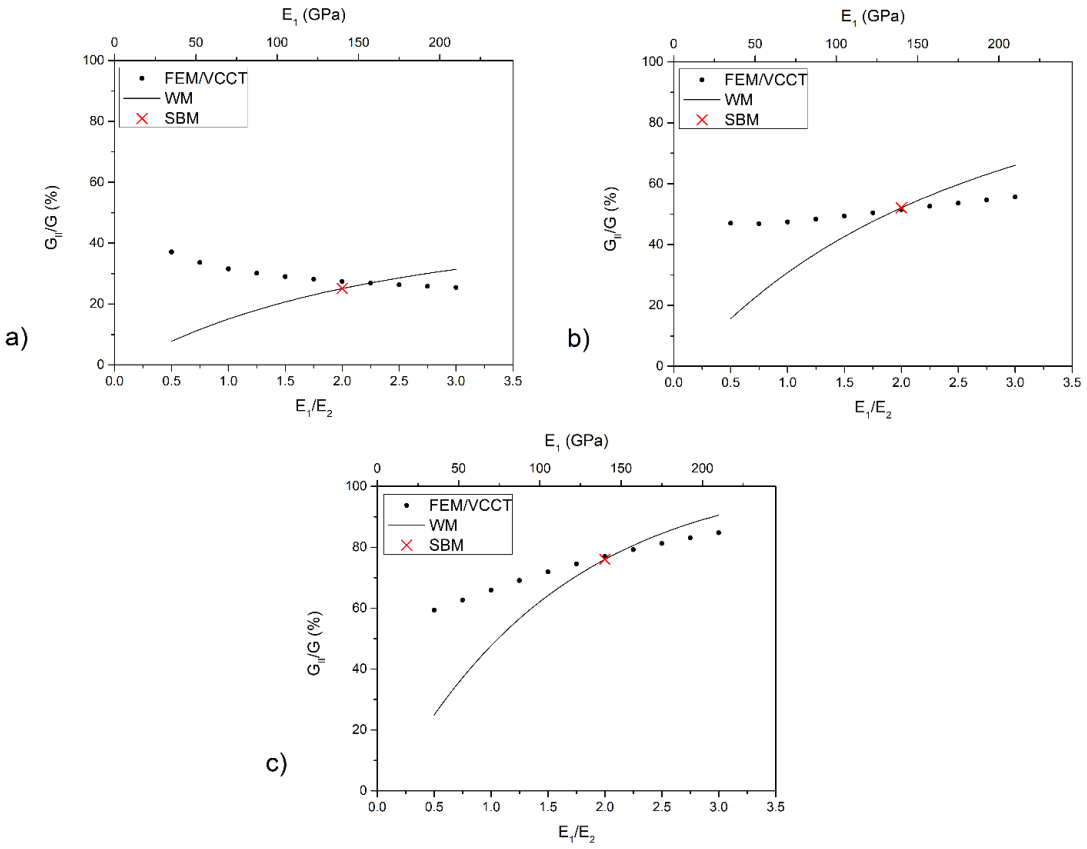


Figure 4.12: Fracture mode ratio with the variation of specimen material: cases (a) 4 – low, (b) 5 – intermediate and (c) 6 – high mode II.

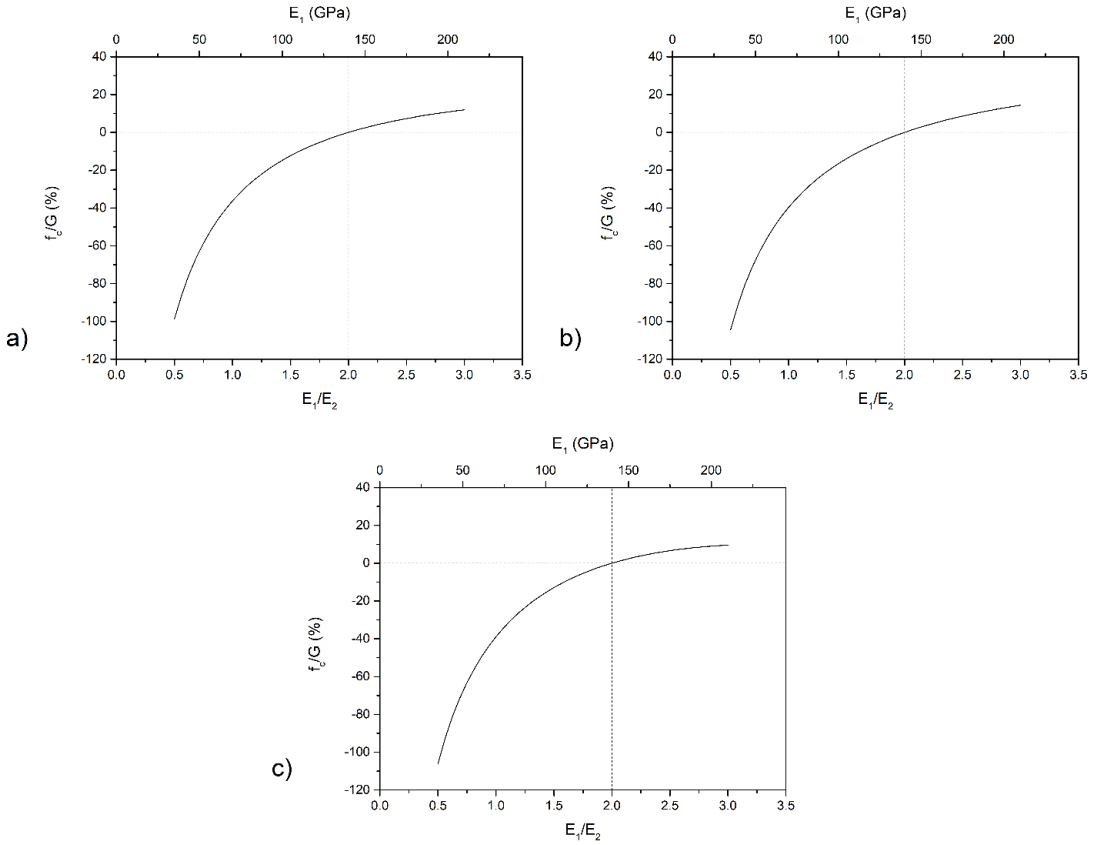


Figure 4.13: Influence of the coupling function on the fracture energy: cases (a) 4 – low, (b) 5 – intermediate and (c) 6 – high mode II.

Table 4.4 shows the results and errors of the analytical model in comparison with the numerical model for the particular condition of strain equivalence proposed in the SBM (see Equation 19). Errors between 1.0% and -8.1% are observed in the calculation of the total fracture energy and between 1.1% and -8.6% in the fracture mode ratio. These errors are in a similar degree as cases 1, 2 and 3 of symmetric condition, presented in Table 4.2. Therefore, it can be implied that the effect of crack tip rotation is also a major cause of the errors produced in cases 4, 5 and 6 of bi-material cracks using the SBM.

Table 4.4: Results and errors of the analytical model in the condition of strain equivalence.

Case	Numerical model		Strain-Based Method (SBM)			
	G (J/m^2)	G_{II}/G (%)	G (J/m^2)	Error (%)	G_{II}/G (%)	Error (%)
4	306.0	27.5	309.0	1.0	25.1	-8.6
5	84.2	51.5	77.4	-8.1	52.1	1.1
6	41.3	77.0	40.5	-2.0	76.0	-1.3

4.5 Case study

In this section, the mixed-mode fracture behavior of a bi-material bonded joint is determined from experiments using the SBM and the FEM. Composite-to-metal bonded specimens were manufactured in thin and thick geometries and tested using the MMB apparatus. The aim is to verify the accuracy of the SBM against significant shear effects and its limitations for the characterization of a crack propagation between different materials and geometry.

4.5.1 Materials and methods

Composite-to-metal bonded specimens were manufactured using similar materials and methods of composite repair application to metal structures in offshore industry [43]. Specimens with two different geometries were produced. Carbon steel plates (ASTM A36) with 6.35 mm and 3.18 mm thickness were selected for the metal adherend. The steel surface was blasted with steel grit (G-40) and degreased with acetone. An epoxy adhesive (NVT201E, Novatec, Brazil) with a glass transition temperature (T_g) of 80 ºC was applied. One layer of glass fiber chopped strand mat with a density of 300 g/m^2 was inserted between the adherends on half of the plate. Bidirectional carbon fiber fabrics (LTC450-C10-C, DEVOLD AMT, Norway) with density of 430 g/m^2 and epoxy lamination resin (PIPEFIX, Polinova S.A., Brazil) with a T_g of 116 °C and working life of 30 minutes were selected for the composite adherend. The composite adherend was manufactured by hand lay up on the treated metal surface. The first unidirectional carbon ply in contact with the glass fiber mat was placed at the length direction (0º). Ten layers of 0/90º carbon fibers were laminated on the thin metal plate and 20 layers were applied on the thick metal plate. The adhesive and resin curing process occurred simultaneously in approximately 2 hours at room temperature. The mechanical properties of the materials were obtained from a previous work [44] and are shown in Table 4.5.

Specimens were cut from the plates using a bandsaw with a high-speed steel blade and cutting oil. Measurements of width and thickness were obtained with a digital caliper at 30 mm from both ends and at center of the specimens. The thick specimens have an average width of 24.9±0.3 mm and an average thickness of 20.1±0.4 mm. The thin specimens have an average width of 25.3±0.2 mm and an average thickness of 9.5±0.2 mm. The average length of both specimens is 180±1 mm and was measured with a ruler. The specimen geometry was designed in accordance with the criterion of strain equivalence between arms (see Equation 19) although a high precision thickness of the composite materials is impracticable. An anti-friction material was applied between the metal plate and the adhesive in order to produce a pre-cracked region of 50 mm length.

Table 4.5: Mechanical properties of the materials.

Material	**Elastic Modulus, E_{11} (GPa)**	**Poisson's Ratio, ν_{12}**
Steel	200	0.27
Composite 0/90	46	0.24
Adhesive	2.25	0.38

MMB tests (see Figure 4.2) were performed using a servo-hydraulic testing machine (MTS 831, MTS Systems Corporation) coupled with a 10 kN load cell. Specimens were positioned with the metal arm on top and the lever length (c) of 78 mm and 110 mm were set for the thick and thin samples, respectively. Table 4.6 shows the test matrix. The half-span (L) of the test is 70 mm and the initial crack length (a_0) of 30 mm was obtained after bonding the end-blocks. The testing load was applied at the quasi-static rate of 0.5 mm/min. with displacement control. Load-displacement points were obtained during the test and a high-resolution camera is positioned for crack length monitoring. The numerical results were obtained from the model of a bi-material crack, as described in section 4.3.2, with the actual properties presented in Table 4.5 and the geometry shown in Table 4.6. The analytical results were calculated using the SBM using the same parameters as the numerical model. The input composite thickness was slightly adapted in order to have the required strain equivalence condition (see Equation 4.19).

Table 4.6: Test matrix.

Test	Specimen	Metal arm thickness, h_1 (mm)	Composite arm thickness, h_2 (mm)	Lever length, c (mm)	Lever center of gravity, c_g (mm)	Lever weight, P_g (kg)
1	thick	6.35	13.35	78	31	17.6
2	thick	6.35	13.35	78	31	17.6
3	thin	3.18	6.34	110	40	17.6
4	thin	3.18	6.34	110	40	17.6

4.5.2 Results and discussion

Results of the MMB tests in thick and thin composite-to-metal specimens are shown in Figure 4.14 and 4.15, respectively. Crack propagation points were obtained for every 1 mm of crack step. Tests 1 and 2 in thick specimens (Figure 4.14a and 4.14b, respectively) reached maximum loads between 800 N and 1000 N at crack initiation and decreased to values between 600 N and 700 N at the final crack length of 65 mm with displacements near 1.5 mm. In the case of thin specimens, tests 3 and 4 (Figure 4.15a and 4.15b, respectively) presented maximum loads between 200 N and 250 N at crack initiation and values between 100 N and 150 N at the final crack length of 65 mm with displacements near 4.0 mm.

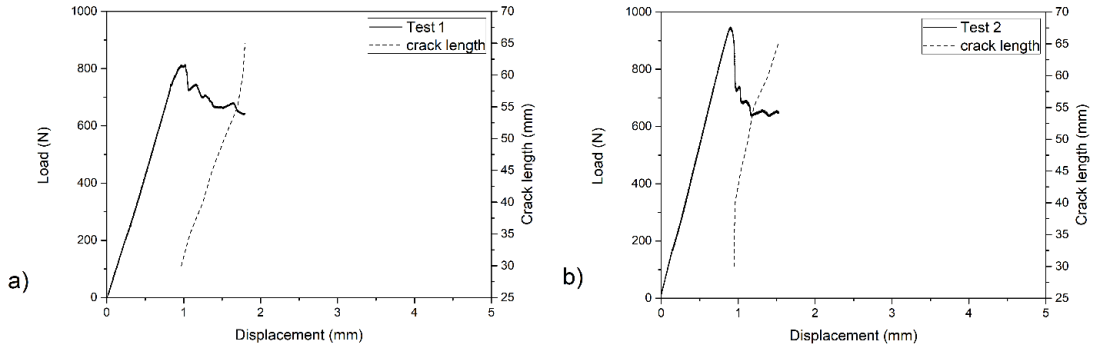


Figure 4.14: MMB test results of thick specimens.

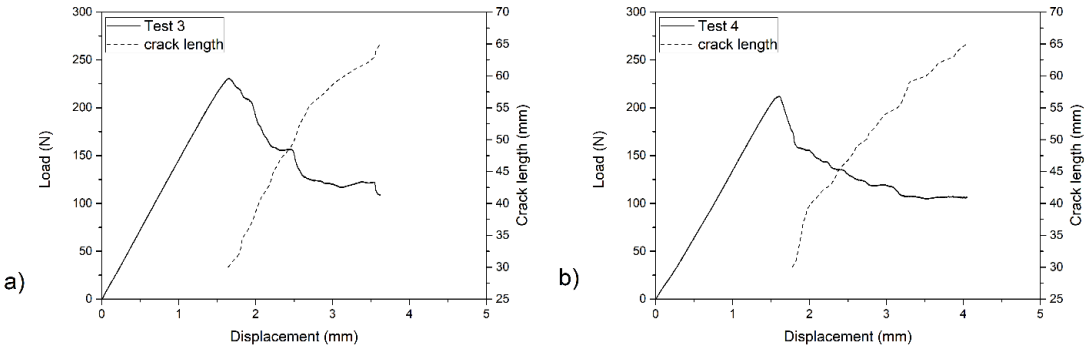


Figure 4.15: MMB test results of thin specimens.

The total fracture energy and mode ratio were obtained at crack propagation using the SBM and the FEM. Figures 4.16a and 4.16b show the total fracture energy of Tests 1 and 2 in thick specimens. The SBM produced an error of 27.8% in the first measurement of crack propagation and reduced as the crack length increases, down to 11.4% in the last propagation point. The fracture mode ratio (G_{II}/G) presented nearly constant values of 23.5% in the SBM and 21.5% in the FEM, as observed in Figure 4.16c. A constant fracture mode ratio is expected from the MMB test. The total fracture energy of Tests 3 and 4, in thin specimens, are presented in Figure 4.17a and 4.17b, respectively. In this geometry, the SBM produced an error of 13.2% in the first measurement of crack propagation and reduced as the crack length increases, down to 2.6% in the last propagation point. The analytical method produced more accurate results in the thin specimens compared to the thick ones. Moreover, the analytical solution showed more accuracy as the crack length increases, similarly to reference [40]. These results are attributed to the reduction of transverse shear effect that are not considered in the analytical model but can be significant in specimens with relatively large thickness Finally, thin specimens presented a nearly constant fracture mode ratio (G_{II}/G) of 19.8% from both the SBM and the FEM. This shows the accuracy of the analytical solution and agrees with the results obtained from the parametric study in the previous section. Overall, the SBM gives reliable results for the calculation of the total fracture energy and mode ratio of bi-material crack as long as the shear effects are negligible.

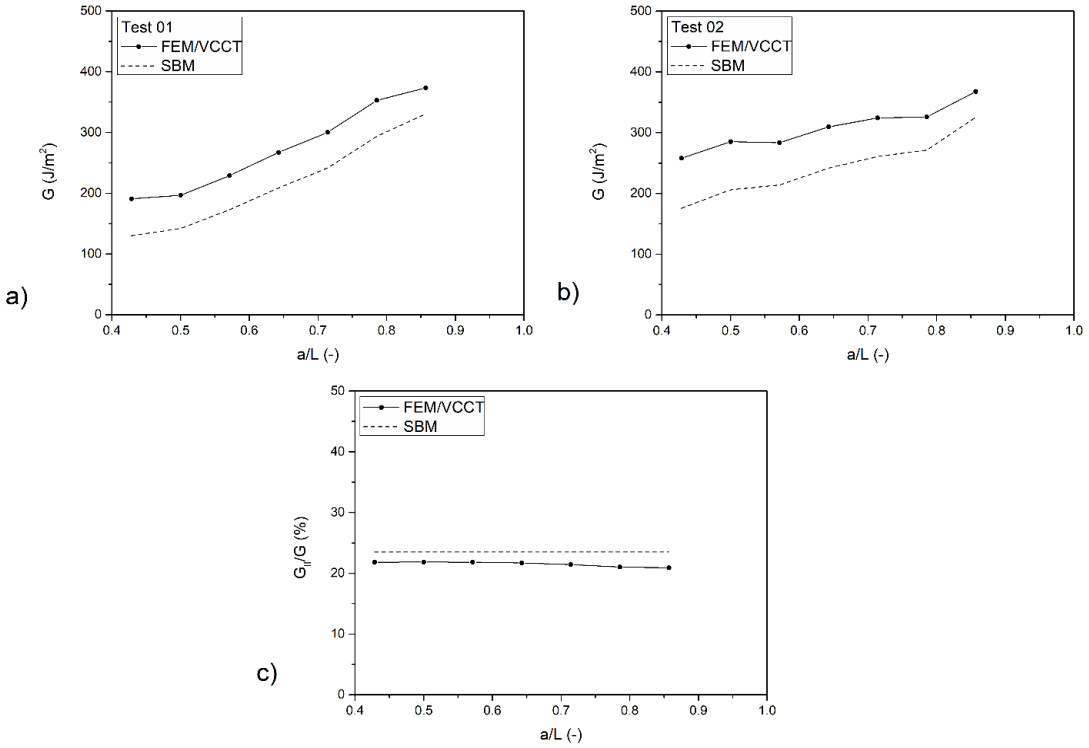


Figure 4.16: Total fracture energy and mode ratio of thick specimens.

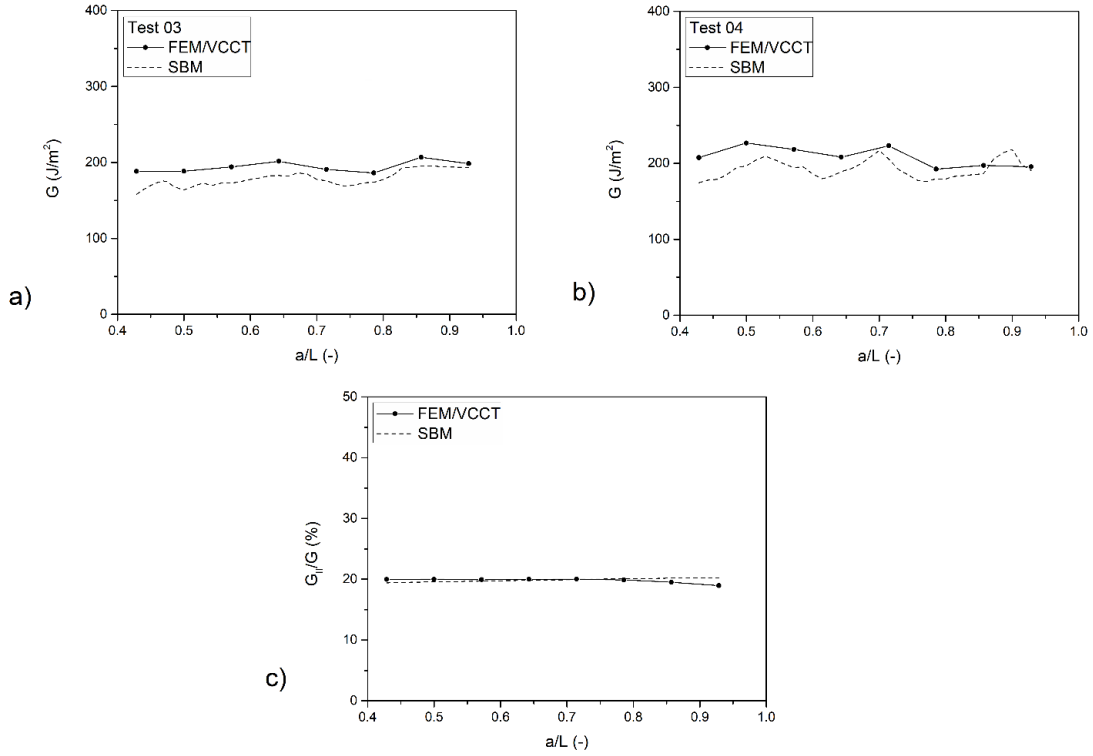


Figure 4.17: Total fracture energy and mode ratio of thin specimens.

4.6 Conclusion

In this Chapter, the strain-based method (SBM) is evaluated for the mixed-mode fracture characterization of asymmetric cracks. The fracture energy at the crack tip of mixed-mode bending (MMB) is determined using SBM, the widely applied Williams' partitioning method (WM) and finite element models using the virtual crack closure technique (VCCT). The total fracture energy and mode ratio is obtained for a wide range of specimen thicknesses and materials.

The analytical methods based on beam analysis give good predictions of the total fracture energy of crack propagation with geometrical and/or material asymmetry. However, WM does not consider the coupling effect of mode I and mode II fracture energy and for that reason produces incorrect results of the fracture mode ratio in asymmetric cracks.

The SBM predicts a coupling relationship between the pure modes that allows obtaining the fracture mode ratio of bi-material cracks through a simple design criterion based on the longitudinal strain equivalence between specimen's arms. SBM shows to be a reliable method that allows characterizing the mixed-mode fracture of asymmetric cracks through a simple formulation. The main limitation identified in the SBM are that it does not consider the transverse shear effect. Using SBM in specimens with relatively large thickness may produce significant errors and, therefore, geometrical limitations should be considered in the specimen design.

References

[1] Budhe, S.; Banea, M.D.; de Barros, S. An updated review of adhesively bonded joints in composite materials. Int. J. Adhes. Adhes. 2017, 72, 30-42.

[2] Mangalgiri, P.D. Composite materials for aerospace applications. Bull. Mater. Sci. 1999, 22, 657-664.

[3] Teixeira de Freitas, S.; Sinke, J. Failure analysis of adhesively-bonded skin-to-stiffener joints: Metal–metal vs. composite–metal. Eng. Failure Anal. 2015, 56, 2-13.

[4] Teixeira de Freitas, S.; Sinke, J. Failure analysis of adhesively-bonded metal-skin-to-composite-stiffener: Effect of temperature and cyclic loading. Compos. Struct. 2017, 166, 27-37.

[5] Taub, A.I.; Krajewski, P.E.; Luo, A.A. The evolution of technology for materials processing over the last 50 years: the automotive example. JOM 2007, 59, 48-57.
[6] McGeorge, D.; Echtermeyer, A.T.; Leong, K.H.; Melve, B.; Robinson, M.; Fischer, K.P. Repair of floating offshore units using bonded fibre composite materials. Compos. Part A 2009, 40(9), 1364-1380.
[7] Saleh, M.N.; Saeedifar, M.; Zarouchas, D.; Teixeira de Freitas, S. Stress analysis of double-lap bi-material joints bonded with thick adhesive. Int. J. Adhes. Adhes. 2020, 97, 102480.
[8] Van Den Einde, L.; Zhao, L.; Seible, F. Use of FRP composites in civil structural applications. Constr. Build. Mater. 2003, 17(6-7), 389-403.
[9] Chaves, F.J.P.; da Silva, L.F.M.; de Moura, M.F.S.F.; Dillard, D.A.; Esteves, V.H.C. Fracture Mechanics Tests in Adhesively Bonded Joints - A Literature Review. J. Adhes. 2014, 90(12), 955-992.
[10] Xiao, F.; Hui, C.-Y.; Kramer, E.J. Analysis of a mixed mode fracture specimen: the asymmetric double cantilever beam. J. Mater. Sci. 1993, 28, 5620-5629.
[11] Park, S.; Dillard, D.A. Development of a simple mixed-mode fracture test and the resulting fracture energy envelope for an adhesive bond. Int. J. Fract. 2007, 148, 261-271.
[12] Russell, A.J.; Street, K.N. Moisture and Temperature Effects on the Mixed-Mode Delamination Fracture of Unidirectional Graphite/Epoxy Delamination and Debonding of Materials. West Conshohocken, PA, ASTM International, 349-370, 1985.
[13] Yoon, S.H.; Hong, C.S. Modified end notched flexure specimen for mixed mode interlaminar fracture in laminated composites. Int. J. Fract. 1990, 43, R3-R9.
[14] Davidson, B.D.; Sundararaman, V. A single leg bending test for interfacial fracture toughness determination. Int. J. Fract. 1996, 78(2), 193-210.
[15] Szekrényes, A.; József, U.J. Over-leg Bending Test for Mixed-mode I/II Interlaminar Fracture in Composite Laminates. Int. J. Damage Mech. 2007, 16(1), 5-33.
[16] Reeder, J.R.; Crews Jr, J.H. Mixed-Mode bending method for delamination testing. AIAA J. 1990, 28(7), 1270-1276.
[17] Reeder, J.R.; Crews Jr., J.H. Redesign of the Mixed-mode Bending Delamination Test to Reduce Non-linear Effects. J. Compos. Technol. Res. 1992, 14(1), 12-19.
[18] Ducept, F.; Gamby, D.; Davies, P. A mixed-mode failure criterion derived from tests on symmetric and asymmetric specimens. Compos. Sci. Technol. 1999, 59(4), 609-619.

[19] Pereira, A.B; de Morais, A.B. Mixed mode I + II interlaminar fracture of glass-epoxy multidirectional laminates – Part 2 Experiments. Compos. Sci. Technol. 2006, 66(13), 1896-1902.

[20] Kim, B.W.; Mayer, A.H. Influence of fiber direction and mixed-mode ratio on delamination fracture toughness of carbon/epoxy laminates. Compos. Sci. Technol. 2003, 63(5), 695-713.

[21] Liu, Z.; Gibson, R.F.; Newaz, G.M. The Use of a Modified Mixed Mode Bending Test for Characterization of Mixed-Mode Fracture Behavior of Adhesively Bonded Metal Joints. J. Adhes. 2010, 78(3), 223-244.

[22] Stamoulis, G.; Carrere, N.; Cognard, J.Y.; Davies, P.; Badulescu, C. On the experimental mixed-mode failure of adhesively bonded metallic joints. Int. J. Adhes. Adhes. 2014, 51, 148-158.

[23] Droubi, M.G.; Mcafee, J.; Horne, R.C.; Walker, S.; Klaassen, C.; Crawford, A.; Prathuru, A.K.; Faisal, N.H. Mixed-mode fracture characteristics of metal-to-metal adhesively bonded joints - experimental and simulation methods. Procedia Structural Integrity 2016, 5, 40-47.

[24] Oliveira, J.M.Q.; de Moura, M.F.S.F.; Silva, M.A.L.; Morais, J.J.L. Numerical analysis of the MMB test for mixed-mode I/II wood fracture. Compos. Sci. Technol. 2007, 67(9), 1764-1771.

[25] de Moura, M.F.S.F.; Oliveira, J.M.Q.; Morais, J.J.L; Dourado, N. Mixed-mode (I + II) fracture characterization of wood bonded joints. Constr. Build. Mater. 2011, 25(4), 1956-1962.

[26] Yoshihara, H. Initiation and propagation fracture toughness of solid wood under the mixed Mode I-II condition examined by mixed-mode bending test. Eng. Fract. Mech. 2013, 104, 1-15.

[27] Pereira, F.A.M.; de Moura, M.F.S.F.; Dourado, N.; Morais, J.J.L.; Silva, F.G.A.; Dias, M.I.R. Bone fracture characterization under mixed-mode I + II loading using the MMB test. Eng. Fract. Mech. 2016, 166, 151-163.

[28] Krueger, R. Virtual crack closure technique: History, approach, and applications. Appl. Mech. Rev. 2004, 57(2), 109-143.

[29] Pereira, A.B.; de Morais, A.B. Mixed mode I + II interlaminar fracture of carbon/epoxy laminates. Compos. Part A 2008, 39(2), 322-333.

[30] Williams, J.G. On the calculation of energy release rates for cracked laminates. Int. J. Fract. 1988, 36, 101-119.
[31] Williams, J.G. End corrections for orthotropic DCB specimens. Comp. Sci. Tech. 1989, 35(4), 367-376.
[32] Wang, Y.; Williams, J.G. Corrections for mode II fracture toughness specimens of composites materials. Compos. Sci. Tech. 1992, 43(3), 251-256.
[33] Shahverdi, M.; Vassilopoulos, A.P.; Keller, T. Mixed-Mode I/II fracture behavior of asymmetric adhesively-bonded pultruded composite joints. Eng. Fract. Mech. 2014, 115, 43-59.
[34] de Morais, A.B.; Pereira, A.B. Mixed-mode I + II interlaminar fracture of glass/epoxy multidirectional laminates – Part 1: Analysis. Compos. Sci. Tech. 2006, 66(13), 1889-1895.
[35] Harvey, C.M.; Wang, S. Experimental assessment of mixed-mode partition theories. Compos. Struct. 2012, 94(6), 2057-2067.
[36] Wang, W.; Teixeira de Freitas, S.; Poulis, J.A.; Zarouchas, D. A review of experimental and theoretical fracture characterization of bi-material bonded joints. Compos. Part B. 2021, 206, 108537.
[37] Arouche, M.M.; Teixeira de Freitas, S.; de Barros, S. On the influence of glass fiber mat on the mixed-mode fracture of composite-to-metal bonded joints. Compos. Struct. 2021, 256, 113109.
[38] Valvo, P.S. On the calculation of energy release rate and mode mixity in delaminated laminated beams. Eng. Fract. Mech. 2016, 165, 114-139.
[39] Wang, W.; Fernandes, R.L.; Teixeira de Freitas, S.; Zarouchas, D. How Pure Mode I Can Be Obtained in Bi-Material Bonded DCB Joints: A Longitudinal Strain-Based Criterion. Compos. Part B 2018, 153, 137-148.
[40] Arouche, M.M.; Wang, W.; Teixeira de Freitas, S., de Barros, S. Strain-based methodology for mixed-mode I+II fracture: A new partitioning method for bi-material adhesively bonded joints. J. Adhes. 2019, 95(5-7), 385-404.
[41] Ouyang, Z.; Ji, G.; Li, G. On Approximately Realizing and Characterizing Pure Mode-I Interface Fracture Between Bonded Dissimilar Materials. J. Appl. Mech. 2011, 78(3), 031020.

[42] Mollón, V.; Bonhomme, J.; Argüelles, A.; Viña, J. Influence of the crack plane asymmetry over GII results in carbon epoxy ENF specimens. Compos. Struct. 2012, 94(3), 1187-1191.
[43] Arouche, M.M.; Budhe, S.; Alves, L.A.; Teixeira de Freitas, S.; Banea, M.D.; de Barros; S. Effect of moisture on the adhesion of CFRP-to-steel bonded joints using peel tests. J. Braz. Soc. Mech. Sci. Eng. 2018, 40,10.
[44] Teixeira de Freitas, S.; Banea, M.D.; Budhe, S.; de Barros, S. Interface adhesion assessment of composite-to-metal bonded joints under salt spray conditions using peel tests. Compos. Struct. 2017, 164, 68-75.

Chapter 5

Design and Manufacturing Parameters

In this Chapter, the influence of a layer of glass fiber mat (GFM) inserted in a bi-material bonded joint interface is investigated as a toughening mechanism to improve the fracture performance of bonded structures. Composite-to-metal bonded specimens were manufactured by hand lay-up using two different consolidation processes: at room pressure or using vacuum bagging. The fracture behavior was evaluated under quasi-static loadings using the mixed-mode bending (MMB) test. Test results revealed an increase of the fracture toughness with the insertion of an adjacent layer of GFM. The toughening mechanism is associated with a more irregular fracture surface profile. It was verified a relationship between the fracture surface roughness and the fracture toughness. The toughening effect showed to be more evident in higher mode II fracture conditions. The insertion of a layer of GFM and the use of vacuum pressure in the consolidation of the composite increase the fracture performance of composite repairs in metal structures.

Keywords: mixed-mode bending (MMB) test, composite materials, bi-material bonded joints, crack propagation, toughening mechanism, fracture surfaces, roughness, fractography.

This chapter is based on the journal article: "On the influence of glass fiber mat on the mixed-mode fracture of composite-to-metal bonded joints", published in Composite Structures 256:113109 (2021).

5.1 Introduction

The requirement of lightweight structures has encouraged the introduction of composite materials in industrial applications [1]. First applications of composite structures are found in aerospace industry [2-3] and have been expanded to many other fields, such as automotive [4] and construction [5]. Adhesive bonding technology is generally the preferred joining method for composite structures as they provide enhanced stress transfer mechanisms and design flexibility [6]. The selection of the manufacturing method usually depends on the analysis of several parameters, such as substrates to be bonded, service conditions and area of application [1, 7-9].

Recently, composite materials technology has been introduced to the maintenance routine in offshore industry [10]. Oil and gas production platforms are projected to remain more than 20 years in operation. The floating vessels are subjected to harsh environment and a large maintenance routine is necessary in order to ensure structural integrity and continuous production. During the life cycle of a plant, repairs on metallic structures are crucial as result of corrosion and fatigue degradation. The composite repair technology arises as a promising alternative for the rehabilitation of pipes [10-11], tanks [12] and ship hull [13]. The technology has the advantage of avoiding hot work, which is safer and does not require to stop the production. A composite patch is bonded to a damaged metallic structure in order to re-establish the structural integrity. In the repair, a carbon fiber composite patch is usually manufactured using hand lay-up [14]. This leads to new applications of adhesively bonded structures between composite and metal adherends.

The fracture mechanics approach is widely applied to improve the design and evaluate the performance of structures. In the cases of delamination and debonding, cracks usually propagate along an interface. In real-life applications, interfacial fracture often propagates in a combination of opening (mode I) and shear (mode II) loadings. A variety of experimental procedures is available for mixed-mode fracture testing [15]. Among them, the mixed-mode bending (MMB) test [16-17] stands out for its easy implementation and capability of testing a wide range of partitioning ratios with only one specimen geometry. The MMB test method was originally developed for fracture propagation of unidirectional symmetric composites and was later extended to

multidirectional laminates [18-19], metal bonded joints [20-21], sandwich specimen face/core debonding [22] and bi-material bonded joints [23].

The crack propagation path in a bonded structure depends on the fracture resistance of the adherends, the interface toughness and the applied fracture mode ratio [24]. An interfacial crack in a composite bonded structure may kink into the composite adherend. Crack migration is encouraged by a relatively low delamination fracture toughness of the composite material compared to the interface and high shear loadings at the crack tip. In these cases, the bonded interface does not influence the fracture toughness. Instead, an interlaminar fracture occurs and the adjacent composite layer to the bonded interface has an important role in the fracture performance of the structure [25]. The fracture performance of a composite laminate may be increased by design optimization of the lay-up sequence [26]. However, the development of composite toughening methods has a greater potential for surpassing the limitations of the current material systems [27]. The choice of a toughening method depends on the structural requirements, in service conditions and available manufacture technology.

Kuwata and Hogg investigated the toughening effect of interleaved fiber veil on a carbon fiber reinforced polymer (CFRP) under pure mode I [28]. They associated the toughening mechanism to the effect of fiber-bridging. The work of Hosseini et al. [29] revealed a decrease in the pure mode I fracture toughness of a woven glass/epoxy composite with inserted glass fiber chopped strand mat at the delamination interface. Regarding the pure mode II fracture, toughening mechanisms are less dependent on fiber bridging and more affected by additional factors beyond the material of the delamination interface [30]. However, these studies address only the pure modes and a limited combination of bonded materials. Additional studies are required in order to understand the fracture toughening mechanisms and improve the performance of structures.

Boccaccini and Winkler [31] correlated the increase in the fracture toughness of a composite with a crack deflection mechanism. An experimental study in sandwich structures showed that the fracture toughness can increased by inserting a layer of mat with randomly oriented fibers between the adherends [32]. Karger-Kocsis et al. [33] obtained higher fracture stresses and enlarged damage zone in polypropylene composite with glass fiber mat compared with long glass fiber reinforcement. Huang et al. [34] analyzed the interlaminar toughening of carbon-fiber/epoxy composite laminates with

chopped aramid fibers. Kopp et al. [35] showed that the topography of the fracture surfaces has an intrinsic effect in the fracture characterization of materials. Sun et al. [36] obtained higher fracture toughness in a composite-to-metal bonded joint by interleaving short aramid fibers and altering surface treatments. These works suggest that the fracture surfaces profile of the delamination interface has an important role in the fracture toughness performance of the structure.

Present literature does not fully address the toughening mechanisms associated to the use of a mat in bonded joints, particularly under mixed-mode fracture conditions. A detailed analysis is required in order to describe the toughening effect in new applications of bonded structures. In this Chapter, the influence of a layer of glass fiber mat (GFM) in the fracture performance of a bi-material bonded joint is investigated. Composite-to-metal bonded specimens are manufactured by hand lay-up with two different consolidation processes: at room pressure or using vacuum bagging. The mixed-mode fracture behavior is assessed under quasi-static loadings using the MMB test. The crack propagation mechanisms resulted from the insertion of a layer of GFM between the adherends is verified with a fracture surface analysis.

5.2. Materials and methods

5.2.1 Specimen design and manufacture

Composite-to-metal bonded specimens were manufactured in order to simulate the application of a composite repair to a metal structure in offshore industry [14]. A carbon steel plate (ASTM A36) of 3.18 mm thickness was selected for the metal adherend. The steel surface was blasted with steel grit (G-40) and degreased with acetone. An anti-friction material was applied in order to produce a pre-cracked region. A brittle epoxy adhesive (NVT201E, Novatec, Rio de Janeiro, Brazil) with a glass transition temperature (T_g) of 80 ºC was applied. One layer of glass fiber chopped strand mat with a density of 300 g/m^2 was inserted between the adherends on half of the plate. Bidirectional carbon fiber fabrics (LTC450-C10-C, DEVOLD AMT, Langevåg, Norway) with density of 430 g/m^2 and epoxy lamination resin (PIPEFIX, Polinova S.A., Rio de Janeiro, Brazil) with a T_g of 116 °C and working life of 30 minutes were selected for the composite adherend.

Two CFRP-to-steel plates were manufactured by hand lay-up of carbon fiber fabrics on the treated steel surface. Hand rollers are used to compact the composite layers. The first plate is consolidated at room pressure and has a total of 10 layers of 0/90 carbon fibers. The second plate was consolidated using vacuum bagging. In this case, 12 layers of 0/90 carbon fibers were laminated in order to produce a similar composite thickness after curing. The layer of 0º carbon fibers adjacent to the adhesive interface was placed at the length direction and the cure process took approximately 2 hours at room temperature. Mechanical properties of the materials [37] are presented in Table 5.1.

Table 5.1: Mechanical properties of the materials.

Material	**Elastic Modulus, E_{11} (GPa)**	**Poisson's Ratio, ν_{12}**
Steel	200	0.27
Composite 0/90	46	0.24
Adhesive	2.25	0.38

Specimens were cut from the plates and measured with a digital caliper from three different regions: 30 mm from the sides and at center of the specimens. The length was obtained with a ruler. Table 5.2 shows the average measurements of the different specimen configurations: manufactured at room pressure without glass fiber mat (RP) and with glass fiber mat (RP/GFM); and manufactured using vacuum bagging without (VB) and with glass fiber mat (VB/GFM).

Table 5.2: Specimen measurements.

Specimens	**Manufacture Process**	**Design**	**Thickness (mm)**	**Width (mm)**	**Length (mm)**
RP	room pressure	without GFM	9.49±0.34	25.11±0.11	180±1
RP/GFM	room pressure	with GFM	9.82±0.45	25.31±0.14	180±1
VB	vacuum bagging	without GFM	9.95±0.27	25.08±0.14	180±1
VB/GFM	vacuum bagging	with GFM	10.07±0.36	25.29±0.10	180±1

5.2.2 Experimental method

The mixed-mode bending (MMB) test was chosen for the experimental mixed-mode fracture analysis of the specimens. In the MMB test, a loading is applied through a roller attached to a lever and loaded just above the mid-plane of the test specimen. The test loading (P) is decomposed in opening (P_I) and shear (P_{II}) loadings in a constant ratio determined by the lever length (c), as shown in Figure 5.1. The mode I fracture ratio increases with the lever length. The lever weight produces a load (P_g) on the specimen at the length of the lever center of gravity (c_g). The test half-span (L) is set to 70 mm and the initial crack length (a) is 30 mm.

Tests were conducted using a servo-hydraulic testing machine (MTS 831, MTS Systems Corporation) coupled with a 10 kN load cell. The testing loads were applied at the quasi-static rate of 0.5 mm/min. with displacement control. Table 5.3 shows the test configurations. Specimens were tested in 75% and 40% mode II fracture ratio. The fracture partitioning ratio was obtained from a finite element model [23]. Load-displacement points were obtained during the test and a high-resolution camera was positioned for crack length monitoring.

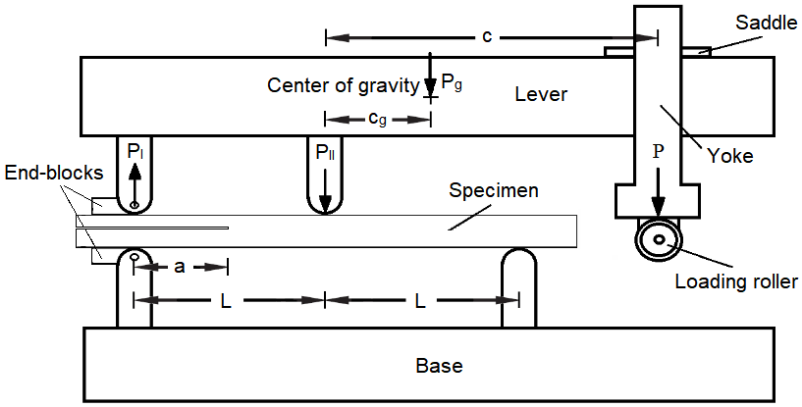


Figure 5.1: MMB test scheme.

Table 5.3: Test matrix.

Test	Specimen	Manufacture Process	Design	Lever length, c (mm)	G_{II}/G (%)
01	RP-1	room pressure	without GFM	42	75
02	RP-2	room pressure	without GFM	42	75
03	RP-3	room pressure	without GFM	42	75
04	RP-4	room pressure	without GFM	42	75
05	RP/GFM-1	room pressure	with GFM	42	75
06	RP/GFM-2	room pressure	with GFM	42	75
07	RP/GFM-3	room pressure	with GFM	42	75
08	RP/GFM-4	room pressure	with GFM	42	75
09	VB-1	vacuum bagging	without GFM	42	75
10	VB-2	vacuum bagging	without GFM	42	75
11	VB-3	vacuum bagging	without GFM	42	75
12	VB/GFM-1	vacuum bagging	with GFM	42	75
13	VB/GFM-2	vacuum bagging	with GFM	42	75
14	VB/GFM-3	vacuum bagging	with GFM	42	75
15	VB-4	vacuum bagging	without GFM	110	40
16	VB-5	vacuum bagging	without GFM	110	40
17	VB/GFM-4	vacuum bagging	with GFM	110	40
18	VB/GFM-5	vacuum bagging	with GFM	110	40

5.3 Test results

Load-displacement curves were obtained from the tests. Tests were performed until the crack length reaches 65 mm and the propagation points were obtained in each 5 mm crack step. Some non-linearity may be observed in the beginning of the test due to the initial load distribution on the testing apparatus. Results of specimens manufactured at room pressure and tested under 75% mode II fracture are shown in Figures 5.2 and 5.3. A more abrupt load drop occurred in three out of the four tests performed in specimens without GFM (Figure 5.2a, 5.2c and 5.2d), while only test RP-2 (Figure 5.2b) presented a stepwise propagation. Regarding the specimens with GFM, Figure 5.3 shows that a stepwise crack propagation occurred in all tests. Additionally, specimens with GFM

(Figure 5.3) presented slightly higher testing loadings compared with the specimens without GFM (Figure 5.2).

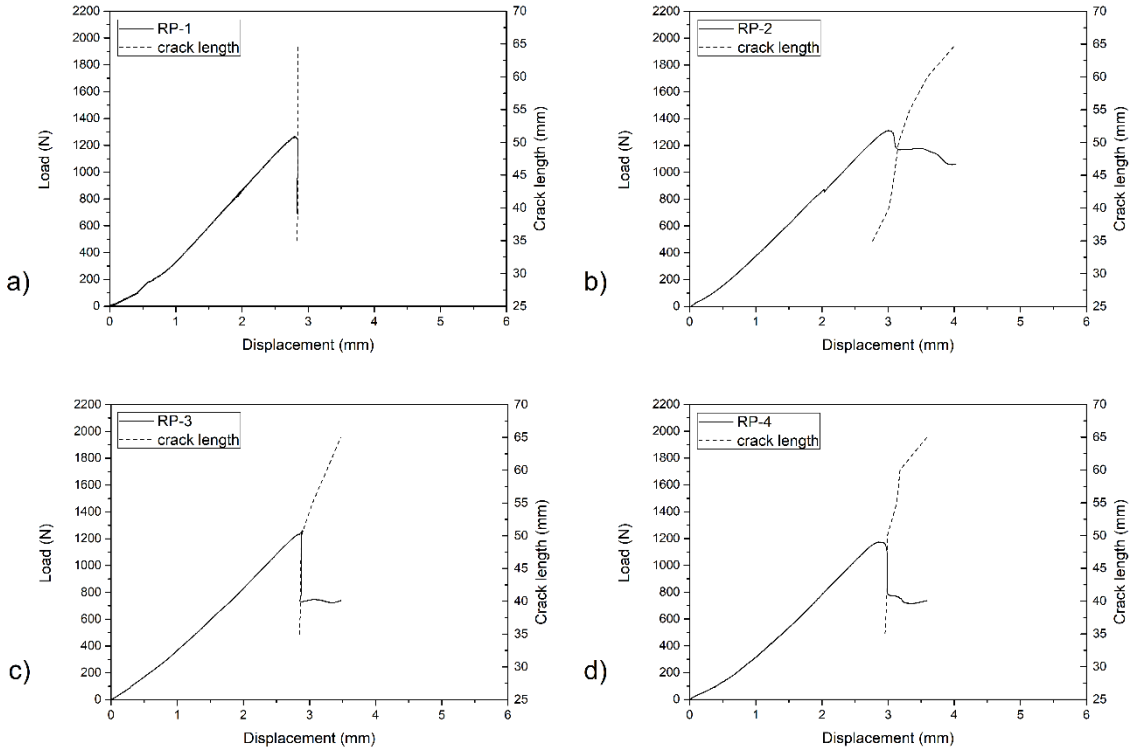


Figure 5.2: Load and crack length curves of specimens manufactured at room pressure without GFM under 75% mode II fracture.

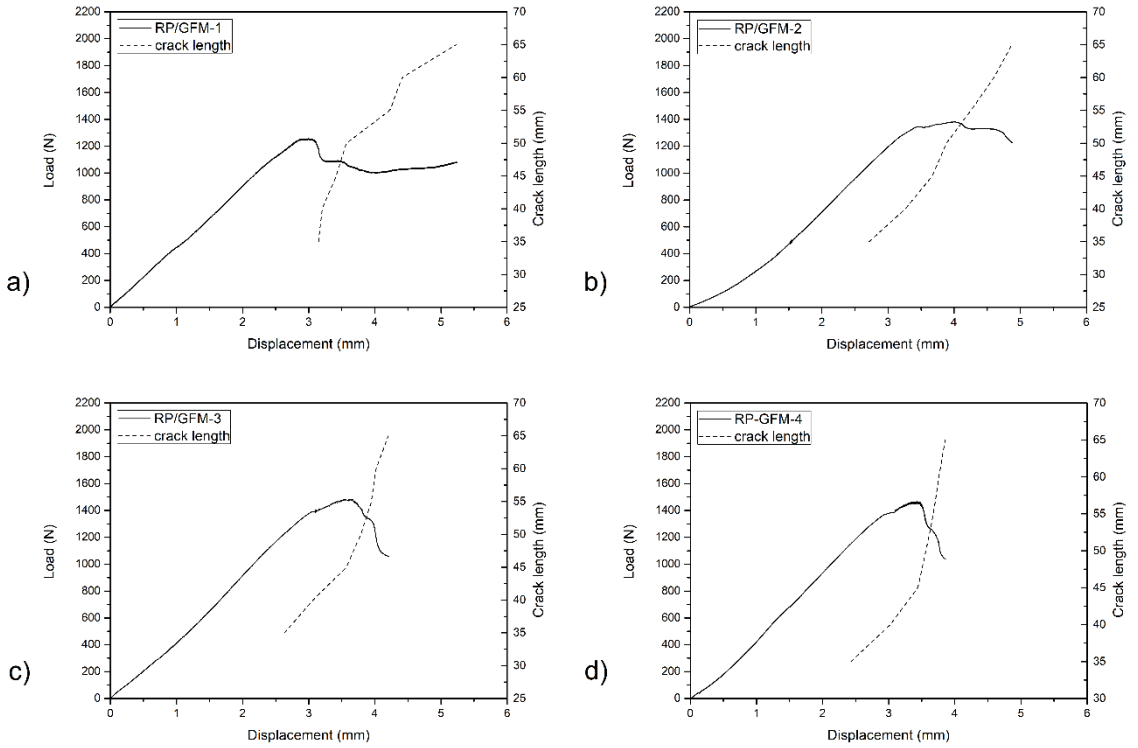


Figure 5.3: Load and crack length curves of specimens manufactured at room pressure with GFM under 75% mode II fracture.

Figures 5.4 and 5.5 show the results of specimens manufactured using vacuum bagging and tested under 75% mode II fracture. All tests presented abrupt load drop during crack propagation. Specimens with an inserted layer of GFM (Figure 5.5) had significant higher test loadings compared to specimens without GFM (Figure 5.4). Tests were also performed under 40% mode II ratio fracture configuration and the results are shown in Figures 5.6 and 5.7. In this condition, all tests presented a smooth variation of the test load during crack propagation. Specimens with an inserted layer of GFM (Figure 5.7) presented slightly higher loadings in compared to the specimens without GFM (Figure 5.6). Overall, the insertion of a layer of GFM between adherends increased the fracture loadings of the bonded joints although in different degree depending on the manufacture process and fracture mode ratio.

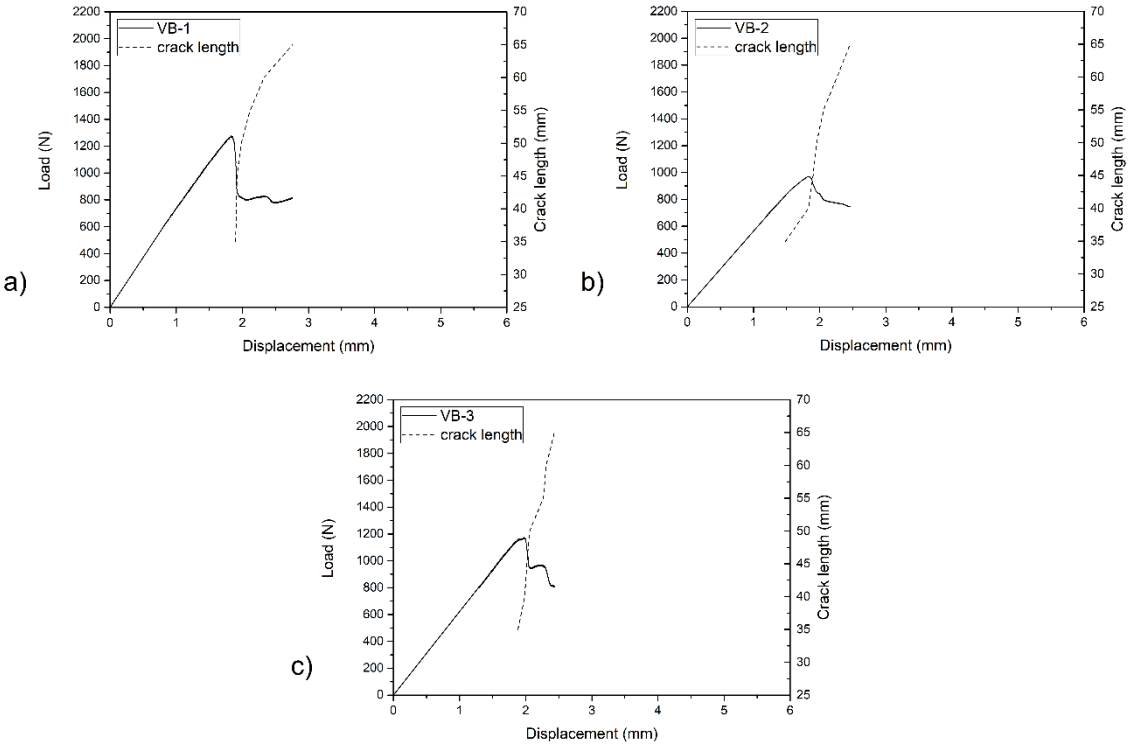


Figure 5.4: Load and crack length curves of specimens manufactured using vacuum bagging without GFM under 75% mode II fracture.

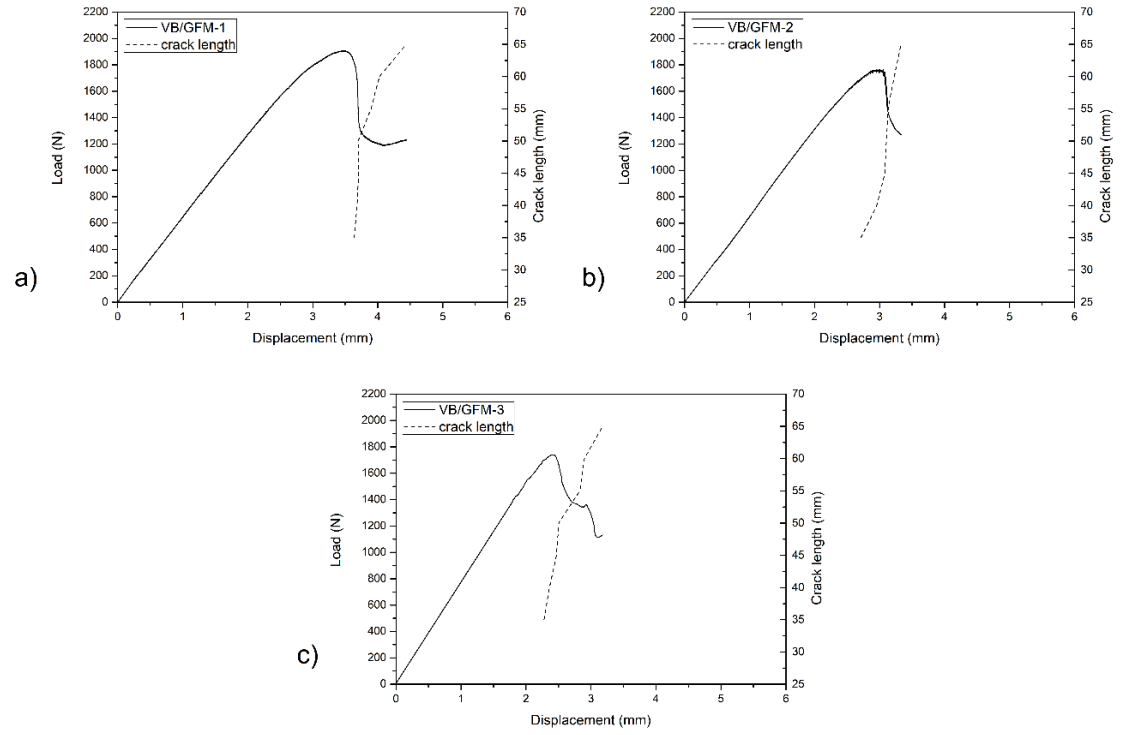


Figure 5.5: Load and crack length curves of specimens manufactured using vacuum bagging with GFM under 75% mode II fracture.

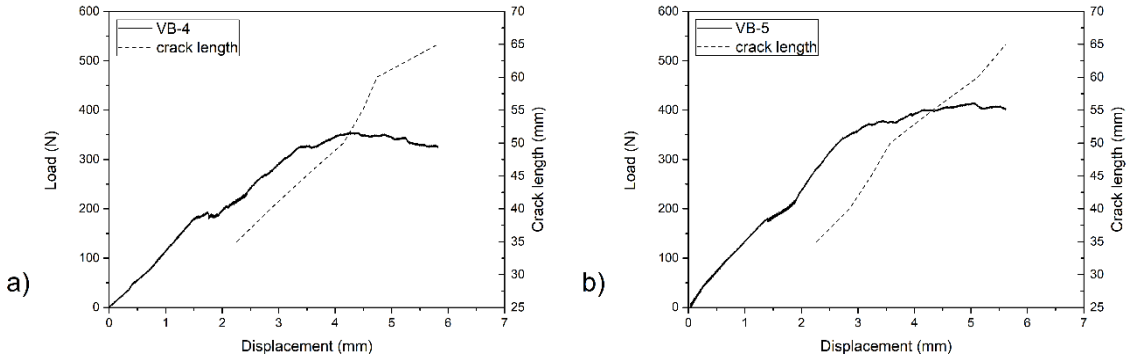


Figure 5.6: Load and crack length curves of specimens manufactured using vacuum bagging without GFM under 40% mode II fracture.

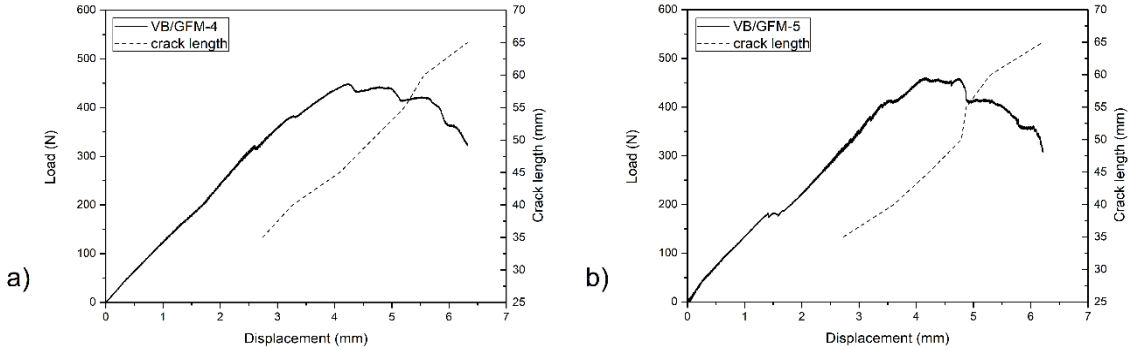


Figure 5.7: Load and crack length curves of specimens manufactured using vacuum bagging with GFM under 40% mode II fracture.

Images of the fracture propagation paths were obtained from an optical microscope. Figure 5.8 shows the typical fracture propagation paths of the specimens without GFM and with a layer of GFM between adherends. Crack migration was observed in all tests. This is attributed to the higher stresses in the upper arm of the specimen caused by the MMB loading configuration. Consequently, crack propagated within the interface between the adhesive layer and the first layer of the composite adherend with fibers at length direction, as observed in Figure 5.8a. The insertion of a layer of GFM between the adherends produced a preferential layer for crack propagation with more irregular path, as seen in Figure 5.8b. This suggests an influence of the fracture surface profile on the higher test loadings produced in specimens with GFM. The test results support previous literature regarding the crucial role of the adjacent layer to the adhesive in the fracture performance of the structure [25, 26, 32-34].

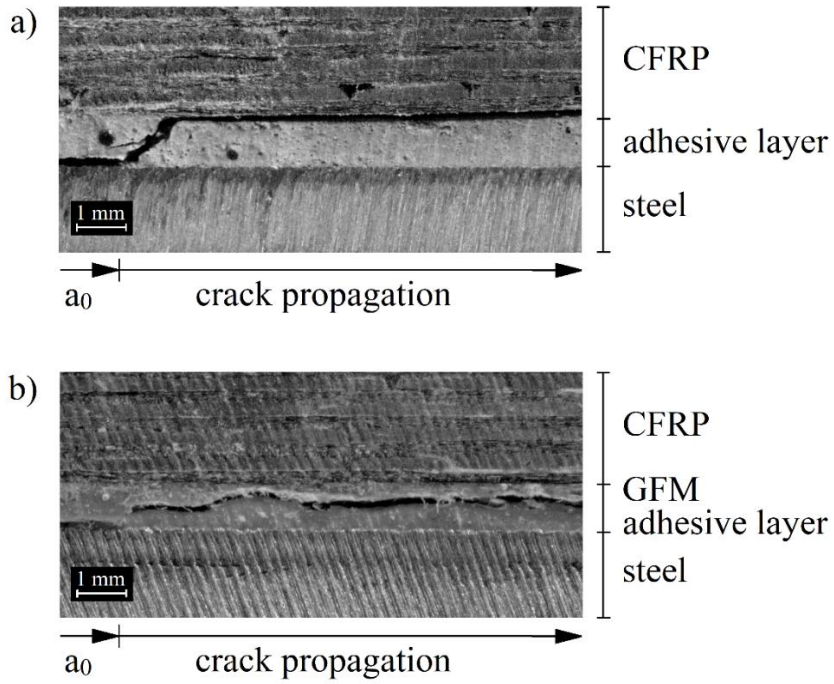


Figure 5.8: Crack propagation paths of (a) specimens without GFM and (b) specimens with GFM.

5.4. Discussion

5.4.1 Fracture toughness

The total fracture energy (G) was calculated from the crack propagation points using the strain-based method (SBM) [23]. The method is derived from beam analysis and requires the longitudinal strain equivalence at the faying surfaces of both arms in order to calculate the fracture mode ratio.

$$E_2 h_2^2 = E_1 h_1^2 \tag{5.1}$$

Where E_1, h_1, E_2 and h_2 are the flexural longitudinal moduli and thickness of the upper and lower arms, respectively. The total fracture energy is determined by the following equation:

$$G = \frac{1}{2B}\left(\frac{M_1^2}{E_1 I_1} + \frac{M_2^2}{E_2 I_2} - \frac{(M_1 + M_2)^2}{E_{eq} I_{eq}}\right) \tag{5.2}$$

Where B is the specimen width, M_1 and M_2 are the bending moments on the section of the crack tip in the upper and lower arms, respectively, E_{eq} is the flexural modulus of the specimen, and I_1, I_2 and I_{eq} are second moments of the area in the section of the crack tip of the upper arm, lower arm and total specimen, respectively.

Figure 5.9 shows the R-curves of the specimens manufactured at room pressure under 75% mode II fracture. Results were obtained from 35 mm to 65 mm crack length. The fracture energy increased substantially with the crack length in specimens with GFM although the fracture mode ratio remains constant during the test. This can be explained by the crack deflection mechanism [31] resulted from the more irregular crack path. Specimens with an inserted layer of GFM presented higher fracture energy during propagation when compared with the specimens without GFM. This reveals the toughening effect caused by the insertion of a layer of GFM between the adherends. A note is given to specimen RP-2 which presented similar results to the specimens with GFM. This will be discussed later in this work.

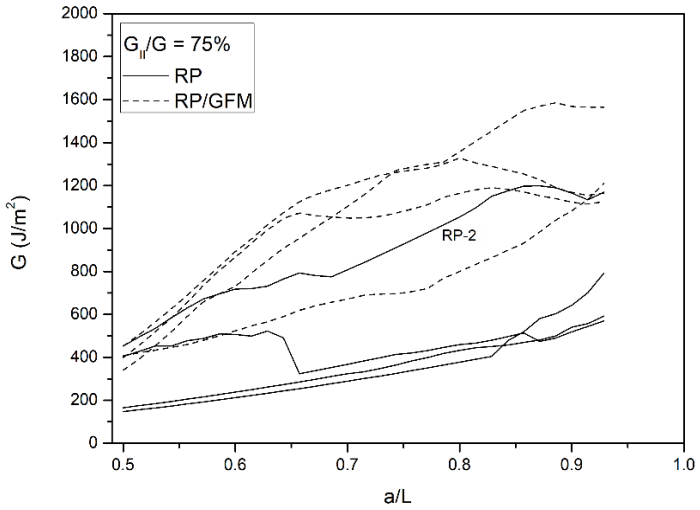


Figure 5.9: Fracture toughness of specimens manufactured at room pressure under 75% mode II fracture.

Figure 5.10 shows the R-curves obtained from specimens manufactured using vacuum bagging and tested under 75% mode II fracture. Specimens with an inserted layer of GFM presented substantially higher fracture energy compared with the specimens without GFM. The toughening effect is shown to be more significant in specimens

manufactured using vacuum bagging. The R-curves from tests under 40% mode II fracture are shown in Figure 5.11. Both specimens without and with GFM presented similar fracture energy.

These experimental results show that the increase in mode I fracture ratio reduced the toughening effect of the GFM. This shows that the toughening mechanism is not only influenced by the specimen design configuration but also the fracture mode ratio. The relationship between the fracture mode ratio and the toughening effect agrees with literature regarding mat-interlayered composites under pure mode I [29] and pure mode II [30] fracture. A more irregular crack propagation path improves the toughening effect as the shear becomes the dominant fracture mode.

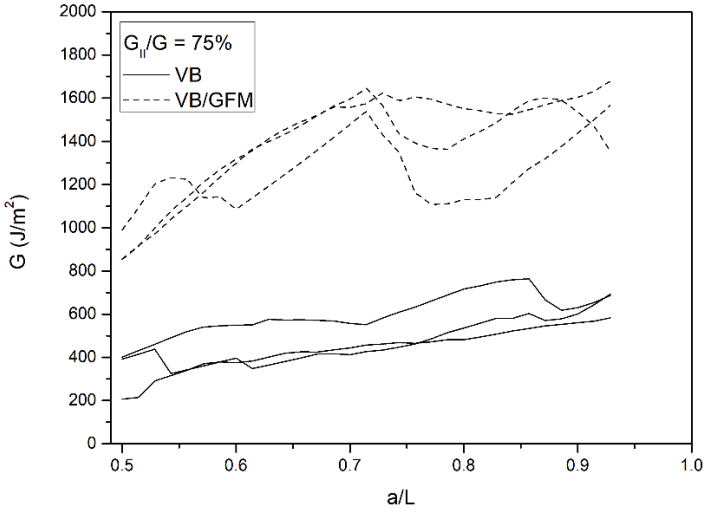


Figure 5.10: Fracture toughness of specimens manufactured using vacuum bagging under 75% mode II fracture.

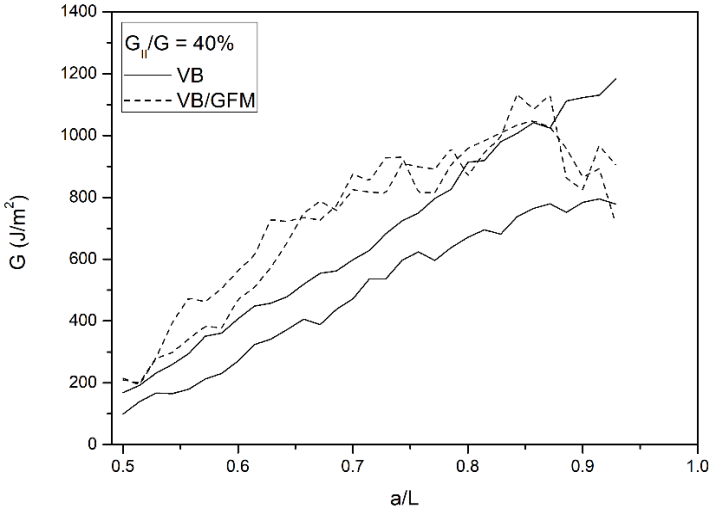


Figure 5.11: Fracture toughness of specimens manufactured using vacuum bagging under 40% mode II fracture.

A comparison between the average fracture energy (G_{ave}) of the specimens is given in Figure 5.12. The insertion of a layer of GFM between adherends is shown to increase the average fracture energy in both manufacturing processes under 75% mode II fracture. However, the toughening effect is more substantial in specimens manufactured using vacuum bagging when compared to room pressure. Regarding the fracture mode, the GFM produced greater improvement in the vacuum bagging manufacture under high mode II condition. Both the manufacturing process and the fracture mode ratio showed to have significant influence in the toughening effect. Moreover, specimens without GFM presented similar average fracture energy although it is slightly higher in specimens manufactured using vacuum bagging tested under high mode I fracture.

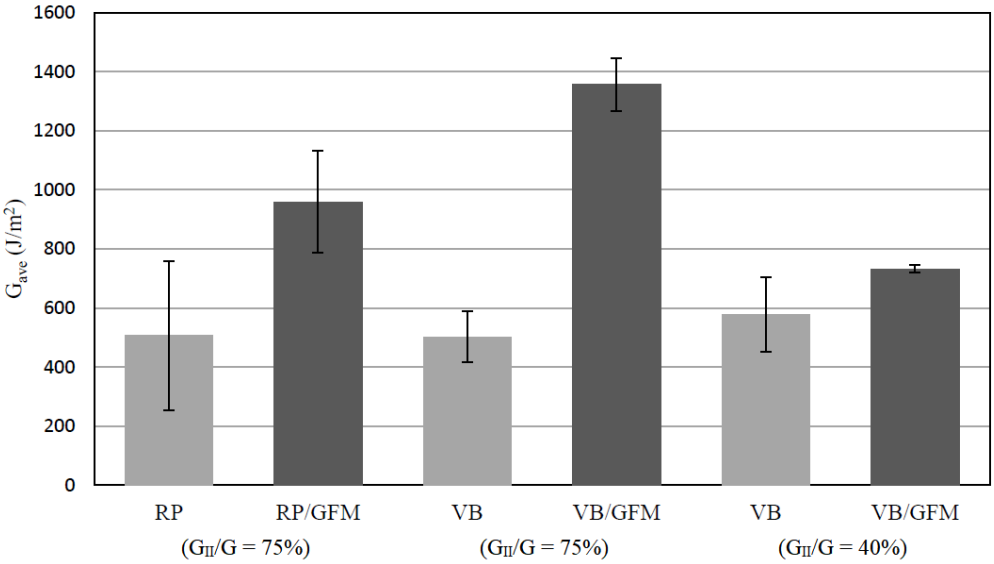


Figure 5.12: Average fracture energy.

5.4.2 Surface profile

An analysis of the fracture surfaces features was performed using a 3D wide-area measuring optical microscope (VR-3200, Keyence Corporation). Fracture surfaces and height profiles were analyzed. The height profiles of the fracture surfaces were obtained from three different paths: center of the surfaces and near the edges on the left and right sides. The aim is to evaluate the influence of the fracture surface profile on the toughening mechanism.

Figure 5.13 shows representative images of the fracture surfaces of specimens manufactured at room pressure under 75% mode II fracture. The specimen without GFM (RP-4) presented a crack propagation between the adhesive layer and the adjacent layer of carbon fibers. Otherwise, the specimen with GFM (RP/GFM-2) showed a combination of fracture propagation within the GFM and interlaminar fracture within the adjacent layer of carbon fibers. Representative height profiles are shown in Figure 5.14. It reveals a more irregular fracture surface in the specimen with GFM. Crack propagations along irregular paths are shown to require more energy to propagate [31]. This explains the higher fracture toughness of the specimens with GFM.

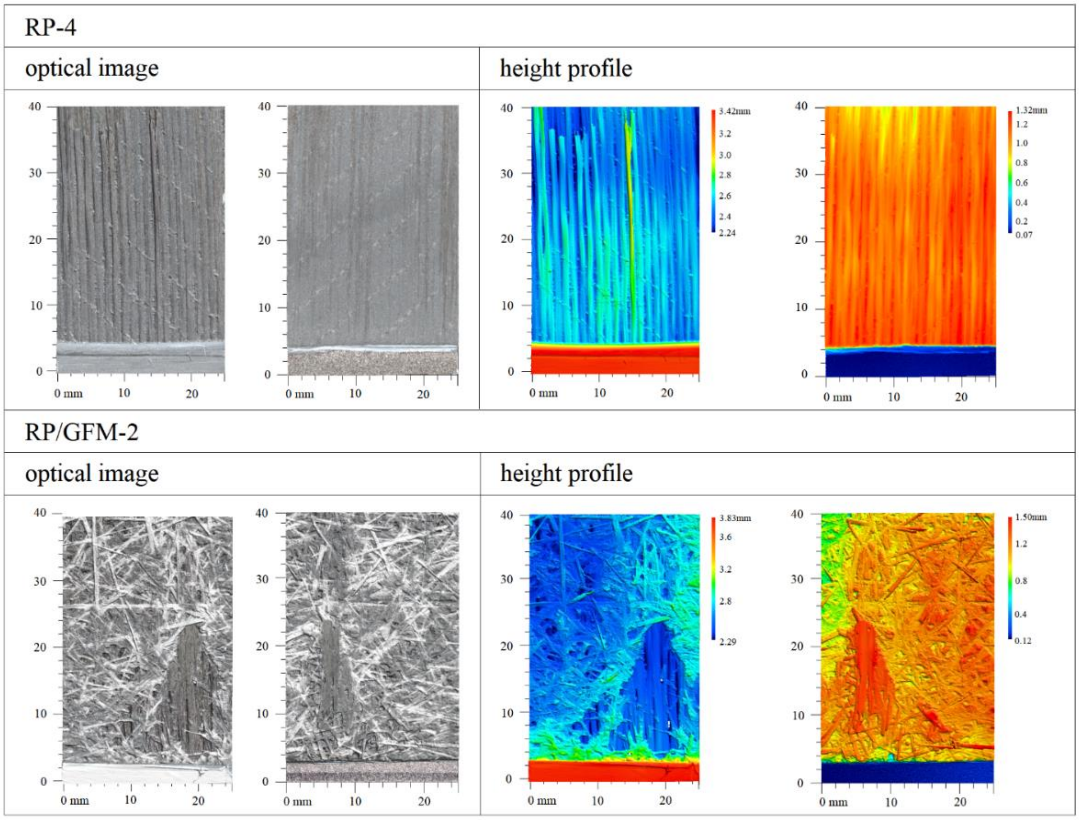


Figure 5.13: Representative fracture surfaces of specimens manufactured at room pressure under 75% mode II fracture.

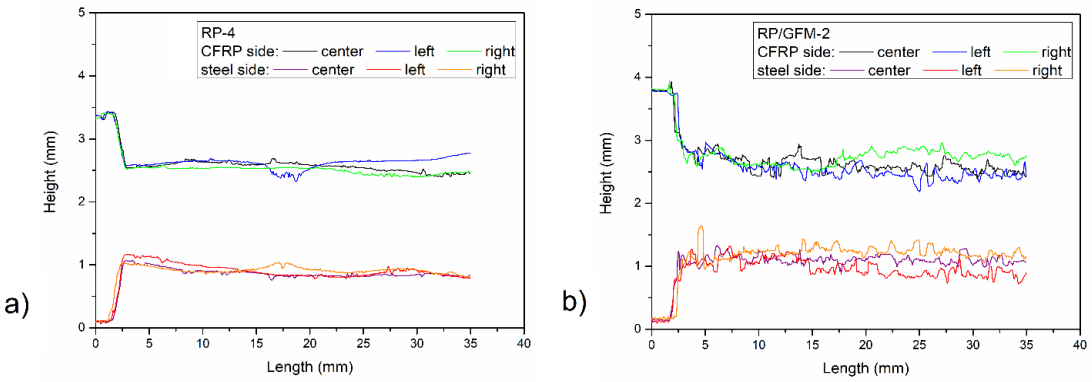


Figure 5.14: Representative fracture height profiles of specimens manufactured at room pressure under 75% mode II fracture (a) without and (b) with GFM.

Figure 5.15 shows representative images of the fracture surfaces of specimens manufactured using vacuum bagging under 75% mode II fracture. The specimen without GFM (VB-2) presented a fracture between the adhesive layer and the adjacent layer of

carbon fibers, similar to the specimen manufactured at room pressure (see Figure 5.13). However, the specimen with GFM (VB/GFM-3) revealed mostly fracture propagation within the layer of GFM. Representative height profiles are shown in Figure 5.16. It reveals a more irregular fracture surface in the specimen with GFM. These results are similar to the specimens manufactured at room pressure (see Figure 5.14). Therefore, the manufacturing process had no notable effect in the height profile of the fracture surfaces.

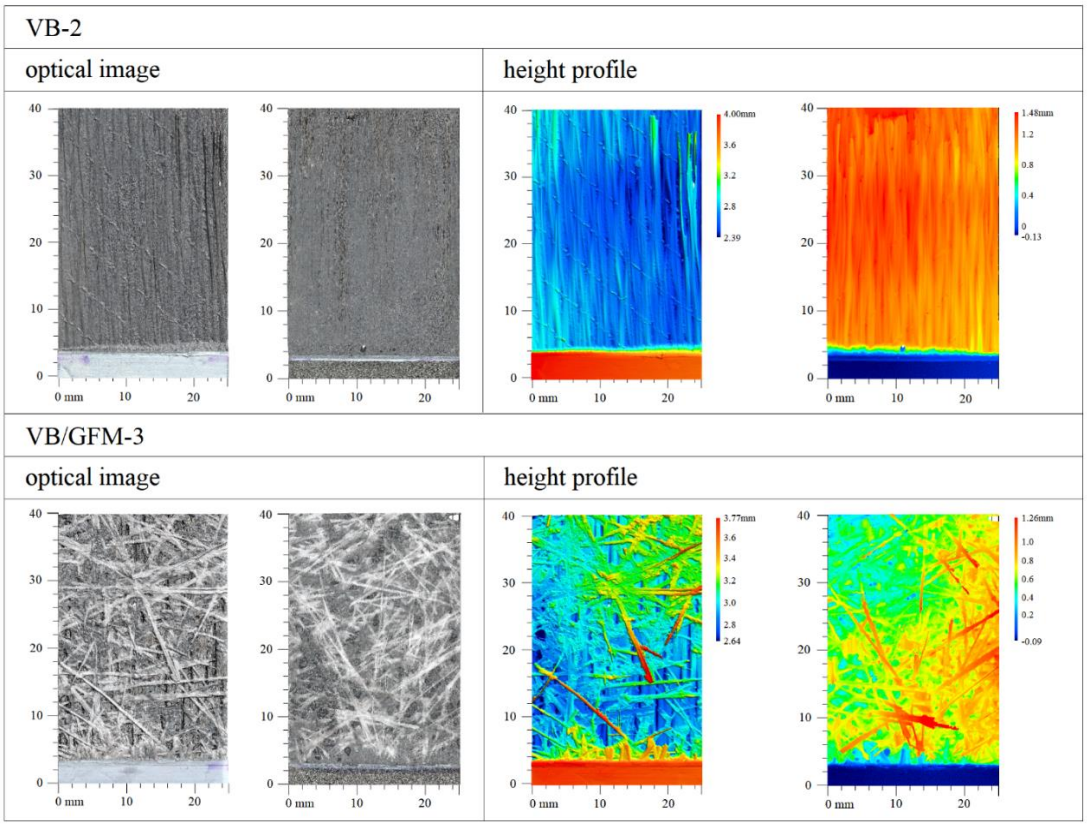


Figure 5.15: Representative fracture surfaces of specimens manufactured using vacuum bagging under 75% mode II fracture.

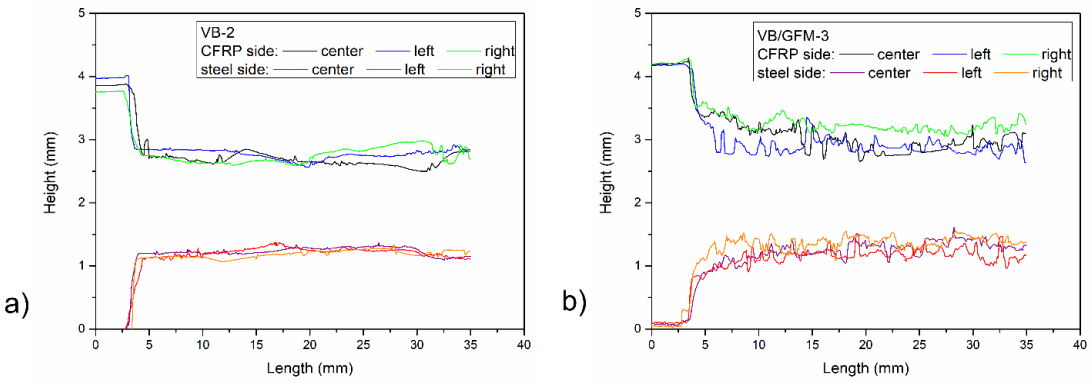


Figure 5.16: Representative fracture height profiles of specimens manufactured using vacuum bagging under 75% mode II fracture (a) without and (b) with GFM.

Figure 5.17 shows representative images of the fracture surfaces of specimens manufactured using vacuum bagging under 40% mode II fracture. The specimen without GFM (VB-5) presented a fracture similar to the previous cases of 75% mode II at room pressure (see Figure 5.13) or using vacuum bagging (see Figure 5.15). Likewise, the specimen with GFM (VB/GFM-5) revealed a fracture propagation within the layer of GFM. Representative height profiles are shown in Figure 5.18. It reveals a more irregular fracture surface in the specimen with GFM. These results are analogous to the previous cases (see Figures 5.14 and 5.16). Therefore, the fracture partitioning ratio had no notable effect in the height profile of the fracture surfaces.

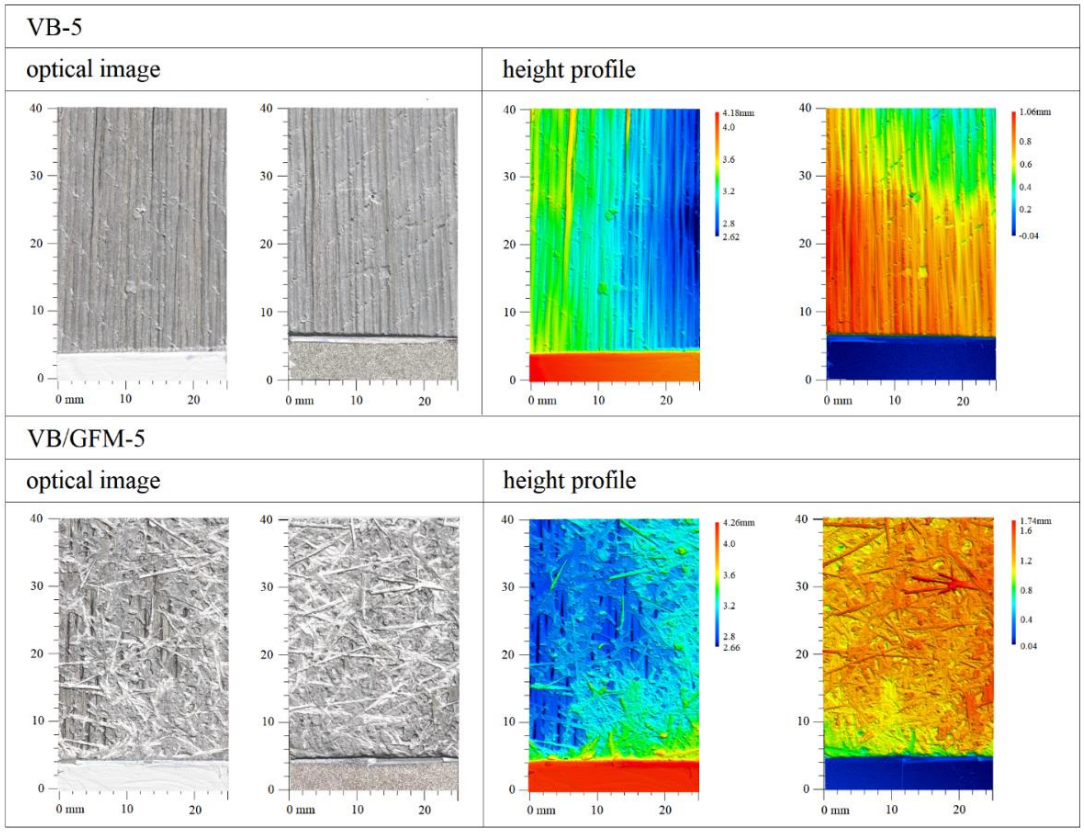


Figure 5.17: Representative fracture surfaces of specimens manufactured using vacuum bagging under 40% mode II fracture.

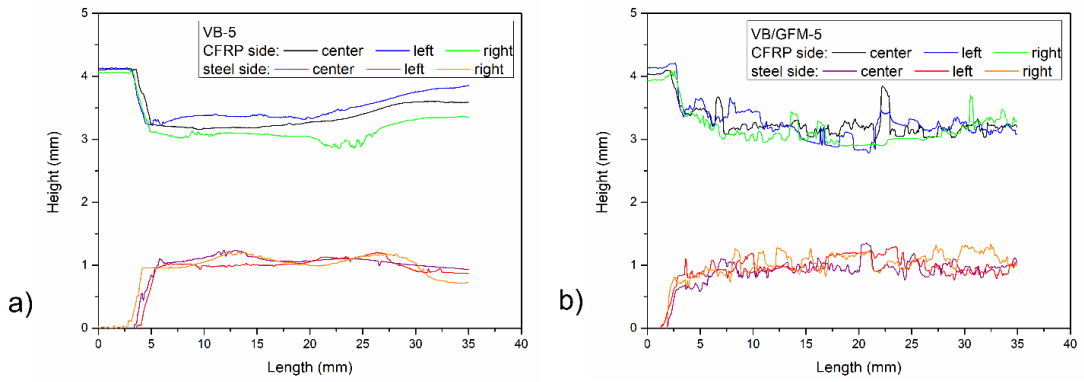


Figure 5.18: Representative fracture height profiles of specimens manufactured using vacuum bagging under 40% mode II fracture (a) without and (b) with GFM.

The roughness of the fracture surfaces was measured from an area of 10 x 10 mm at the center of the fracture surfaces. Table 5.4 presents the roughness, in terms of the root mean square height (Sq), obtained from the CFRP and steel sides of the tested

specimens. Results from every specimen revealed similar roughness in both sides of the crack. Cracks within the GFM showed mostly rougher fracture surfaces. It is observed that specimen RP-2 presented a rougher surface compared with the others of the same design and manufacturing process. This can be related to the more stepwise propagation (see Figure 5.2) and higher fracture energy (see Figure 5.9) obtained from this test.

Table 5.4: Roughness of the fracture surfaces.

Specimen	G_{II}/G	Adherend side	Roughness, Sq (μm)
RP-1	75%	CFRP	88.4
		steel	70.2
RP-2	75%	CFRP	135.9
		steel	133.6
RP-3	75%	CFRP	71.8
		steel	65.9
RP-4	75%	CFRP	84.5
		steel	68.7
RP/GFM-1	75%	CFRP	150.0
		steel	167.4
RP/GFM-2	75%	CFRP	129.4
		steel	112.1
RP/GFM-3	75%	CFRP	121.4
		steel	117.8
RP/GFM-4	75%	CFRP	144.9
		steel	125.7
VB-1	75%	CFRP	59.5
		steel	60.4
VB-2	75%	CFRP	68.8
		steel	67.9
VB-3	75%	CFRP	97.6
		steel	84.9
VB/GFM-1	75%	CFRP	149.8
		steel	155.0

VB/GFM-2	75%	CFRP	184.5
		steel	172.5
VB/GFM-3	75%	CFRP	136.8
		steel	158.2
VB-4	40%	CFRP	91.3
		steel	88.0
VB-5	40%	CFRP	88.6
		steel	68.7
VB/GFM-4	40%	CFRP	169.5
		steel	154.9
VB/GFM-5	40%	CFRP	163.9
		steel	162.4

The relationship between the surface roughness and the fracture energy is presented in Figure 5.19. The average surface roughness (Sq_{ave}) presented in x-axis is the average between the CFRP and steel fracture surfaces of the specimen. The data is clustered in three series: RP (G_{II}/G = 75%), VB (G_{II}/G = 75%) and VB (G_{II}/G = 40%). For each of these three clustered series, it is observed a common trend of increasing the fracture energy with surface roughness as a result of inserting a layer of GFM. This can be observed by the positive slope of the three linear fits for all three clustered series. Specimens manufactured at room pressure and tested under 75% mode II fracture - RP (G_{II}/G = 75%) show an increase of 49% in the Sq_{ave} with the presence of GFM, which resulted in 89% increase in the G_{ave}. Specimens manufactured using vacuum bagging and tested under the same ratio - VB (G_{II}/G = 75%), show an increase of 118% in the Sq_{ave} with the presence of the GFM, which resulted in 170% increase in the G_{ave}. Therefore, specimens tested under the same fracture mode ratio, the ones manufactured using vacuum bagging produced higher fracture surface roughness and consequently higher fracture energy. Finally, specimens manufactured with vacuum bagging and tested under lower fracture mode ratio of 40% mode II - VB (G_{II}/G = 40%), the Sq_{ave} increased 93% with the insertion of the GFM but the G_{ave} increased only 27%. Although the surface roughness increased in a similar extent for all specimens manufactured under vacuum bagging, the toughening effect is more evident under high mode II fracture.

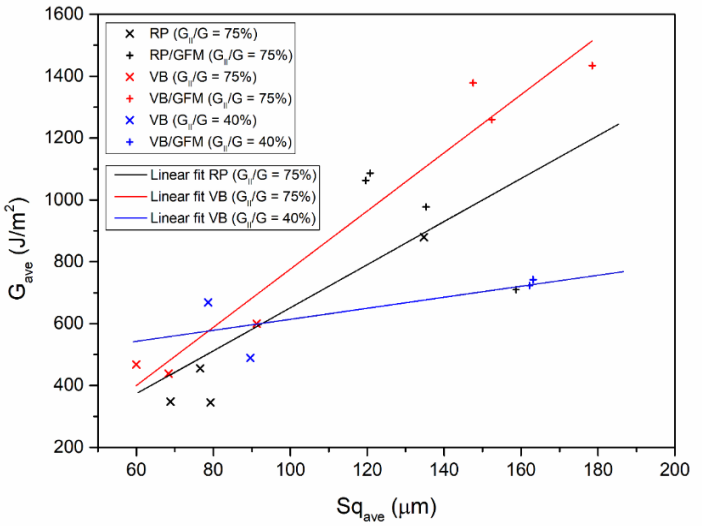


Figure 5.19: Relationship between surface roughness and fracture energy.

5.4.3 Fractography

In order to better understand the effect of the manufacturing process on the fracture surface features, a fractography analysis was performed using a field emission scanning electron microscope (SEM) (JEOL JSM-7500F, Japan). Prior to examination, the samples were coated with a thin layer of gold (Au) using a sputter coater (Quorum Q300T D, United Kingdom). SEM images were obtained from the steel side of the fracture in magnification of 500x.

Figure 5.20 shows representative SEM images of the fracture surface of the specimens without GFM. Specimens manufactured at room pressure and tested under 75% mode II presented a combination of cohesive and interlaminar failure within the first layer of carbon fibers, as shown in Figure 5.20a. Similar failure modes are observed in Figure 5.20b for specimens manufactured using vacuum bagging and tested under the same ratio. Nevertheless, the specimens tested under 40% mode II fracture presented dominant cohesive failure, as observed in Figure 5.20c. This fracture features explain the similar fracture energy of specimens without GFM from both manufacturing processes (RP and VB) and the slightly higher performance under 40% mode II fracture ratio (see Figure 5.12). The increase in mode I fracture increases the cohesive failure mode within the adhesive layer. For mode II dominated fracture, cracks tend to propagate in the inner

layer of the laminate. This relationship between fracture mode ratio and crack propagation path is also noticed in the literature [24].

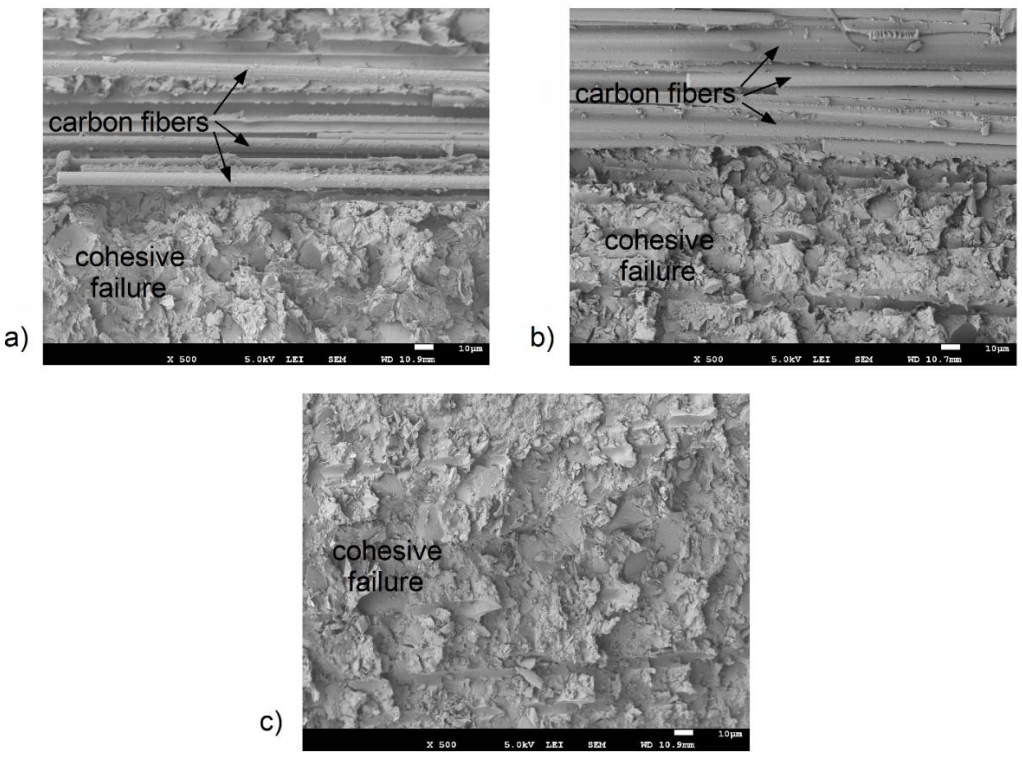


Figure 5.20: SEM images of the steel side of specimens without GFM (a) RP-4 (G_{II}/G = 75%), (b) VB-2 (G_{II}/G = 75%) and (c) VB-5 (G_{II}/G = 40%).

Figure 5.21 shows representative SEM images of the fracture surfaces of the specimens with an inserted layer of GFM. The glass fiber/matrix interactions are visible showing the crack path inside the GFM. The fracture surfaces are significantly different from the ones without GFM, in Figure 5.20, where the crack path developed at the CFRP/adhesive interface. Figure 5.21a shows the specimens manufactured at room pressure with GFM and tested with 75% mode II fracture. It is clearly shown the presence of loose fibers and bare fibers. Specimens manufactured using vacuum bagging and tested under the same fracture mode ratio, shown in Figure 5.21b, exhibited higher compaction and better fiber/matrix adhesion. This is a consequence of the vacuum pressure applied for consolidation of the composite during manufacture. A higher compaction of the mat contributes to an increased fracture performance [31], and consequently the toughening effect is more evident in specimens manufactured using vacuum bag than specimens

manufactured at room pressure (see Figure 5.12). Moreover, good fiber/matrix compaction is observed in Figure 5.21c for a dominant mode I fracture, similar to the case of high mode II fracture (Figure 5.21b). Therefore, the inferior performance of specimens tested under 40% mode II regards only the loading conditions and not the failure mode.

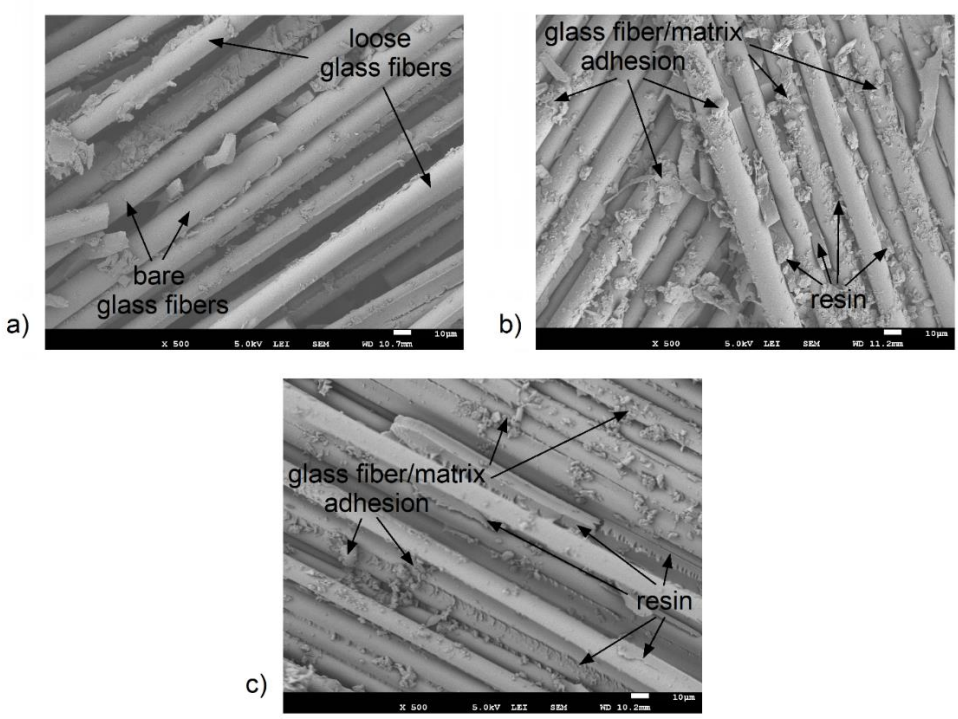


Figure 5.21: SEM images of the steel side of specimens with GFM (a) RP/GFM-2 (G_{II}/G = 75%), (b) VB/GFM-3 (G_{II}/G = 75%) and (c) VB/GFM-5 (G_{II}/G = 40%).

5.5 Conclusion

The influence of a layer of glass fiber mat inserted in a bi-material bonded joint interface has been investigated as a toughening mechanism to improve the fracture performance of bonded structures. Composite-to-metal bonded specimens were manufactured by hand lay-up using two different consolidation processes: at room pressure or using vacuum bagging. The mixed-mode fracture behavior was evaluated under quasi-static loadings using the MMB test. Fracture toughening mechanisms were investigated through the test results and fractography analysis.

Crack tends to propagate in the interface between the adhesive layer and the upper arm of the specimen due to the higher stresses caused by the MMB loading configuration. In the case of a CFRP adherend without GFM, cohesive failure within the

adhesive layer is the dominant failure mode under high mode I fracture while a combination of cohesive and interlaminar failure occurs in high mode II fracture condition.

The insertion of a layer of GFM between adherends prevented the crack migration to the CFRP adherend and introduced a preferential crack propagation path within the GFM. The crack propagation within the GFM produced more irregular fracture surface height profiles when compared to the specimens without GFM. A more irregular crack path resulted in higher fracture toughness due to the increase of the energy required for the crack to propagate. Therefore, the adjacent composite layer to the adhesive interface has an important role in the fracture performance of the bonded joint since it affects the crack propagation path.

The manufacturing process affected the performance of the specimens with GFM. The vacuum bagging technique produced a better fiber/matrix compaction of the GFM and resulted in rougher fracture surfaces when compared to room pressure. On the other hand, no change was observed in the fracture surfaces of specimens without GFM despite the manufacturing process. The relationship between fracture surface roughness and fracture performance is observed in both manufacturing processes although the toughening effect is more evident in higher mode II fracture conditions.

Even though the values measured for the fracture toughness appear coherent, only the principles of LEFM have been considered for the evaluation of the fracture performance. The non-linearity effects of the plastic zone developed around the crack tip has not been taken into account. The integration of a non-linear analysis may potentially improve the understanding over the fracture behavior of composite-to-metal bonded joints.

The insertion of a layer of GFM is expected to increase the fracture performance of composite repairs in metal structures. The use of vacuum pressure in the consolidation of the composite, when feasible, is recommended for optimizing the fracture performance of the bonded structure.

References

[1] Budhe, S.; Banea, M.D.; de Barros, S. An Updated Review of Adhesively Bonded Joints in Composite Materials. Int. J. Adhes. Adhes. 2017, 72, 30-42.

[2] Mangalgiri, P.D. Composite materials for aerospace applications. Bull. Mater. Sci. 1999, 22, 657-664.

[3] Budhe, S.; Banea, M.D.; de Barros, S. Bonded repair of composite structures in aerospace application: a review on environmental issues. Appl. Adhes. Sci. 2018, 6, 3.

[4] Taub, A.I.; Krajewski, P.E.; Luo, A.A. The evolution of technology for materials processing over the last 50 years: the automotive example. JOM 2007, 59, 48-57.

[5] Van Den Einde L, Zhao L, Seible F. Use of FRP composites in civil structural applications. Constr. Build. Mater. 2003, 17(6-7), 389-403.

[6] Katnam, K.B.; da Silva, L.F.M.; Young, T.M. Bonded repair of composite aircraft structures: A review of scientific challenges and opportunities. Prog. Aerosp. Sci. 2013, 61, 26-42.

[7] Arouche, M.M.; Budhe, S.; Alves, L.A.; Teixeira de Freitas, S.; Banea, M.D.; de Barros, S. Effect of moisture on the adhesion of CFRP-to-steel bonded joints using peel tests. J. Braz. Soc. Mech. Sci. Eng. 2018, 40, 10.

[8] Arouche, M.M.; Budhe, S.; Banea, M.D.; Teixeira de Freitas, S.; de Barros, S. Interlaminar adhesion assessment of carbon-epoxy laminates under salt water ageing using peel tests. Proc. IMechE Part L 2019, 233(8), 1555-1563.

[9] Rudawska, A. Comparison of the adhesive joints' strength of the similar and dissimilar systems of metal alloy/polymer composite. Appl. Adhes. Sci. 2019, 7, 7.

[10] de Barros, S.; Banea, M.D.; Budhe, S.; de Siqueira, C.E.R.; Lobão, B.S.P.; Souza, L.F.G. Experimental analysis of metal-composite repair of floating offshore units (FPSO). J Adhes. 2016, 93(1-2), 147-158.

[11] da Costa Mattos, H.S.; Reis, J.M.L.; Paim, L.M.; da Silva, M.L.; Lopes Junior, R.; Perrut, V.A. Failure analysis of corroded pipelines reinforced with composite repair systems. Eng. Fail. Anal. 2016, 59, 223-236.

[12] McGeorge, D.; Echtermeyer, A.T.; Leong, K.H.; Melve, B.; Robinson, M.; Fischer, K.P. Repair of floating offshore units using bonded fibre composite materials. Compos. Part A 2009, 40(9), 1364-1380.

[13] Meniconi, L.C.; Lana, L.D.; Morikawa, S.R. Experimental fatigue and aging evaluation of the composite patch repair of a metallic ship hull. Appl. Adhes. Sci. 2014, 2, 27.

[14] DNV-RP-C301. Design, Fabrication, Operation and Qualification of Bonded Repair of Steel Structures. Det Norske Veritas AS, 2015.

[15] Chaves, F.J.P.; da Silva, L.F.M.; de Moura, M.F.S.F.; Dillard, D.A.; Esteves, V.H.C. Fracture Mechanics Tests in Adhesively Bonded Joints - A Literature Review. J. Adhes. 2014, 90(12), 955-992.

[16] Reeder, J.R.; Crews Jr, J.H. Mixed-Mode bending method for delamination testing. AIAA J. 1990, 28(7), 1270-1276.

[17] Reeder, J.R.; Crews Jr, J.H. Redesign of the Mixed-mode Bending Delamination Test to Reduce Non-linear Effects. J. Compos. Technol. Res. 1992, 14(1), 12-19.

[18] Pereira, A.B.; de Morais, A.B. Mixed mode I + II interlaminar fracture of carbon/epoxy laminates. Compos. Part A 2008, 39(2), 322–333.

[19] Shahverdi, M.; Vassilopoulos, A.P.; Keller, T. Mixed-Mode I/II Fracture Behavior of Asymmetric Adhesively-Bonded Pultruded Composite Joints. Eng. Fract. Mech. 2014, 115, 43-59.

[20] Liu, Z.; Gibson, R.F.; Newaz, G.M. The Use of a Modified Mixed Mode Bending Test for Characterization of Mixed-Mode Fracture Behavior of Adhesively Bonded Metal Joints. J. Adhes. 2010, 78(3), 223-244.

[21] Stamoulis, G.; Carrere, N.; Cognard, J.Y.; Davies, P.; Badulescu, C. On the Experimental Mixed-Mode Failure of Adhesively Bonded Metallic Joints. Int. J. Adhes. Adhes. 2014, 51, 148-158.

[22] Quispitupa, A.; Berggreen, C.; Carlsson, L.A. On the analysis of a mixed mode bending sandwich specimen for debond fracture characterization. Eng. Fract. Mech. 2009, 76(4), 594-613.

[23] Arouche, M.M.; Wang, W.; Teixeira de Freitas, S.; de Barros, S. Strain-based methodology for mixed-mode I+II fracture: A new partitioning method for bi-material adhesively bonded joints. J. Adhes. 2019, 95(5-7), 385-404.

[24] Quispitupa, A.; Berggreen, C.; Carlsson, L.A. Face/core interface fracture characterization of mixed mode bending sandwich specimens. Fatigue Fract. Eng. Mater. Struct. 2011, 34(11), 839-853.

[25] Kim, B.W.; Mayer, A.H. Influence of fiber direction and mixed-mode ratio on delamination fracture toughness of carbon/epoxy laminates. Compos. Sci. Technol. 2003, 63(5), 695-713.

[26] Andersons, J.; König, M. Dependence of fracture toughness of composite laminates on interface ply orientations and delamination growth direction. Compos. Sci. Technol. 2004, 64(13-14), 2139-2152.
[27] Sela, N.; Ishai, O. Interlaminar fracture toughness and toughening of laminated composite materials: a review. Compos. 1989, 20(5), 423-435.
[28] Kuwata, M.; Hogg, P.J. Interlaminar toughness of interleaved CFRP using non-woven veils: Part 1. Mode-I testing, Compos. Part A: Appl. Sci. Manuf. 2011, 42(10), 1551-1559.
[29] Hosseini, M.R.; Taheri-Behrooz, F.; Salamat-talab, M. Mode I interlaminar fracture toughness of woven glass/epoxy composites with mat layers at delamination interface. Polym. Test. 2019, 78, 105943.
[30] Kuwata, M.; Hoggm P.J. Interlaminar toughness of interleaved CFRP using non-woven veils: Part 2. Mode-II testing, Compos. Part A: Appl. Sci. Manuf. 2011, 42(10), 1560-1570.
[31] Boccaccini, A.R.; Winkler, V. Fracture surface roughness and toughness of Al2O3-platelet reinforced glass matrix composites. Compos. Part A 2002, 33(1), 125-131.
[32] Lundsgaard-Larsen, C.; Berggreen, C.; Carlsson, L.A. Tailoring Sandwich Face/Core Interfaces for Improved Damage Tolerance – Part II: Experiments. Appl. Compos. Mater. 2010, 17, 621-637.
[33] Karger-Kocsis, J.; Harmia, T.; Czigány, T. Comparison of the fracture and failure behavior of polypropylene composites reinforced by long glass fibers and by glass mats. Compos. Sci. Technol. 1995, 54(3), 287-298.
[34] Huang, B.-Z.; Hu, X.-Z.; Liu, J. Modelling of inter-laminar toughening from chopped Kevlar fibers, Compos. Sci. Technol. 2004, 64(13-14), 2165-2175.
[35] Kopp, J.-B.; Schmittbuhl, J.; Noel, O.; Lin, J.; Fond, C. Fluctuations of the dynamic fracture energy values related to the amount of created fracture surface. Eng. Fract. Mech. 2014, 126, 178-189.
[36] Sun, Z.; Shi, S.; Hu, X.; Guo, X.; Chen, J.; Chen, H. Short-aramid-fiber toughening of epoxy adhesive joint between carbon fiber composites and metal substrates with different surface morphology. Compos. Part B 2015, 77, 38-45.

[37] Teixeira de Freitas, S.; Banea, M.D.; Budhe, S.; de Barros, S. Interface adhesion assessment of composite-to-metal bonded joints under salt spray conditions using peel tests. Comp. Struct. 2017, 164, 68-75.

Chapter 6

Environmental Ageing

This Chapter contemplates the effect of long-term environmental exposure on the performance of composite-to-metal bonded joints. Specimens are manufactured using a carbon fiber reinforced polymer (CFRP) co-bonded to a steel member with epoxy adhesive and aged in a salt spray chamber. The mixed-mode fracture behavior of the non-aged and aged specimens is assessed using the mixed-mode bending (MMB) test apparatus. The fracture energy is calculated using the finite element method and an analytical approach, the strain-based method (SBM). The SBM showed to be a simple and accurate method to obtain the total fracture energy and the fracture mode ratio of the bi-material specimen. Ageing increased the fracture toughness at crack initiation by 27% for specimens loaded at 20% mode II and 7% for specimens loaded at 15% mode II. This can be related to the shear behavior and plasticization of the adhesive material. During crack propagation, the fracture toughness remained similar for specimens loaded at 20% mode II and decreased by 15% in specimens loaded at 15% mode II. Fractography analysis together with chemical characterization showed that the penetration of moisture at the edges of the fracture surface produced adhesive failure in these regions affected by moisture. Moreover, the failure mode at the unaffected regions of the fracture surface shifted from cohesive to a combination of thin-layer cohesive and adhesive failure after ageing. The results contributed to describe the effect of ageing on the fracture behavior of bonded materials.

Keywords: fracture toughness, crack propagation, bi-material bonded joints, adhesion, fracture surfaces, fractography, ageing

This chapter is based on the journal article: “Effect of salt spray ageing on the fracture composite-to-metal bonded joints”, published in International Journal of Adhesion and Adhesives 108:102885 (2021).

6.1 Introduction

The requirement of lightweight structures has encouraged the introduction of composite materials in industrial applications. Advanced composite materials, which usually consist of a polymer matrix reinforced with continuous fibers, can provide high strength with a relatively low weight and thus enable superior structural performance to be achieved. Novel design of structures can be developed as manufacturers replace traditional materials with advanced composite materials. In addition, adhesive bonding technology is generally the preferred joining method for composite parts as it provides enhanced stress transfer mechanisms and design flexibility [1]. First applications of advanced composites are found in aerospace industry [2] and have expanded to many other fields, such as automotive [3], civil construction [4] and maritime [5]. In recent years, composite repair technology has emerged as a promising alternative for the rehabilitation of structures. In the repair, fiber reinforced polymers (FRPs) are usually bonded to a metal damaged element, such as in aircrafts [6], vessels [7-8] and pipes [9-11].

The design optimization of these structures requires the understanding of several parameters, such as substrates to be bonded, service conditions and area of application [1]. In aircraft structures, moisture absorption was observed to cause reduction of structural performance in composite bonded joints [12-13]. Resins that are not fully cured are most affected by moisture absorption and degradation of composite repairs in civil applications [14]. Moisture conditioning resulted in a significant decrease in the performance of concrete/epoxy bond [15]. Wet environment is also one of the main factors that affect the strength of adhesive joints in vehicles [16]. These environmental parameters affect the long-term performance of bonded structures and thus represent a critical barrier to the expansion of their applications.

Several authors studied the effect of environmental degradation on the tensile strength of adhesive bonded joints. Early investigation in metal single lap joints (SLJs) showed that the moisture penetrates in the joint by diffusion through the adhesive, and consequently the degradation relates with time and tends to level off at the saturation level [17-18]. The main contributions to the loss of strength of metal bonded joints are described to be the hydrodynamic displacement at the interface, adhesive plasticization and corrosion at the substrates [19]. Sugiman et al. [20] showed that residual stresses due

to thermal and swelling strains in the adhesive layer have no significant effect on the joint strength. Li et al. [21] developed a numerical model for the prediction of long-term degradation of bonded joints based of the degradation of the adhesive properties. Papanicolaou et al. [22] verified that the strength of metal SLJs decreases as a consequence of salt spray ageing.

Regarding composite bonded joints, the work of Park et al. [23] addressed the effect of manufacturing process on the strength of composite SLJs under environmental conditions. They obtained a higher performance of co-cured composite joints in elevated temperatures and wet conditions. Jeong et al. [24] evaluated the effect of secondary bonded joints immersed in tap water and salt water. Results showed an increase of strength in pre-saturated specimens and decrease in specimens with saturated moisture content. The major failure modes of the composite bonded joints were found to be delamination and intralaminar failure of the composite adherend. Moreover, a decrease in the interlaminar adhesion was observed in carbon-epoxy laminates subjected to salt water ageing [25].

Recently, several works have been carried out on the degradation of bi-material bonded joints between composite and metal adherends. The tensile strength of dissimilar joints showed to be higher than composite joints due to the different behavior between the permeable composite adherend and impermeable metal adherend under moisture degradation [26]. A reduction of peel strength in composite-to-metal bonded joints was related with the moisture penetration in salt water [27] and salt spray [28], as a consequence of the change in the failure mechanism from cohesive to adhesive failure after ageing. Heshmati et al. [29] revealed a higher influence of moisture content on the degradation of a glass fiber reinforced polymer (GFRP) compared to a carbon fiber reinforced polymer (CFRP) in composite-to-metal double lap shear (DLS) joints due to the low permeability of the CFRP in comparison with GFRP. The work also showed that the diffusion rate of distilled water is higher than salt water, causing more degradation to the interlaminar strength in short-term immersion. However, with longer exposure times, salt water resulted in more damaging effects to the resin/fiber interface. A study performed by Sugiman et al. [30] obtained a similar outcome regarding the diffusion rate in an epoxy adhesive. Additionally, the diffusion rate showed to be much higher in the fiber direction than the through-thickness direction of unidirectional composites. The

effect of salt water under fluctuating condition was more severe than the effect of both distilled and salt water under steady condition. Similarly, the effect of salt fog cycles caused severe degradation in CFRP-steel double strap joints [31]. Yang et al. [32] detected the degradation of a laminate due to galvanic coupling developed from corrosion product depositions over steel and exposed carbon fibers. Although these studies provide valuable and insightful information, there remain a number of aspects that require investigation of the mechanical properties of bi-material bonded joints.

The fracture mechanics approach is widely applied to improve the design and evaluate the performance of bonded structures [33]. In this regard, limited work is available on the fracture behavior of bonded materials subjected to environmental conditions. Some authors addressed the degradation of the fracture properties of metal bonded joints using open-faced specimens [34-36]. The fracture energy was primarily associated with the moisture content and independent of test method and time [34]. The combined effects of temperature and water caused an initial increase in strength due to plasticization followed by a reduction due to degradation [35]. Tests in open-faced epoxy-aluminum specimens revealed that the fracture toughness decreases as the crack grows closer to the interface for a given level of degradation regardless of the fracture mode ratio [36]. Fernandes et al. [37] evaluated the effect of ageing in metal bonded joints using a secondary bonding method with aged adhesive plates. They detected an increase of the fracture toughness after exposure to salt water due to plasticization of the adhesive, while degradation of the fracture toughness was observed in distilled water as consequence of a substantial reduction of the glass transition temperature. Although the ageing methods previously mentioned are time-efficient, their results may differ from the actual degradation mechanisms in real bonded structures.

Further authors [38-39] observed the degradation of the pure mode I fracture toughness of aluminum bonded joints exposed to moist conditions. In general, aged specimens fail adhesively while non-aged specimens usually show cohesive failure. In the case of composite bonded materials, Markatos et al. [40] detected a considerable reduction of the fracture toughness at crack initiation in bonded CFRP laminates after immersion in de-mineralized water. Interfacial failure also showed to become the dominant failure mode. Fernandes et al. [41] verified a relationship between physical alterations of the adhesive material and the reduction of pure mode I and pure mode II

fracture energy of composite bonded joints under the effect of moisture. However, these studies address only the pure modes. In real-life applications, cracks in bonded joints propagate in a combination of opening (mode I) and shear (mode II) loadings.

Recently, few authors addressed the effect of moisture on the fracture of symmetric composites. LeBlanc and LaPlante [42] investigated the delamination growth of a carbon-epoxy composite aged in distilled water. The fracture energy increased in pure mode I while the pure mode II and mixed-mode conditions were weakened. Silva et al. [43] obtained similar results for the pure modes using composite bonded joints aged in humid atmosphere. However, specimens tested in mixed-mode conditions presented a reduction in the mechanical properties. Additionally, fracture energy decreased after ageing in salt fog. In general, fracture properties degrade with the exposure time with non-negligible effects at early stages followed by a stabilization trend. However, these studies focused on the quantitative analysis of the fracture toughness. The analysis of failure mechanisms and their association to the degradation of mechanical properties may reveal additional data to improve the design of adhesively bonded structures.

Finally, a review on available literature reveals insufficient information regarding the fracture of bi-material bonded joints [44]. In this matter, some authors successfully applied the mixed-mode bending (MMB) test method for the analysis of sandwich specimen face/core debonding [45], dissimilar composite bonded joints [46] and composite-to-metal bonded joints [47]. The MMB test proved to be a simple and reliable technique to evaluate the fracture performance of dissimilar bonded specimens under mixed-mode loadings. The experimental procedure shows potential to be further extended for the evaluation of the effect of environmental conditions in bi-material bonded joints.

In this Chapter, the effect of long-term environmental exposure on the performance of composite-to-metal bonded joints is investigated. Specimens are manufactured using a CFRP co-bonded to steel with an epoxy adhesive. Samples are aged in a salt spray chamber. The mixed-mode fracture behavior of non-aged and aged specimens is assessed using the MMB test apparatus. The fracture energy is calculated using numerical and analytical approaches. A fracture surface analysis together with a chemical characterization are performed in order to evaluate the failure mechanisms in

association with the performance of the bonded joint subjected to environmental exposure.

6.2 Materials and methods

6.2.1 Specimen manufacturing

Composite-to-metal bonded specimens were manufactured in order to simulate the application of a composite repair to a metal structure in offshore industry [48]. A steel plate (ASTM A36) of 3.18 mm thickness was selected for the metal adherend. The steel surface was blasted with steel grit (G-40) and degreased with acetone. An epoxy adhesive (NVT201E, Novatec, Rio de Janeiro, Brazil) with a glass transition temperature (T_g) of 80 ºC was applied. One layer of glass fiber chopped strand mat with a density of 300 g/m^2 was inserted between the adhesive and the composite. Bidirectional carbon fiber fabrics (LTC450-C10-C, DEVOLD AMT, Langevåg, Norway) with density of 430 g/m^2 and epoxy lamination resin (PIPEFIX, Polinova S.A., Rio de Janeiro, Brazil) with a T_g of 116 ºC and working life of 30 min. were selected for the composite adherend. A composite-to-metal plate was manufactured by hand lay up on the treated metal surface. The composite adherend has 10 layers of 0/90º carbon fibers. The first unidirectional carbon ply in contact with the glass fiber mat was placed at the length direction (0º). The adhesive and resin curing process occurred simultaneously in approximately 2 hours at room temperature. The properties of the materials were obtained from a previous work [28] and are shown in Table 6.1.

Specimens were cut from the plates using a bandsaw with a high-speed steel blade and cutting oil. Measurements of width and thickness were obtained with a digital caliper at 30 mm from both ends and at center of the specimens. Specimen geometry is shown in Figure 6.1. The specimens have an average width of 25.28±0.18 mm and an average thickness of 9.52±0.19 mm. The average length of 180±1 mm was measured with a ruler. An anti-friction material was applied between the metal plate and the adhesive in order to produce a pre-cracked region.

Table 6.1: Mechanical properties of the materials.

Material	Elastic Modulus, E_{11} (GPa)	Poisson's Ratio, ν_{12}
Steel	200	0.27
Composite 0/90	46	0.24
Adhesive	2.25	0.38

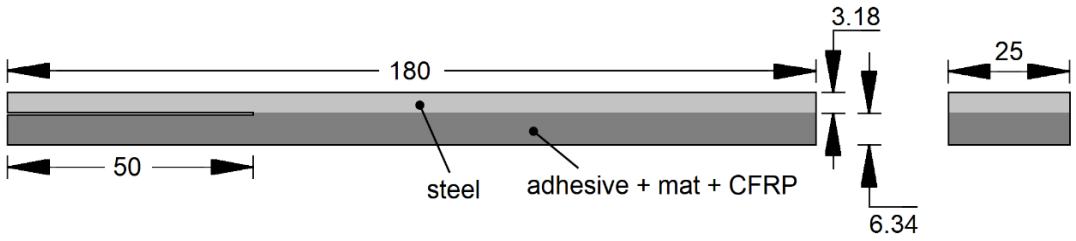


Figure 6.1: Specimen geometry (dimensions in millimeters).

6.2.2 Conditioning

Specimens were placed for ageing in a salt spray chamber. A solution of 5% mass sodium chloride [NaCl] was atomized at 200 ml/h and 35 ºC. The exposure zone remained in a relative humidity between 95% and 98% and pH between 6.5 and 7.2, according to the ASTM B117 standard practice [49]. Specimen's top and bottom surfaces were covered with a layer of tape to avoid degradation of the adherends as shown in Figure 6.2.

The average weight of 144.4 ±1.7 g was measured from the specimens before ageing using a precision balance with 0.01 g. The ageing period was chosen based on the results of previous work with similar materials [27, 28]. After an ageing period of 137 days, specimens were gently washed in clean running water and dried with paper and their weight was measured again.

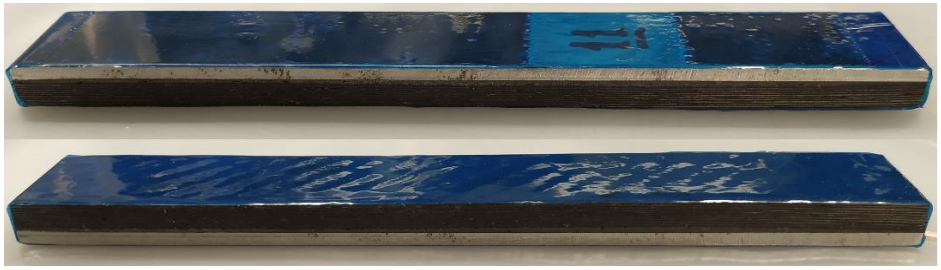


Figure 6.2: A specimen prepared for ageing.

6.2.3 Experimental method

The MMB test was chosen for the experimental mixed-mode fracture analysis of the specimens. During the procedure, loading is applied from a yoke to rollers attached to a lever and loaded just above the mid-plane of the test specimen, as shown in Figure 6.3. The test loading (P) is decomposed in opening (P_I) and shear (P_{II}) loadings in a constant ratio determined by the lever length (c). The mode I fracture ratio increases with the lever length. The lever weight produces a load (P_g) on the specimen at the length of the lever center of gravity (c_g). The test half-span (L) is set to 70 mm and the initial crack length (a) is 30 mm. The MMB test configuration produces higher stresses in the upper side of the specimen. Therefore, specimens were tested with the metal arm on top in order to prevent crack propagation within the composite material.

End-blocks of the same width as the specimens were bonded on both sides of the specimens using a structural epoxy adhesive. A thin layer of white correction fluid was coated on the specimen sides and millimeter paper was bonded in order to facilitate crack length measurements. Tests were conducted using a servo-hydraulic testing machine (MTS 831, MTS Systems Corporation) equipped with a 10 kN load cell. The testing load was applied at a quasi-static rate with a controlled displacement of 0.5 mm/min. Load-displacement points were obtained during the tests and a high-resolution camera, synchronized with the test output data, is positioned for crack length monitoring.

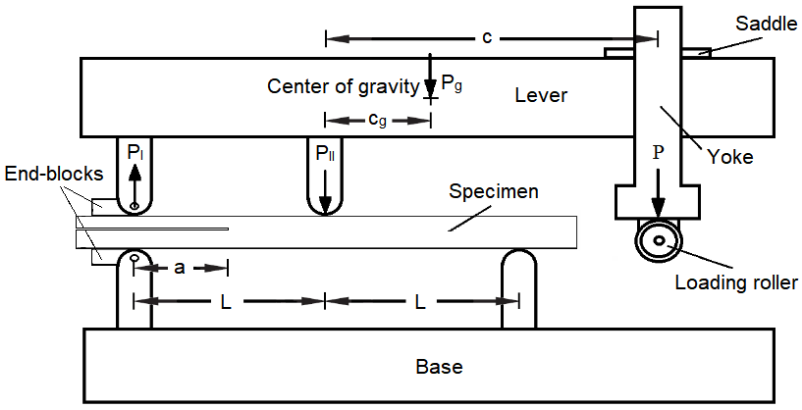


Figure 6.3: MMB test scheme.

6.3 Fracture data analysis

6.3.1 Numerical model

A 2D finite element (FE) model was developed in Abaqus Standard (version 2019.HF2). The geometry was modelled based on the specimen measurements, as presented in Figure 6.4. Loadings and contour conditions were applied in order to simulate the MMB test conditions. Boundary conditions were defined by constraining displacements in x and y directions at the left side and displacements in y direction at the right side of the beam. The opening and shear loadings were applied at the top surface. Isotropic materials were selected from the properties presented in Table 6.1. A FE mesh of 4-node bilinear plane strain quadrilateral solid elements (CPE4) was applied in the whole model for optimized computational cost.

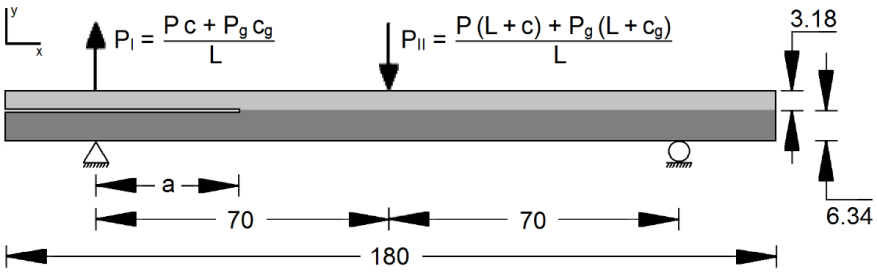


Figure 6.4: Model geometry and contour conditions.

The calculation of the fracture energy was performed using the finite element method with the virtual crack closure technique (FEM/VCCT). The VCCT is based on linear elastic fracture mechanics (LEFR). This is valid as long as the energy dissipated on the fracture process zone (FPZ) ahead of the crack tip is in a small scale in relation to the macroscopic elastic response. In this work, the tested specimens have relatively thick adherends which increase the elastic response on a macroscopic scale. Additionally, the use of a thin adhesive layer with a brittle epoxy adhesive contributes for a smaller plastic zone.

A mesh sensitivity analysis was performed using the model of the MMB test with a crack length (a) of 30 mm. The results are shown in Figure 6.5. The calculated fracture mode ratio (G_{II}/G) of a model without the adhesive layer showed dependency on the element size around the crack tip (Δa) and did not represent the actual fracture

development. In order to circumvent the problem, literature suggests modelling an artificial interlayer around the crack [46-47]. Therefore, thin layers of 0.2 mm thickness with adhesive properties (see Table 6.1) were modelled on both sides of the crack. The effect of the adhesive layer on the stiffness of the arms is negligible. The calculated fracture mode (G_{II}/G) of the model with adhesive layer is independent from the element size. A global mesh with elements of 0.1 mm was chosen for the determination of the fracture energy at the load-crack length points, as shown in Figure 6.6.

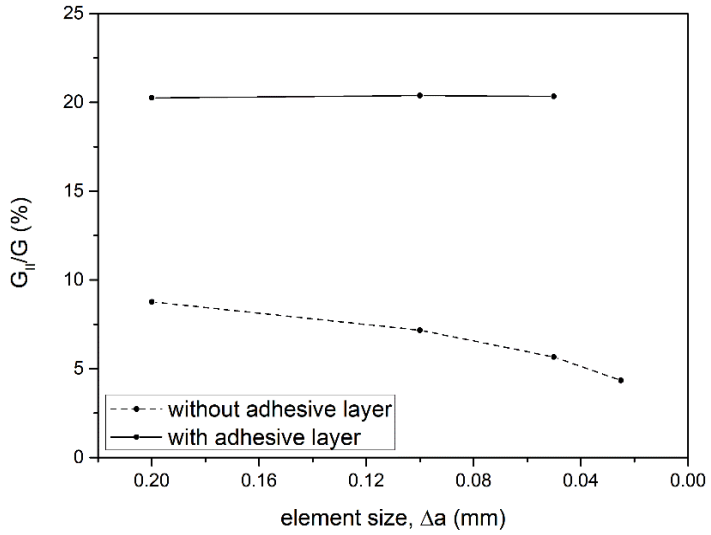


Figure 6.5: Mesh sensitivity analysis.

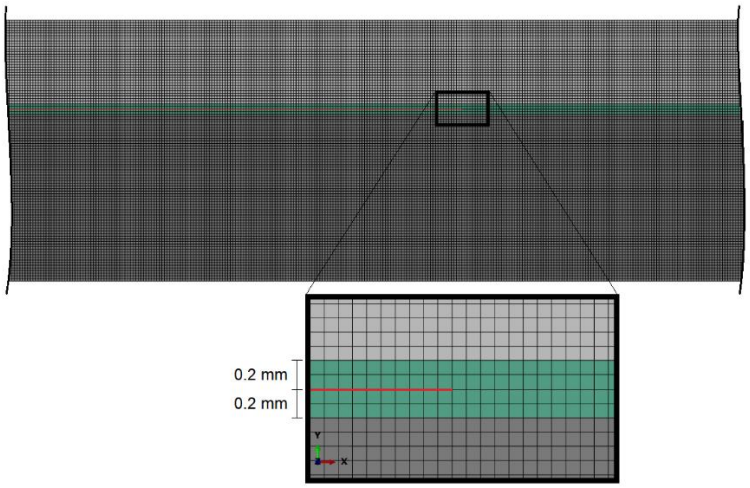


Figure 6.6: Detail of the FE mesh around crack tip.

6.3.2 Analytical model

The strain-based partitioning method (SBM) [47] is based on beam analysis and allows determining the fracture mode and total fracture energy of bi-material cracks. The method requires a design condition of longitudinal strain equivalence between the sides of the crack to be satisfied. This means, under bending loadings:

$$E_1 h_1^2 = E_2 h_2^2 \tag{6.1}$$

Where E_1 h_1, E_2 and h_2 are the flexural longitudinal moduli and the thickness of the upper and lower arms, respectively. The SBM assumes that pure mode II is produced when the longitudinal strain distribution at the faying surfaces of both arms must be identical, and pure mode II is obtained when the curvatures in the two arms are the same [47].

The mode I, mode II and total fracture energy of MMB test specimens can be obtained by the following equations:

$$G_I = \frac{(\psi M_1 - M_2)^2}{2B(\psi + 1)^2}\left(\frac{1}{E_1 I_1} + \frac{1}{E_2 I_2}\right) \tag{6.2}$$

$$G_{II} = \frac{(M_1 + M_2)^2}{2B(\psi + 1)}\left(\frac{1}{E_1 I_1} + \frac{(\psi + 1)}{E_{eq} I_{eq}}\right) \tag{6.3}$$

$$G = G_I + G_{II} \tag{6.4}$$

Where B is the specimen's width, M_1 and M_2 are the bending moments at the section of the crack tip in the upper and lower arms, respectively. E_{eq} is the flexural longitudinal modulus of the beam, I_1, I_2 and I_{eq} are the second moments of the area at the section of the crack tip in the upper arm, lower arm and beam, respectively. The bending stiffness ratio between the upper and lower arms is given by:

$$\psi = \frac{E_1 I_1}{E_2 I_2} \tag{6.5}$$

The SBM is a promising method for the easy and reliable fracture characterization of bi-material bonded joints [47, 50]. It is important to notice that the method requires linear-elastic conditions. The same parameters used in the FE model were applied to the calculation of the fracture energy using the SBM. Material properties were selected from Table 6.1 and geometrical parameters are indicated in Figure 6.4. Moreover, Equations. 6.2 and 6.3 do not consider effects of shear and crack tip rotation that are accounted in the numerical method.

6.4 Results and discussion

6.4.1 Effect of ageing on the materials

Figure 6.7 shows the outer surface of the steel arm of non-aged and aged specimens. The effect of corrosion on the outer steel surface is negligible. This can be observed by comparing non-aged specimens (Figure 6.7a) with the condition after ageing (Figure 6.7b). The application of tape on the outer surfaces of the specimens showed to be effective in diminishing the degradation of metal adherends aged in salt fog. However, the average weight measured from the aged specimens is 142.9±1.7 g, which means a decrease of 1.1% of the initial weight. This shows that the weight reduction due to corrosion of the steel member under long-term exposure to harsh environmental conditions had dominant effect against the weight increase due to moisture absorption of the adhesive [16] and the composite laminate [25]. These combined parameters make it difficult to determine the degree of moisture saturation at the bonded interface based on the measured weight during the conditioning process.

The effect of corrosion is noted on the sides of specimens, as shown in Figure 6.8. The presence of corrosion products is observed over the metal and composite sides of aged specimens (Figure 6.8b), in comparison with the non-aged sample (Figure 6.8a). This shows the degradation of the sides of the steel member exposed during the ageing period. Literature states the galvanic corrosion of the composite material occurs as consequence of corrosion product depositions, acting as electric bridges between steel and exposed carbon fibers [32]. Overall, only the sides of the specimens were significantly affected by the ageing conditions.

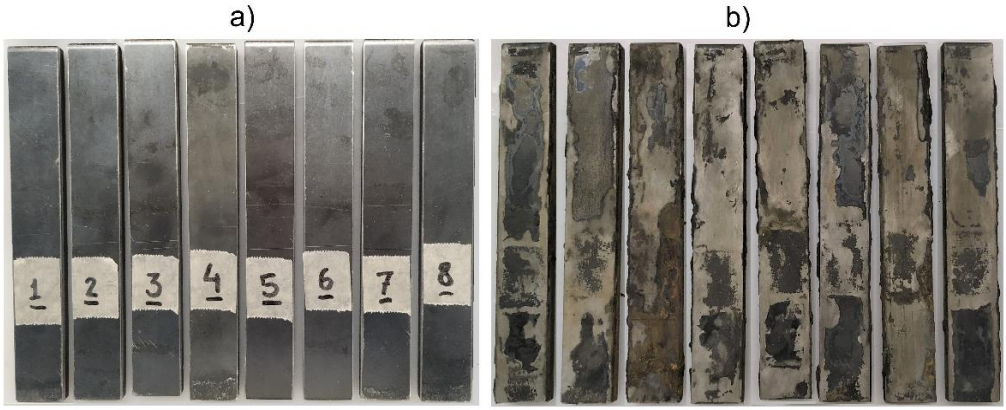


Figure 6.7: Steel outer surface (a) non-aged and (b) aged conditions.



Figure 6.8: Side view of a section of (a) non-aged and (b) aged specimens.

6.4.2 Test results

Non-aged and aged specimens were tested using the MMB test method described in section 6.2.3. Aged specimens were abraded on the sides with sandpaper prior to the experiments to ensure accurate crack length monitoring during tests. Tests were performed in two different configurations, i.e., two lever lengths, as shown in Table 6.2. The lever length of 110 mm is the limitation obtained from the numerical model for which linear elastic behavior of the metal arm is guaranteed and the SBM can be evaluated for the fracture characterization. The lever length of 150 mm corresponds to the maximum length of the available equipment.

Table 6.2: Test matrix.

Specimen	Condition	Lever length, c (mm)	Lever weight, P_g (N)	Lever center of gravity, c_g (mm)
01-04	non-aged	110	17.6	40

05-08	non-aged	150	28.7	130
09-12	aged	110	17.6	40
13-16	aged	150	28.7	130

Figure 6.9 shows the load-displacement curves obtained from the MMB tests. Composite-to-metal bonded joints exhibited typical curves, similar to standard symmetric specimens subjected to ageing conditions [42]. Results of non-aged and aged specimens tested with a lever length of 110 mm are presented in Figure 6.9a. It can be noticed that the maximum load achieved by the aged sample is higher than the non-aged ones. This means that the bonded structure required higher loadings for crack initiation after ageing in saline atmosphere. However, specimens tested with a lever length of 150 mm presented similar curves in both non-aged and aged condition, as shown in Figure 6.9b. The ageing process did not affect the performance of the bonded joint when tested at 150 mm. The overall stiffness of the structure was hardly affected by the ageing conditions, given the reduced effect of corrosion at the steel member (see Figure 6.7) as well as the stability of carbon fibers in the presence of moisture [26]. Moreover, the effect of galvanic coupling seems to be negligible to the stiffness of the laminate.

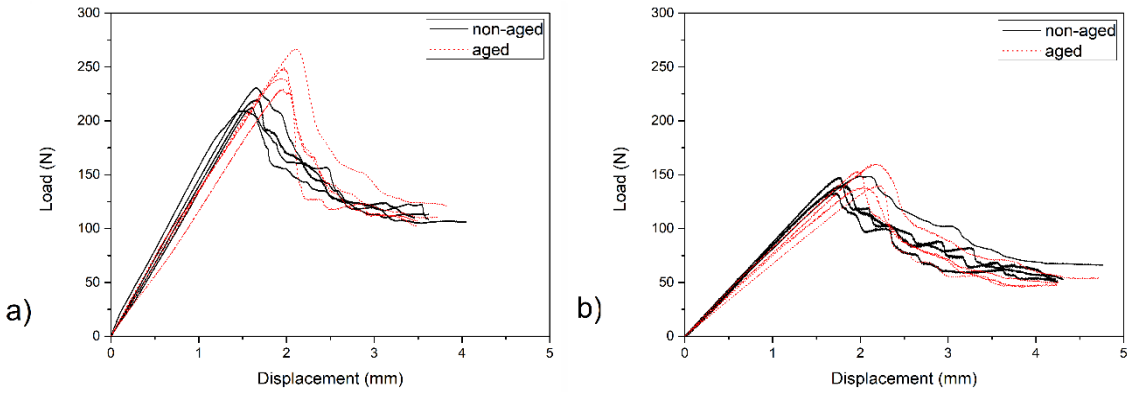


Figure 6.9: Load-displacement curves of tests with lever length of (a) 110 mm and (b) 150 mm.

6.4.3 Fracture toughness

The effect of ageing on the interface fracture of the bonded materials is measured by the variation of the fracture toughness. It is assumed that the mechanical properties of

the adherends remain the same after the ageing process. Therefore, only the adhesion mechanisms are considered in the analysis. The fracture toughness was obtained in terms of the total fracture energy (G) and the fracture mode ratio (G_{II}/G) using the numerical and analytical methods described in sections 6.3.1 and 6.3.2, respectively. The numerical results were calculated every 5 mm and the analytical results were calculated every 1 mm of the crack propagation.

Figure 6.10 shows comparative results of the fracture energy obtained from the FEM/VCCT and the SBM in the two different testing configurations. Numerical values of the total fracture energy are shown to be consistent along crack propagation. Results calculated using the SBM deviated by 15% from the FEM/VCCT at crack initiation and converged as the crack length increases. This is attributed to the effects of transverse shear stresses that are not considered in the SBM but can be significant when testing beams with high thickness-to-span ratio [47].

The fracture mode ratio obtained from numerical and analytical methods is presented in Figure 6.11. Numerical results (FEM/VCCT) presented nearly constant results along the crack propagation with a slight reduction of the mode II portion at the crack propagation points near the specimen half-length. In addition, the global mode ratio at the whole specimen, obtained from the SBM, showed good agreement with the local mode ratio at the crack tip, obtained from the numerical simulations. This indicates that the effect of the FPZ is negligible. The SBM predicted, with accuracy, the partitioning ratio of the composite-to-metal bonded joints. The test configuration with a lever length of 110 mm produced 20% mode II and the lever length of 150 mm resulted in 15% mode II fracture ratio.

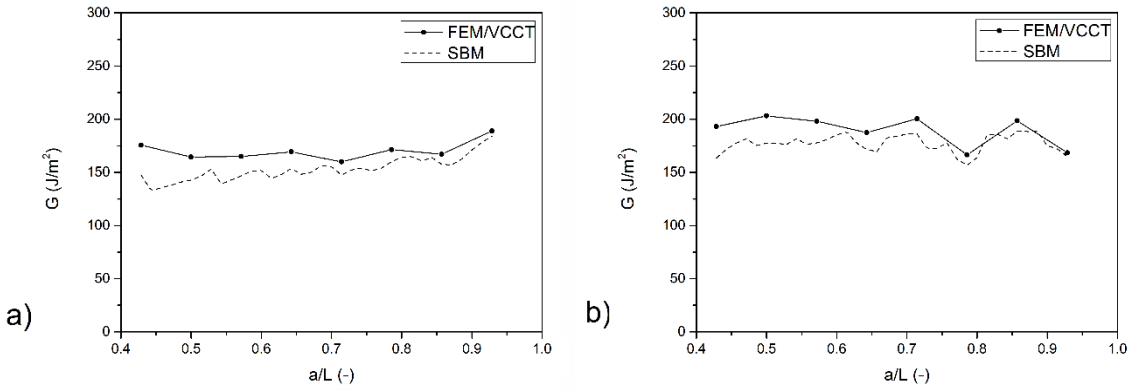


Figure 6.10: Fracture energy of a representative specimen tested at a lever length of (a) 110 mm and (b) 150 mm.

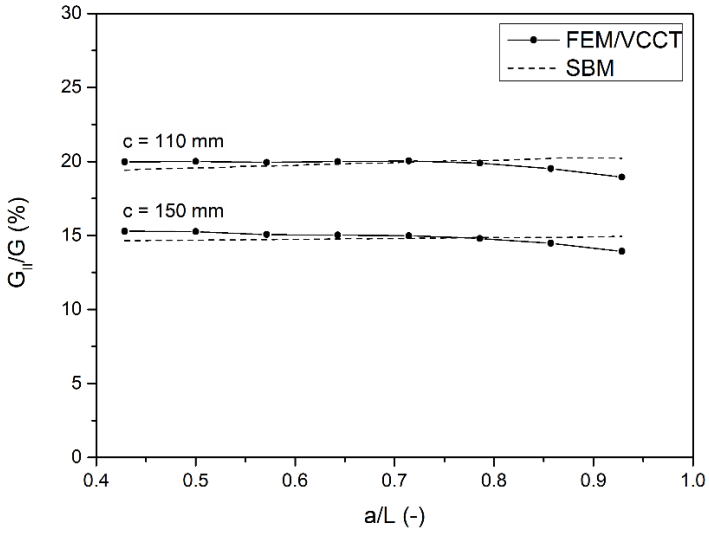


Figure 6.11: Fracture mode ratio.

The average fracture energy (G_{ave}), presented in Figure 6.12, provides a comparable data for the evaluation of the ageing effect on the fracture performance of the tested specimens. Figure 6.12a shows the mean fracture energy at crack initiation of the 4 repeats of each configuration. It reveals a significant increase of 27% of the fracture energy at crack initiation when tested in 20% mode II. In the case of specimens tested in 15% mode II, the fracture energy showed a slight increase of 7% at crack initiation. The region of crack initiation is directly affected by the moisture across the whole width and resulted in an increase of the fracture toughness. This seems to be related to the shear behavior of the adhesive and is attributed to the effect of plasticization [35, 37]. Figure 6.12b shows the mean fracture energy at crack propagation points (from 35 to 65 mm crack length) of the 4 repeats of each configuration. A negligible variation is observed of 3% of the fracture energy at 20% mode II during crack propagation, while a reduction 15% of the fracture energy is noted at 15% mode II. As expected, the SBM showed good agreement with the numerical results. Moreover, the average fracture energy obtained from the SBM deviated by 15% from the FEM/VCCT at crack initiation (Figure 6.12a) and 6% during propagation (Figure 6.12b), as observed in Figure 6.10.

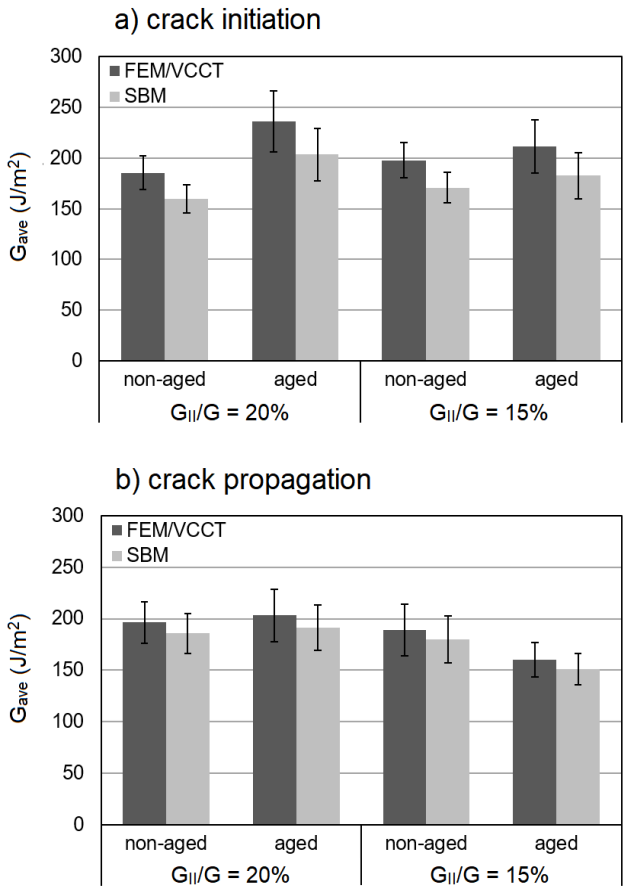


Figure 6.12: Average fracture energy at (a) crack initiation and (b) propagation.

6.4.4 Fractography

Representative images of the fracture surfaces are presented in Figure 6.13. Both non-aged and aged specimens presented most of the adhesive stuck to the composite adherend (lower surface), while a thin layer of adhesive remained on the metal side (upper surface). Overall, the non-aged specimens (Figure 6.13a) exhibited thin-layer cohesive failure as the triggering failure mode. This observation confirms good bond quality and ensures high joint efficiency. In the case of the aged specimens (Figure 6.13b), moisture penetration is noticed on both side edges of the fracture surfaces.

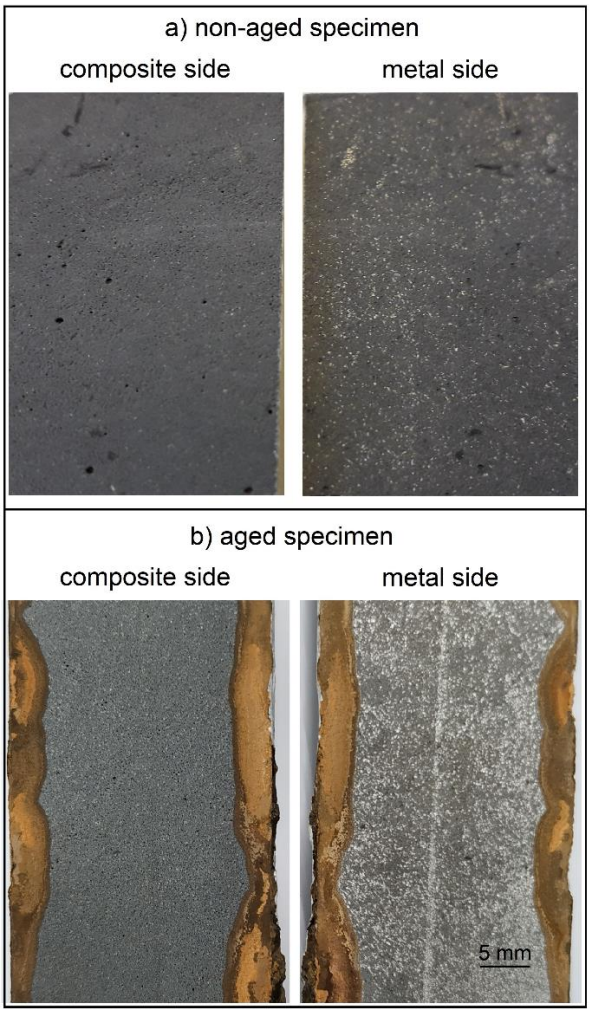


Figure 6.13: Fracture surfaces of (a) non-aged and (b) aged specimens.

A detailed analysis of the fracture surfaces was performed using a field emission scanning electron microscope (SEM) (JSM-7500F, JEOL, Japan). Prior to examination, samples were coated with two ultra-thin (15 microns) layers of gold using a sputtering system (Q300T D, Quorum Technologies, United Kingdom) for the SEM analysis of non-conductive materials. Figure 6.14 shows typical fracture surfaces from the metal side of non-aged specimens using magnifications of 100 and 500 times. Crack propagation direction is from the left to the right side of the images. Both test configurations of 20% mode II (Figures 6.14a and 6.14b) and 15% mode II (Figures 6.14c and 6.14d) demonstrated similar surfaces of cohesive failure with the presence of air voids and scarps. These features confirm that the fracture occurred with dominant mode I loadings in both test configurations [25, 28]. No significant difference in the failure mechanisms was noticed between the two mode ratios.

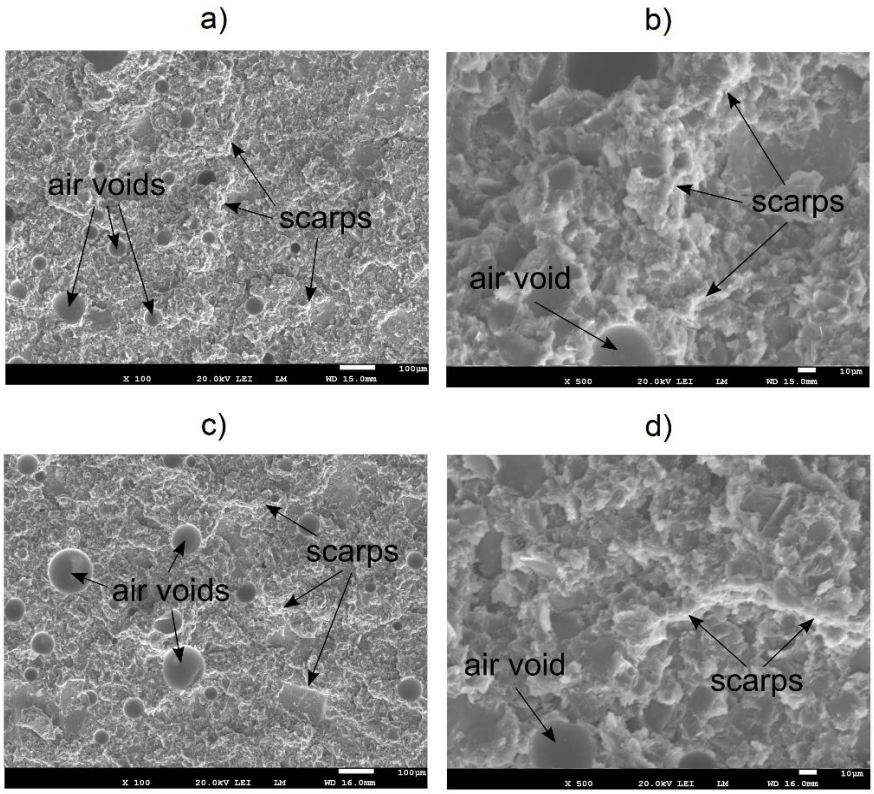


Figure 6.14: SEM images of non-aged specimen tested with c = 110 mm (20% mode II) at (a) x100 and (b) x500 and tested with c = 150 mm (15% mode II) at (c) x100 and (d) x500.

Figure 6.15 shows the fracture surfaces from the metal side of an aged specimen using magnifications of 100 and 500 times. Images were obtained in three different regions: at the center of the surface, near the edge, and in an intermediate region. Images from the center (Figures 6.15a and 6.15b) and intermediate (Figures 6.15c and 6.15d) regions show the presence of adhesive attached to the metal surface indicating cohesive failure, such as the non-aged specimens in Figure 6.14. However, slight less scarps on the adhesive surface can be observed, indicating a certain variation of the failure mechanism in these regions. Images obtained from regions affected by moisture (Figures 6.15e and 6.15f) showed remarkably distinct fracture surfaces of seemingly adhesive failure. The occurrence of micro-cracks observed at high magnification (Figure 6.15f) indicates the presence of corrosion products at the interface due to the degradation of the metal adherend.

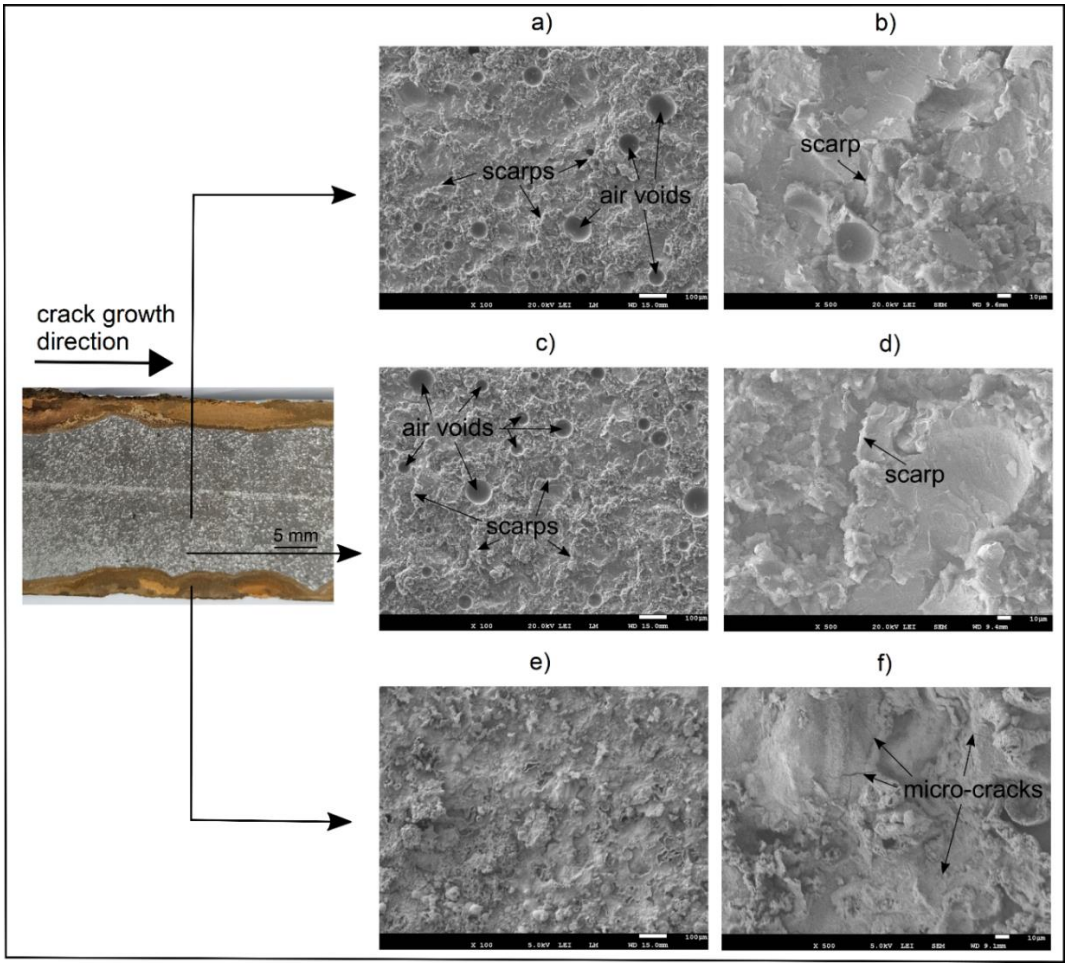


Figure 6.15: SEM images of aged specimen in 100x and 500x, respectively, at (a, b) center, (c, d) intermediate and (e, f) edge regions of the fracture surface.

In order to have a better understanding of the failure mechanisms, a chemical characterization was performed by using Energy-Dispersive Spectroscopy (EDS), available in the SEM equipment. Figure 6.16 shows the chemical spectrum of the regions presented in Figure 6.15, in terms of counts per second per electron-volt (cps/eV). Results reveal the presence of chloride [Cl] in the region of moisture penetration near the edge of the fracture surfaces (Figure 6.16c), while it was not found at the center and intermediate regions (Figures 6.16a and 6.16b). The incidence of salt traces at the fracture surface is an indication of adhesive failure due to degradation and ingress of salt within the interface [28]. Additionally, the higher content of iron [Fe] and oxygen [O] elements confirm the presence of corrosion products at the interface, as noticed in Figure 6.15e and 6.15f. Moreover, minor amounts of aluminum [Al] and silicon [Si] contaminations are observed

at the center and intermediate regions. The presence of these elements can be attributed to the surface preparation of the metal adherend.

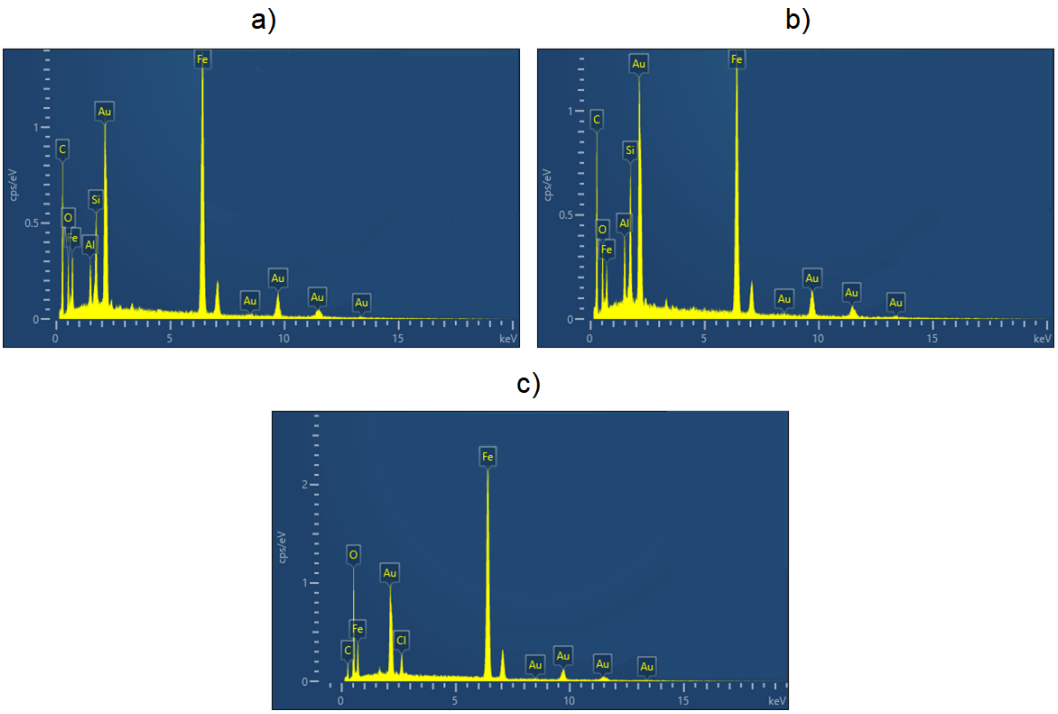


Figure 6.16: EDS of aged specimen at (a) center, (b) intermediate and (c) edge regions.

Figure 6.17 shows the relative weight content of the chemical components at the fracture surfaces of non-aged and aged specimens. The gold [Au] content was excluded from this analysis. The non-aged specimens demonstrated a high content of carbon [C] and oxygen [O] elements in contrast to the slight presence of iron [Fe], which shows the dominant presence of adhesive in the fracture surfaces. In the case of aged specimens, the increased incidence of iron [Fe] indicates an exposed metal interface at center and intermediate regions. This suggests a combination of cohesive and adhesive failure in regions unaffected by the moisture, occurred closer to the interface with the incidence of the interfacial fracture.

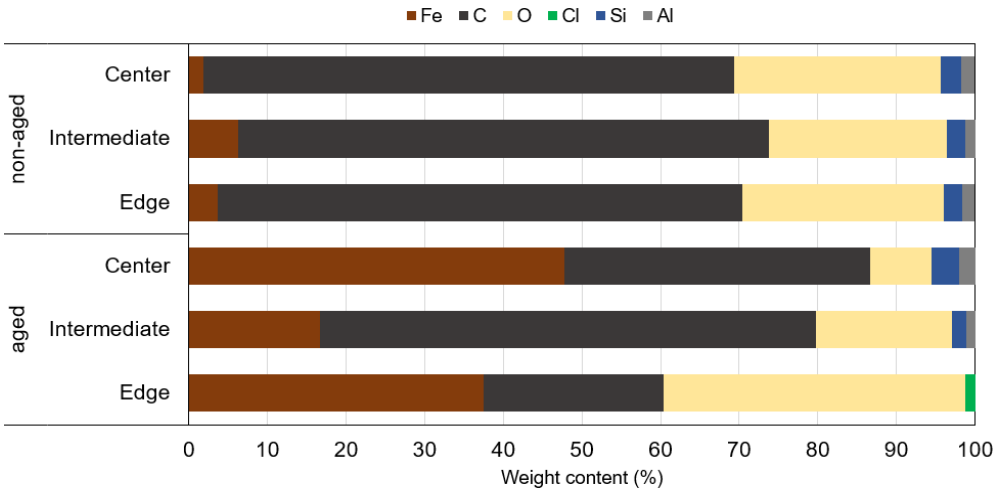


Figure 6.17: EDS of aged specimen at center, intermediate and edge regions of the fracture surface.

The results obtained from the fractographic analysis help to explain the effect of salt spray ageing on the mechanical behavior of the bonded joint. The failure mode shifted from thin-layer cohesive to to adhesive failure in the regions where the ingress of moisture and salt is observed. Additionally, the ageing process also affected the metal-adhesive interface in regions where the ingress of moisture was not observed, changing from thin-layer cohesive failure to a combination of thin-layer cohesive and adhesive failure. This degradation mechanism is important since a very long exposure time is needed in order to have a significant penetration of moisture within the interface. Therefore, the decrease of the fracture toughness observed at crack propagation can be related to the degradation of the interfacial adhesion between metal adherend and adhesive. Moreover, the increase of the fracture toughness observed at crack initiation may be related mainly to the mechanical behavior of the adhesive material than the failure mode.

6.5 Conclusion

The effect of long-term environmental exposure on the performance of composite-to-metal bonded joints was investigated. Bi-material bonded specimens with steel and CFRP adherends were manufactured and aged in salt fog. MMB tests were performed for non-aged and aged specimens and the mixed-mode fracture ratios were obtained using the virtual crack closure technique (FEM/VCCT) and the strain-based method (SBM). The fracture surfaces were analysed in order to evaluate the failure

mechanisms and their association with the performance of the bonded materials subjected to environmental exposure.

The metal adherend suffered significant damage during ageing in salt spray environment. The combined effects of corrosion on the metal and moisture uptake on the adhesive and composite made it difficult to determine the degree of moisture saturation at the bonded interface based on the measured weight during the conditioning process. Overall, the long-term exposure to salt spray environment did not have a drastic effect on the adhesive layer although it was extremely aggressive to the steel adherend. The presence of corrosion products resulted from the steel degradation was observed at the sides of the specimens and at the interface, together with the salt and moisture.

The strain-based method (SBM) predicted, with accuracy, the fracture mode ratio of bi-material bonded joints. It proved to be an easy and reliable solution based on closed form equations with parameters obtained directly from the experiments that allows the characterization of fracture behavior of cracks between different materials. In contrast, the use of numerical solutions requires the use of complex models and high computational cost.

Non-aged specimens demonstrated thin-layer cohesive failure occurring near the metal adherend. The effect of ageing resulted in an increase of the fracture toughness at crack initiation. This seems to be related to the shear behavior and plasticization of the adhesive. At the same time, the penetration of moisture at the edges of the fracture surface produced adhesive failure in these regions affected by moisture. Additionally, the failure mode at the unaffected regions of the fracture surface of aged specimens shifted from thin-layer cohesive failure to a combination of thin-layer cohesive and adhesive failure. This may explain the typical changes of the mechanical behavior of bonded joints at initial stages of ageing followed by a steady condition when pure adhesive failure is reached.

References

[1] Budhe, S.; Banea, M.D.; de Barros, S. An updated review of adhesively bonded joints in composite materials. Int. J. Adhes. Adhes. 2017, 72, 30-42.

[2] Mangalgiri, P.D. Composite materials for aerospace applications. Bull. Mater. Sci. 1999, 22, 657-664.

[3] Taub, A.I.; Krajewski, P.E.; Luo, A.A. The evolution of technology for materials processing over the last 50 years: the automotive example. JOM 2007, 59, 48-57.
[4] Van Den Einde, L.; Zhao, L.; Seible, F. Use of FRP composites in civil structural applications. Constr. Build. Mater. 2003, 17(6-7), 389-403.
[5] Saeedifar, M.; Saleh, M.N.; Teixeira de Freitas, S.; Zarouchas, D. Damage characterization of adhesively-bonded Bi-material joints using acoustic emission. Compos. Part B 2019, 176, 107356.
[6] Katnam, K.B.; da Silva, L.F.M.; Young, T.M. Bonded repair of composite aircraft structures: A review of scientific challenges and opportunities. Prog. Aerosp. Sci. 2013, 61, 26-42.
[7] Meniconi, L.C.; Lana, L.D.; Morikawa, S.R. Experimental fatigue and aging evaluation of the composite patch repair of a metallic ship hull. Appl. Adhes. Sci. 2014, 2, 27.
[8] Saleh, M.N.; Saeedifar, M.; Zarouchas, D.; Teixeira de Freitas, S. Stress analysis of double-lap bi-material joints bonded with thick adhesive. Int. J. Adhes. Adhes. 2020, 97, 102480.
[9] da Costa-Mattos, H.S; Reis, J.M.L; Sampaio, R.F.; Perrut, V.A. An alternative methodology to repair localized corrosion damage in metallic pipelines with epoxy resins. Mater. Des. 2009, 30(9), 3581-3591.
[10] de Barros, S.; Banea, M.D.; Budhe, S.; de Siqueira, C.E.R.; Lobão, B.S.P.; Souza, L.F.G. Experimental analysis of metal-composite repair of floating offshore units (FPSO). J. Adhes. 2016, 93(1-2), 147-158.
[11] da Costa Mattos, H.S.; Reis, J.M.L.; Paim, L.M.; da Silva, M.L.; Lopes Junior, R.; Perrut, V.A. Failure analysis of corroded pipelines reinforced with composite repair systems. Eng. Fail. Anal. 2016, 59, 223-236.
[12] Oudad, W.; Madani, K.; Bachir Bouiadjra, B.; Belhouari, M.; Cohendoz, S.; Touzain, S.; Feaugas, X. Effect of humidity absorption by the adhesive on the performances of bonded composite repairs in aircraft structures. Compos. Part B 2012, 43(8), 3419-3424.
[13] Budhe, S.; Banea, M.D.; de Barros, S. Bonded repair of composite structures in aerospace application: a review on environmental issues. Appl. Adhes. Sci. 2018, 6, 3.

[14] Böer, P.; Holliday, L.; Kang, T.H.-K. Independent environmental effects on durability of fiber-reinforced polymer wraps in civil applications: A review. Constr. Build. Mater. 2013, 48, 360-370.
[15] Lau, D.; Büyüköztürk, O. Fracture characterization of concrete-epoxy interface affected by moisture. Mech. Mater. 2010, 42(12), 1031-1042.
[16] Viana, G.; Costa, M.; Banea, M.D.; da Silva, L.F.M. A review on the temperature and moisture degradation of adhesive joints. Proc. Inst. Mech. Eng., Part L. 2017, 231(5), 488-501.
[17] Brewis, D.M.; Comyn, J.; Tegg, J.L. The durability of some epoxide adhesive-bonded joints on exposure to moist warm air. Int. J. Adhes. Adhes. 1980, 1(1), 35-39.
[18] Brewis, D.M.; Comyn, J.; Shalash, R.J.A. The effect of moisture and temperature on the properties of an epoxide-polyamide adhesive in relation to its performance in single lap joints. Int. J. Adhes. Adhes. 1982, 2(4), 215-222.
[19] Pethrick, R.A. Design and ageing of adhesives for structural adhesive bonding – A review. Proc. Inst. Mech. Eng., Part L. 2015, 229(5), 349-379.
[20] Sugiman, S.; Crocombe, A.D.; Aschroft, I.A. Experimental and numerical investigation of the static response of environmentally aged adhesively bonded joints. Int. J. Adhes. Adhes. 2013, 40, 224-237.
[21] Li, W.D.; Ma, M.; Han, X.; Tang, L.P.; Zhao, J.N.; Gao, E.P. Strength Prediction of Adhesively Bonded Single Lap Joints Under Salt Spray Environment Using a Cohesive Zone Model. J. Adhes. 2016, 92(11), 916-937.
[22] Papanicolaou, G.C.; Charitidis, P.; Mouzakis, D.E.; Karachalios, E.; Jiga, G.; Portan, D.V. Experimental and numerical investigation of balanced Boron/Epoxy single lap joints subjected to salt spray aging. Int. J. Adhes. Adhes. 2016, 68, 9-18.
[23] Park, Y.-B.; Song, M.-G.; Kim, J.-J.; Kweon, J.-H.; Choi, J.-H. Strength of carbon/epoxy composite single-lap bonded joints in various environmental conditions. Compos. Struct. 2010, 92(9), 2173-2180.
[24] Jeong, M.-G.; Kweon, J.-H.; Choi, J.-H. Effect of various hygrothermal environments on the failure of adhesively bonded composite single-lap joints. J. Compos. Mater. 2013, 47(17), 2061-2073.

[25] Arouche, M.M.; Budhe, S.; Banea, M.D.; Teixeira de Freitas, S.; de Barros, S. Interlaminar adhesion assessment of carbon-epoxy laminates under salt water ageing using peel tests. Proc. Inst. Mech. Eng., Part L. 2019, 233(8), 1555-1563.
[26] Mariam, M.; Afendi, M.;Abdul Majid, M.S.; Ridzuan, M.J.M.; Azmi, A.I.; Sultan, M.T.H. Influence of hydrothermal ageing on the mechanical properties of an adhesively bonded joint with different adherends. Compos. Part B 2019, 165, 572-585.
[27] Arouche, M.M.; Budhe, S.; Alves, L.A.; Teixeira de Freitas, S.; Banea, M.D.; de Barros, S. Effect of moisture on the adhesion of CFRP-to-steel bonded joints using peel tests. J Braz. Soc. Mech. Sci. Eng. 2018, 40:10.
[28] Teixeira de Freitas, S.; Banea, M.D.; Budhe, S.; de Barros S. Interface adhesion assessment of composite-to-metal bonded joints under salt spray conditions using peel tests. Compos. Struct. 2017, 164, 68-75.
[29] Heshmati, M.; Haghani, R.; Al-Emrani, M. Durability of bonded FRP-to-steel joints: Effects of moisture, de-icing salt solution, temperature and FRP type. Compos. Part B 2017, 119, 153-167.
[30] Sugiman, S.; Setyawan, P.D.; Salman, S.; Ahmad, H. Experimental and numerical investigation of the residual strength of steel-composites bonded joints: Effect of media and aging condition. Compos. Part B 2019, 173, 106977.
[31] Silva, M.A.G.; Biscaia, H.; Ribeiro, P. On factors affecting CFRP-steel bonded joints. Constr. Build. Mater. 2019, 226, 360-375.
[32] Yang, Y.; Silva, M.A.G.; Silva, R.J.C. Material degradation of cfrp-to-steel joints subjected to salt fog. Compos. Part B 2019, 173, 106884.
[33] Chaves, F.J.P.; da Silva, L.F.M.; de Moura, M.F.S.F.; Dillard, D.A.; Esteves, V.H.C. Fracture Mechanics Tests in Adhesively Bonded Joints - A Literature Review. J. Adhes. 2014, 90(12), 955-992.
[34] Loh, W.K.; Crocombe, A.D.; Abdel Wahab, M.M.; Ashcroft, I.A. Environmental degradation of the interfacial fracture energy in an adhesively bonded joint. Eng. Fract. Mech. 2002, 69(18), 2113-2128.
[35] Wylde, J.W.; Spelt, J.K. Measurement of adhesive joint fracture properties as a function of environmental degradation. Int. J. Adhes. Adhes. 1998, 18(4), 237-246.
[36] Ameli, A.; Papini, M.; Spelt, J.K. Fracture R-curve of a toughened epoxy adhesive as a function of irreversible degradation. Mater. Sci. Eng. A. 2010, 527(20), 5105-5114.

[37] Fernandes, P.; Viana, G.; Carbas, R.J.C.; Costa, M.; da Silva, L.F.M.; Banea, M.D. The influence of water on the fracture envelope of an adhesive joint. Theor. Appl. Fract. Mech. 2017, 89, 1-15.
[38] Viana, G.; Costa, M.; Banea, M.D.; da Silva, L.F.M. Moisture and temperature degradation of double cantilever beam adhesive joints. J. Adhes. Sci. Technol. 2017, 31(16), 1824-1838.
[39] Costa, M.; Viana, G.; da Silva, L.F.M.; Campilho, R.D.S.G. Effect of humidity on the mechanical properties of adhesively bonded aluminium joints. Proc. Inst. Mech. Eng., Part L. 2018, 232(9), 733-742.
[40] Markatos, D.N.; Tserpes, K.I.; Rau, E.; Markus, S.; Ehrhart, B.; Pantelakis, Sp. The effects of manufacturing-induced and in-service related bonding quality reduction on the mode-I fracture toughness of composite bonded joints for aeronautical use. Compos. Par B 2013, 45(1), 556-564.
[41] Fernandes, R.L.; de Moura, M.F.S.F.; Moreira, R.D.F. Effect of moisture on pure mode I and II fracture behaviour of composite bonded joints. Int. J. Adhes. Adhes. 2016, 68, 30-38.
[42] LeBlanc, L.R.; LaPlante, G. Experimental investigation and finite element modeling of mixed-mode delamination in a moisture-exposed carbon/epoxy composite. Compos. Part A 2016, 81, 202-213.
[43] Silva, F.G.A.; de Moura, M.F.S.F.; Moreira, R.D.F. Influence of adverse temperature and moisture conditions on the fracture behaviour of single-strap repairs of carbon-epoxy laminates. Int. J. Adhes. Adhes. 2020, 96, 102452.
[44] André, A.; Haghani, R.; Biel, A. Application of fracture mechanics to predict the failure load of adhesive joints used to bond CFRP laminates to steel members. Constr. Build. Mater. 2012, 27(1), 331-340.
[45] Quispitupa, A.; Berggreen, C.; Carlsson, L.A. On the analysis of a mixed mode bending sandwich specimen for debond fracture characterization. Eng. Fract. Mech. 2009, 76(4), 594-613.
[46] Shahverdi, M.; Vassilopoulos, A.P.; Keller, T. Mixed-Mode I/II Fracture Behavior of Asymmetric Adhesively-Bonded Pultruded Composite Joints. Eng. Fract. Mech. 2014, 115, 43-59.

[47] Arouche, M.M.; Wang, W.; Teixeira de Freitas, S.; de Barros, S. Strain-based methodology for mixed-mode I+II fracture: A new partitioning method for bi-material adhesively bonded joints. J. Adhes. 2019, 95(5-7), 385-404.
[48] DNV-RP-C301. Design, fabrication, operation and qualification of bonded repair of steel structures. Det Norske Veritas AS, 2015.
[49] ASTM B117-18. Standard Practice of Operation Salt Spray (Fog) Apparatus. ASTM International, 2018.
[50] Arouche, M.M.; Teixeira de Freitas, S.; de Barros, S. On the influence of glass fiber mat on the mixed-mode fracture of composite-to-metal bonded joints. Compos. Struct. 2021, 256, 113109.

Chapter 7

Conclusions and Final Remarks

This Chapter summarises the main conclusion and contributions from each of the interconnected topics studied in this Thesis. At the end, it provides a list of the scientific papers resulted from this research project.

7.1 Main conclusions and contributions

The improvement of structural performance requires innovative applications of composite materials to replace traditional materials in the design of structures. In the offshore industry, the composite repair technology has emerged as a promising alternative for the rehabilitation of metal structures subjected to harsh environment. In this sense, adhesive bonding technology is usually the preferred joining method for composite and metal parts. Literature reveals challenges and limitations in the present methodologies for optimizing the design and ensuring structural integrity of composite-to-metal bonded structures. In this Thesis, the mixed-mode fracture behavior of bonded joints was investigated and a new methodology was developed for the fracture characterization of bi-material crack propagation. The fracture behavior of composite-to-metal bonded joints was assessed under mixed-mode loadings. Then, the effect of design and manufacturing parameters on the performance of the structure was evaluated. After that, the influence of environmental conditions was addressed.

7.1.1 Mixed-mode fracture characterization of bi-material cracks

An analytical method based on beam analysis was proposed for the calculation of the total fracture energy and mode partitioning of bi-material crack propagation: the strain-based method (SBM). A validation of the SBM was performed though a parametric study using the finite element method (FEM) with the virtual crack closure technique (VCCT). The methodology was applied on the experimental analysis of a composite-to-metal bonded joint using the mixed-mode bending (MMB) test. Effects of design parameters, manufacturing and environmental conditions on the performance of the bi-material bonded structure were evaluated.

The MMB test method showed potential for the experimental evaluation of the mixed-mode fracture of bi-material bonded joints. The strain-based specimen design was successfully applied to the MMB test although the metal yielding point imposes limitations on the maximum contribution of mode II fracture in the MMB test.

A finite element (FE) model of the MMB test using the VCCT with a bi-material joint produces mesh size dependent results. This problem can be circumvented by modelling a thin layer with the same material on both sides of the crack. Then, the total fracture energy and mode ratio of bi-material cracks can be predicted.

The fracture energy calculated from the SBM was benchmarked against FE models. The SBM predicts a coupling relationship between the pure modes and allows obtaining the fracture mode ratio of bi-material cracks through a simple design criterion based on the longitudinal strain equivalence between arms of the specimen. The total fracture energy and mode ratio were obtained for a wide range of specimen thicknesses and materials. Then, it was applied to the fracture characterization of composite-to-metal bonded joints. The SBM proved to be an easy and reliable method that allows characterizing mixed-mode fracture behavior of a crack propagation between different materials through a simple formulation. In contrast, the use of numerical solutions requires the use of complex models and high computational cost.

Limitations of the SBM include considerations of transverse shear effect and crack tip rotation. Specimens with relatively large thickness may produce significant errors in the analytical model and, therefore, geometrical limitations should be considered in the specimen design. Additionally, the SBM relies on the principles of linear elastic fracture mechanics (LEFM). Effects of the fracture process zone (FPZ) developed ahead of the crack tip are not taken into account, but may be significant in bonded structures using a ductile adhesive and thick adhesive layer.

7.1.2 Effect of design and manufacturing parameters on composite-to-metal bonded joints

The SBM was applied to investigate the influence of an inserted layer of glass fiber mat as a toughening mechanism to improve the fracture performance of composite-to-metal bonded structures. Specimens were manufactured by hand lay-up using two different consolidation processes: at room pressure or using vacuum bagging. Results showed that crack tends to propagate in the interface between the adhesive layer and the upper arm of the specimen due to the higher stresses caused by the MMB loading configuration. In the case of a CFRP adherend without GFM, cohesive failure within the adhesive layer is the dominant failure mode under high mode I fracture while a combination of cohesive and interlaminar failure occurs in high mode II fracture condition. The insertion of a layer of GFM between adherends prevented the crack migration to the CFRP adherend and introduced a preferential crack propagation path within the GFM. The crack propagation within the GFM produced more irregular fracture

surface height profiles when compared to the specimens without GFM. A more irregular crack path resulted in higher fracture toughness due to the increase of the energy required for the crack to propagate. Therefore, the adjacent composite layer to the adhesive interface has an important role in the fracture performance of the bonded joint since it affects the crack propagation path.

The manufacturing process affected the performance of the specimens with GFM. The vacuum bagging technique produced a better fiber/matrix compaction of the GFM and resulted in rougher fracture surfaces when compared to room pressure. On the other hand, no change was observed in the fracture surfaces of specimens without GFM despite the manufacturing process. The relationship between fracture surface roughness and fracture performance is observed in both manufacturing processes although the toughening effect is more evident in higher mode II fracture conditions. The insertion of a layer of GFM is expected to increase the fracture performance of composite repairs in metal structures. The use of vacuum pressure in the consolidation of the composite, when feasible, is recommended for optimizing the fracture performance of the bonded structure.

7.1.3 Effect of environmental conditions on composite-to-metal bonded joints

The effect of long-term environmental exposure on the performance of composite-to-metal bonded joints aged in salt fog was investigated. The metal adherend suffered significant damage during ageing in salt spray environment. The combined effects of corrosion on the metal and moisture uptake on the adhesive and composite made it difficult to determine the degree of moisture saturation at the bonded interface based on the measured weight during the conditioning process. Overall, the long-term exposure to salt spray environment did not have a drastic effect on the adhesive layer although it was extremely aggressive to the steel adherend. The presence of corrosion products resulted from the steel degradation was observed at the sides of the specimens and at the interface, together with the salt and moisture.

Non-aged specimens demonstrated cohesive failure occurring near the metal adherend. The effect of ageing resulted in an increase of the fracture toughness at crack initiation. This seems to be related to the shear behavior and plasticization of the adhesive. At the same time, the penetration of moisture at the edges of the fracture surface produced

adhesive failure in these regions affected by moisture. Additionally, the failure mode at the unaffected regions of the fracture surface of aged specimens shifted from thin-layer cohesive to a combination of cohesive and adhesive failure. This may explain the typical changes of the mechanical behavior of bonded joints at initial stages of ageing followed by a steady condition when pure adhesive failure is reached.

7.2 Future works

In this project, a literature review was carried out on the theories and approaches for mixed-mode fracture characterization. It was noticed that methodologies for the analysis of composite delamination of symmetric specimens are well stablished. However, the real-life application of symmetric structures is limited. The development of simple and reliable procedures for the analysis of multi-material structures is needed. The analysis of asymmetric beams under pure mode I and pure mode II fracture are current objects of research. In the case of mixed-mode fracture crack propagation between different materials, the partitioning between pure modes I and II is still challenging. Additionally, the expansion in applications of composite laminates requires the development of models that incorporate the complex mechanical behavior of these materials. The fracture characterization of cracks between multidirectional laminates is a relevant topic for future studies.

The strain-based method (SBM) was proposed for the mixed-mode fracture characterization of cracks between different materials. The model showed potential to characterize the crack propagation of beams with dissimilar materials. However, there may be limitations regarding the analysis of composite materials. A deeper study is required in order to evaluate the condition for pure mode II fracture considering the bending-extension coupling of the materials.

Finally, the effect of degradation of composite-to-metal bonded joints in moist environment was evaluated under mixed-mode fracture conditions. However, in operational conditions, variety of different parameters, such as temperature and cyclic loads, will also affect the long-term performance of the bonded structure. Future endeavors may focus on the evaluation of different independent parameters as well as the combined effects, such as hydrothermal ageing. Since the glass transition temperature of

adhesives and resins are relatively low, the thermal condition is expected to have a major influence on the performance of these structures.